# Self-repair rejuvenates mechanically stressed microtubules

Laura Schaedel

Communauté
UNIVERSITÉ Grenoble Alpes

# THÈSE

Pour obtenir le grade de

**DOCTEUR DE LA COMMUNAUTÉ UNIVERSITÉ GRENOBLE ALPES**

Spécialité : **Physique Pour Les Sciences Du Vivant**

Arrêté ministériel : 7 août 2006


Présentée par

**Laura SCHAEDEL**

Thèse dirigée par **Manuel THERY**

préparée au sein du **Laboratoire de Physiologie Cellulaire et Végétale** dans **l'École Doctorale de Physique**


# Self-repair rejuvenates mechanically stressed microtubules

Thèse soutenue publiquement le **1 juillet 2016,** devant le jury composé de :

**Mr Bertrand FOURCADE**
Professeur, Laboratoire Interdisciplinaire de Physique, UGA Grenoble (Président)
**Mme Marileen DOGTEROM**
Professeur, Delft University of Technology – Netherlands (Rapporteur)
**Mr Denis CHRETIEN**
Directeur de Recherche, Université de Rennes 1 (Rapporteur)
**Mme Isabelle ARNAL**
Chargée de Recherche, Grenoble Institut des Neurosciences (Examinateur)
**Mr Gary BROUHARD**
Professeur, McGill University – Canada (Examinateur)
**Mr Igor KULIC**
Chargé de Recherche, Institut Charles Sadron Strasbourg (Examinateur)
**Mr Jean-Christophe GABRIEL**
Ingénieur Chercheur, CEA Grenoble (Examinateur)

# Contents

**List of Abbreviations** **1**

**1 Introduction** **3**

1.1 The eukaryotic cytoskeleton . . . . . 3

1.2 Microtubule networks in cells . . . . . 6

1.3 Microtubule structure . . . . . 9

1.4 The tubulin heterodimer is a GTPase . . . . . 12

1.5 Microtubule dynamics . . . . . 16

1.6 Microtubule mechanical properties . . . . . 23

1.7 Microtubule mechanics in cells . . . . . 26

1.7.1 Mechanical properties of cellular microtubules . . . . . 26

1.7.2 Forces on cellular microtubules . . . . . 27

1.8 Motivation . . . . . 33

**2 Results** **35**

2.1 Study 1. Schaedel *et al.*, Nature Materials, 2015 . . . . . 35

2.1.1 Introduction . . . . . 35

2.1.2 Conclusions and perspectives . . . . . 68

2.1.3 Limitations of the study . . . . . 73

2.2 Study 2. Aumeier / Schaedel *et al.*, Nature Cell Biology, 2016 . . . . 77

2.2.1 Introduction . . . . . 77

2.2.2 Conclusions and perspectives . . . . . 102

2.2.3 Limitations of the study . . . . . 106

**3 Conclusions and Perspectives** **108**

**A References** **112**

**B Summary** **132**

# List of Abbreviations

| | |
|---|---|
| +TIP | Microtubule plus end directed motor |
| AF | Actin filament |
| ATP | Adenosine triphosphate |
| BRB | Brinkley Reassembly Buffer |
| CLASP | CLIP-associating protein |
| CLIP | Cytoplasmic linker protein |
| $E$ | Young's modulus |
| EB3 | End binding protein 3 |
| F-actin | Filamentous actin |
| Gamma-TuRC | Gamma-tubulin ring complex |
| GDP | Guanosine diphosphate |
| GTP | Guanosine triphosphate |
| I | Moment of inertia |
| IF | Intermediate filament |
| $\kappa$ | Bending stiffness |
| $k_B$ | Boltzmann constant |
| $L$ | Length |
| $L_P$ | Persistence length |
| MACF | Microtubule-actin crosslinking factor |
| MAP | Microtubule Associated Protein |
| MT | Microtubule |
| MTOC | Microtubule-organizing center |
| PEG | Poly(ethylene)glycol |
| $t_{1/2}$ | half-life period |
| TIRFm | Total internal reflection fluorescence microscopy |

# 1 Introduction

## 1.1 The eukaryotic cytoskeleton

The eukaryotic cytoskeleton is essentially an intracellular biopolymer scaffold and it is, contrary to what its name may suggest, a highly dynamic system far from thermodynamic equilibrium. Yet it is well-ordered; the high degree of internal organization in cells is mostly due to the cytoskeleton (Huber *et al.*, 2013; Gupta *et al.*, 2015). Apart from spatially organizing cellular content, it also serves to connect the cell to the extracellular space, transports cargoes across the cell and generates forces that allow the cell to move and change shape (Fletcher and Mullins, 2010). The cytoskeletal organization is extremely variable from one cell to another and even, temporally and spatially, within the same cell, reflecting another important property: Fast adaptation to cellular needs, requiring rapid turnover and reorganization (Komarova *et al.*, 2002). The prize the cell pays to maintain an array that can rapidly adapt is energy in the form of adenosine triphosphate (ATP) or guanosine triphosphate (GTP); hydrolysis of these nucleotides is an exothermic process and the energy released can fuel fast cytoskeletal remodeling.

The cytoskeleton of eukaryotic cells consists of three classes of filaments: Actin filaments (AFs), microtubules (MTs) and intermediate filaments (IFs) (see Fig. 1), which are all fiber-like structures made of many individual building blocks (monomers or dimers). All three polymers grow and shrink by addition and subtraction of these building blocks. While actin filaments mostly appear in the form of cross-linked networks, microtubules are hollow polymer tubes that mostly appear as individual fibers or bundles (Fletcher and Mullins, 2010; Huber *et al.*, 2013). Intermediate filaments are more heterogeneous; there are several types made of different protein components (Wagner *et al.*, 2009).

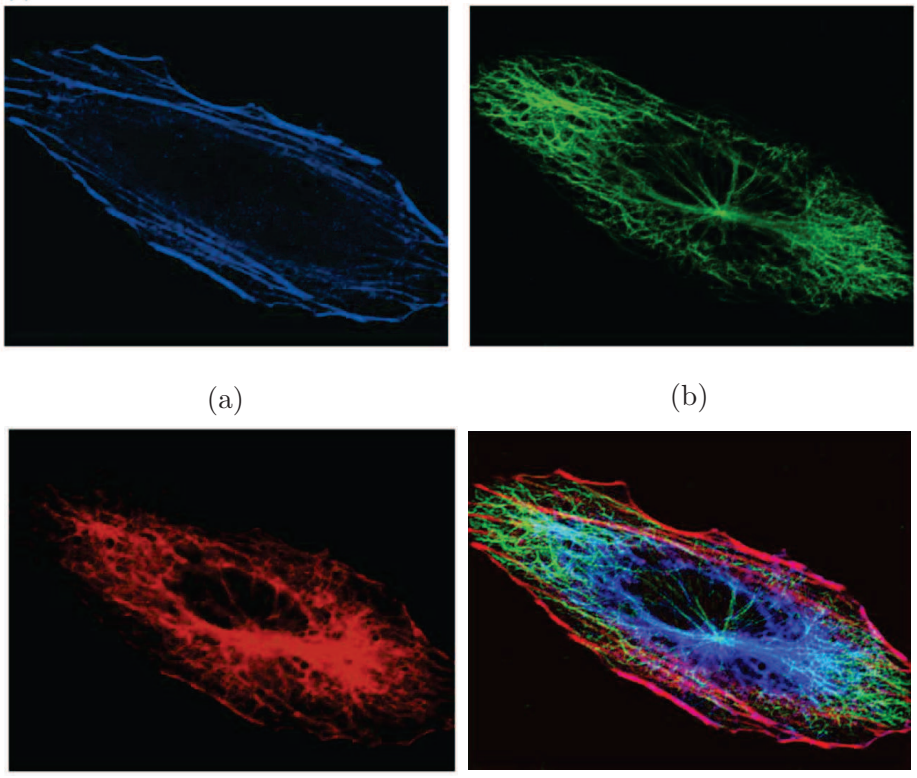


Figure 1: *Actin filaments (a), microtubules (b) and intermediate filaments (c) are the three major components of the cytoskeleton. The images show the organization of the different filaments in a Huh7 cultured human hepatocyte cell. (d) shows a superimposed image. (From Omary et al., 2006)*

A way to characterize the stiffness of cytoskeletal filaments is the persistence length. The persistence length $L_P$ is the length over which a (bio-)polymer bends significantly under thermal fluctuations (see Fig. 2), and can be defined as

$$\langle \boldsymbol{t}(0) \cdot \boldsymbol{t}(s) \rangle_t = e^{-s/L_P}$$

where $s$ is the distance between two points along the polymer, $\boldsymbol{t}(s)$ is the tangent vector to the curve at position s, and $\langle\rangle_t$ denotes the average over time (t) (Boal

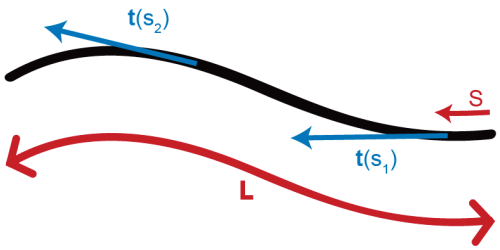


Figure 2: *The persistence length of a polymer is the characteristic distance over which the tangent vectors along the polymer become uncorrelated due to thermal fluctuations.*

2002; Martin 2013). The persistence length is related to the bending stiffness $\kappa$ by

$$L_P = \frac{\kappa}{k_B T} = \frac{EI}{k_B T}$$

where $k_B$ is the Boltzmann constant, $T$ the absolute temperature, $E$ the Young's modulus and $I$ the moment of inertia of the polymer.
The persistence length of microtubules is on the order of millimeters. As microtubule lengths $L$ in cells are typically on the order of micrometers and therefore $L << L_P$, microtubules are considered rigid on the scale of cells, contrary to the semi-flexible actin filaments and the flexible intermediate filaments (see Fig. 3).

Dynamics and organization of cytoskeletal filaments are not only determined by the inherent properties of their components, but also by interactions with associated proteins that can nucleate, sever, cross-link, weaken, strengthen, or transport filaments (Eriksson *et al.*, 2009; van der Vaart *et al.*, 2009; Roll-Mecak and McNaly, 2010; Su *et al.*, 2012; Huber *et al.*, 2013). Cytoskeletal components don't fulfill a single task, their multi-functionality is one of their fundamental properties. For instance, microtubules are essential for cell division, but also for intracellular transport and cell motility.

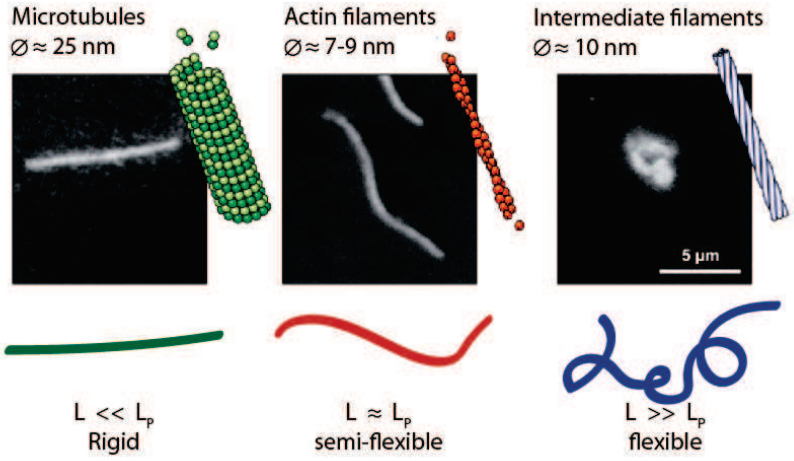


Figure 3: *Microtubules are rigid on cellular length scales, while actin filaments are semi-flexible and intermediate filaments are considered flexible. (Adapted from* `www.uni-leipzig.de/~pwm/web/?section=introduction&page=cytoskeleton` *)*

## 1.2 Microtubule networks in cells

In cells, microtubules fulfill a variety of tasks. They are implied in intracellular transport, cell migration and cell division and constitute in large part axons, cilia and flagella (Mimori-Kiyosue, 2011). Cellular microtubules are mostly nucleated and grow from microtubule-organizing centers (MTOCs). Examples of MTOCs are basal bodies, which are associated with cilia and flagella, and centrosomes, which are e.g. involved in chromosome segregation during cell division. Additionally, non-centrosomal nucleation is found in cells (Bartolini and Gundersen, 2006).

Microtubules in cells are several orders of magnitude longer than their diameter, and often span the intracellular space to be able to carry cargoes efficiently and drive changes in cell shape (Hawkins *et al.*, 2010). Yet they rapidly turn over, with a half-life period of $t_{1/2} \approx 10$ min (Gundersen and Bulinski, 1988). A subset of microtubules, however, is sometimes selectively stabilized, like during neuronal axon determination (Hammond *et al.*, 2010; Stiess *et al.*, 2010; Winans *et al.*, 2016) and at

the leading edge of migrating cells (Gundersen and Bulinski, 1988; Waterman-Storer and Salmon 1997; Wadsworth 1999). A way for the cell to tag a subpopulation of microtubules e.g. for stabilization is by post-translational modifications. Microtubule post-translational modifications are enzymatic modifications on the amino acids at various sites, including acetylation, glutamylation and detyrosination, which can occur both before and after polymerization (Gundersen and Bulinski, 1988; Song and Brady, 2015).

In addition, a variety of microtubule-associated proteins (MAPs) and microtubule plus-end tracking proteins (+TIPs) can influence microtubule dynamics and therefore control and actively remodel microtubule networks (Cassimeris 1993; Levy *et al.*, 2005; Vandecandelaere *et al.*, 1996). They can also slide, pull, anchor and guide microtubules, and, in this way, affect their organization in the cell (Mimori-Kiyosue 2011).

Microtubules interact with other cytoskeletal components by different means (see Fig. 4). Due to the dense packing of filaments e.g. at the periphery of the cell, where actin filaments form dense networks, steric interactions alone can lead to entanglement of microtubules and translocate them: Retrograde flow from the lamellum pushes on microtubules, making them move along with the filamentous actin (F-actin). F-actin bundles can also guide the growth of microtubules, which are often found to align with the bundles (Salmon *et al.*, 2002; Mandato and Bement 2003; Huber *et al.*, 2015). Additionally, there are specific proteins that mediate interactions between cytoskeletal filaments, like the cross linking of actin filaments and microtubules by MACF (Leung *et al.*, 1999, Sun *et al.*, 2001) and kinesin-mediated transport of intermediate filaments along microtubules (Prahlad *et al.*, 1998; Hermann and Aebi, 2000). Moreover, microtubules and actin filaments can influence each other's organization in a more indirect way, through biochemical signaling pathways (Waterman-Storer *et al.*, 1999; Zaoui *et al.*, 2008; Pertz 2010).

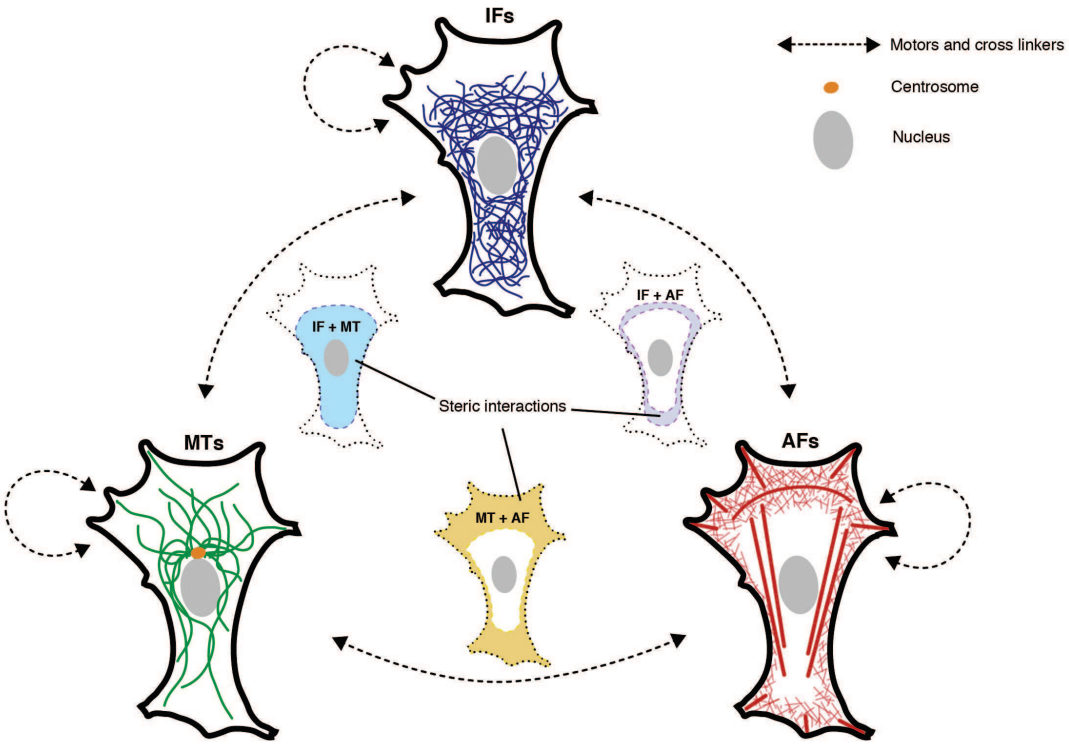


Figure 4: *Microtubules (MTs), intermediate filaments (Ifs) and actin filaments (Ifs) interact via different mechanisms with another: Unspecific, steric interactions occur in overlapping regions as well as crosslinking and motor protein mediated interactions. (Adapted from Huber et al., 2015)*

## 1.3 Microtubule structure

Microtubules are biopolymers made of tubulin heterodimers. Each dimer consists of two closely related 55 kDa globular proteins called alpha and beta tubulin. The dimers assemble longitudinally into so-called protofilaments, which form lateral bonds between each other and, in this way, arrange into a closed tube of approx. 25 nm outer diameter and 17 nm inner diameter (Desai and Mitchison, 1997, see Fig. 5a). Microtubules undergo assembly and disassembly by non-covalent addition and subtraction of tubulin dimers at the ends.

Bonds between protofilaments are anisotropic and three-dimensional (Nogales *et al*, 1999; Sui *et al.*, 2010; Huber *et al.*, 2013) and are either formed between equal subunits (alpha-alpha and beta-beta), yielding a B-lattice configuration, or between unequal subunits (alpha-beta), resulting in an A-lattice (see Fig. 5b). B-lattice configurations are by far more common *in vitro*, while *in vivo* A-lattice configurations can be observed in cilia, where microtubules with an A-lattice have a non-complete B-lattice microtubule attached to them (Amos and Klug, 1974). Axonemes *in vivo* also nucleate A-lattice microtubules (Scheele *et al.*, 1982). There is evidence that the configuration of the microtubule lattice influences microtubule stability (Katsuki *et al.*, 2014).

Energy values of lateral and longitudinal bonds between dimers have been estimated by simulations in silico or inferred from experiments by various groups; values vary from -3 kT to -15 kT for lateral bonds and -6 kT to - 20 kT for longitudinal bonds (VanBuren *et al.*, 2002; VanBuren *et al.*, 2005; Efremov *et al.*, 2007; Molodtsov *et al.*, 2005; Wu *et al.*, 2009; Wu *et al.*, 2012). Most groups found longitudinal bonds to be considerably stronger than lateral bonds. Lateral interactions are mediated by loop-loop interactions. Loops are rather disordered secondary protein structures, which in case of tubulin have been proposed to provide the necessary flexibility to accommodate different lateral bond angles (Sui and Downing, 2010; see Fig. 6).

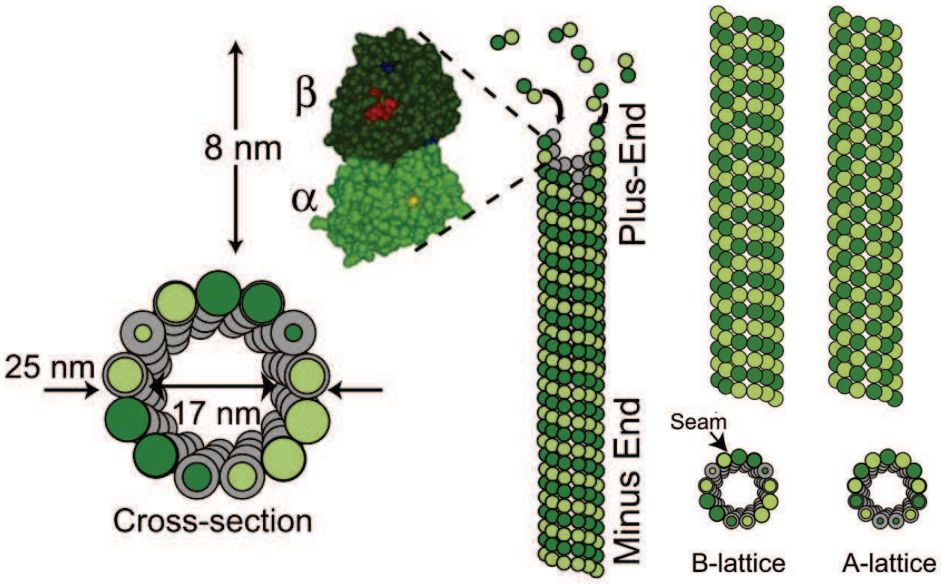


(a) (b)

Figure 5: *(a) Microtubules are made of tubulin dimers. Each dimer consists of two globular, structurally similar 55 kDa proteins, called alpha (light green) and beta (dark green) tubulin. Dimers associate longitudinally into protofilaments, which form lateral bonds and close into a hollow tube of 25 nm diameter. (b) In a B-lattice, lateral bonds are formed between equal subunits (alpha-alpha and beta-beta interactions). The helical staggering of dimers leads to a discontinuity called 'seam', where lateral bonds between alpha and beta subunits form. In an A-lattice, lateral interactions form exclusively between unequal subunits, and there is no seam. (From Hawkins et al., 2010)*

Cellular microtubules usually consist of 13 protofilaments (Ledbetter and Porter, 1964; Evans *et al.*, 1985), though protofilament numbers between 9 and 17 have been observed (Chrétien and Wade, 1991; McIntosh *et al.*, 2009). Indeed post-translational modifications such as acetylation (Cueva *et al.*, 2012) and drugs like taxol (Díaz *et al.*, 1998) are known to favor a specific protofilament number, respectively. Interestingly, the protofilament number can vary not only from one microtubule to another, but even along the length of the same microtubule, creating a protofilament mismatch (Chrétien *et al.*, 1992).

Neighboring protofilaments are staggered, yielding a helical arrangement of dimers in the microtubule lattice and establishing another important parameter to characterize the microtubule lattice: The so-called helix start number is defined as the number of monomers that the helix spans in each turn in the longitudinal direction. For an uneven helix start number and a B-lattice, a discontinuity is created where an alpha subunit interacts laterally with a beta subunit at the so-called seam, breaking the helical symmetry of the microtubule (see Fig. 5b). Even protofilament numbers on the other hand lead to helical symmetry, involving only alpha-alpha and beta-beta subunit interactions. Three- and four-start helices are most common (Sui and Downing, 2010). In all but the 13-3 lattice (13 protofilaments, three-start helix), protofilaments are slightly skewed, resulting in a super twist that is left-handed for 14-3 microtubules and right-handed for 11-3, 12-3, 15-4 and 16-4 microtubules (Wade *et al.*, 1990; Sui and Downing, 2010; see Fig. 6). The biological function of the seam is not yet clear; however, it has been proposed that it presents a weak structure in the microtubule (Sept *et al.*, 2003). Indeed microtubules with ectopic A-lattice seams polymerized *in vitro* are less stable than B-lattice microtubules (Katsuki *et al.*, 2014).

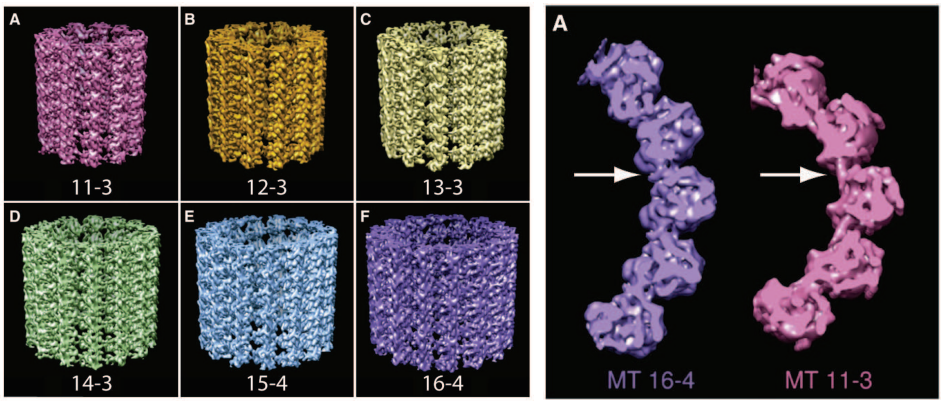


(a) (b)

Figure 6: *(a) Except for the 13-3 lattice configuration, the protofilaments exhibit a slight supertwist. (b) Lateral curvature of a 16 protofilament and an 11 protofilament lattice. The difference in curvature is thought to be accommodated by flexible lateral interactions. (From Sui and Downing, 2010)*

## 1.4 The tubulin heterodimer is a GTPase

Microtubule dynamics is powered by the energy released during GTP hydrolysis. Each alpha beta tubulin dimer binds two nucleotides (GTP or GDP), each one at the interface between two monomers, respectively, so that the nucleotide in one monomer interacts with the next monomer at the longitudinal interface (see Fig. 7). The nucleotide bound to alpha tubulin is buried at the intradimer interface (called N-site) and is therefore non-hydrolyzable and non-exchangeable (Nogales *et al.*, 1998). It has been proposed that it has a structural role (Menendez *et al.*, 1998). The nucleotide bound to beta tubulin on the other hand can be hydrolyzed and exchanged. It is located at the E-site of beta tubulin and it is exposed to the solvent at the microtubule plus end (Nogales *et al.*, 1998).

During microtubule growth, the incoming alpha tubulin interacts with the GTP binding site in the beta subunit, which is thought to contribute to GTP hydrolysis.

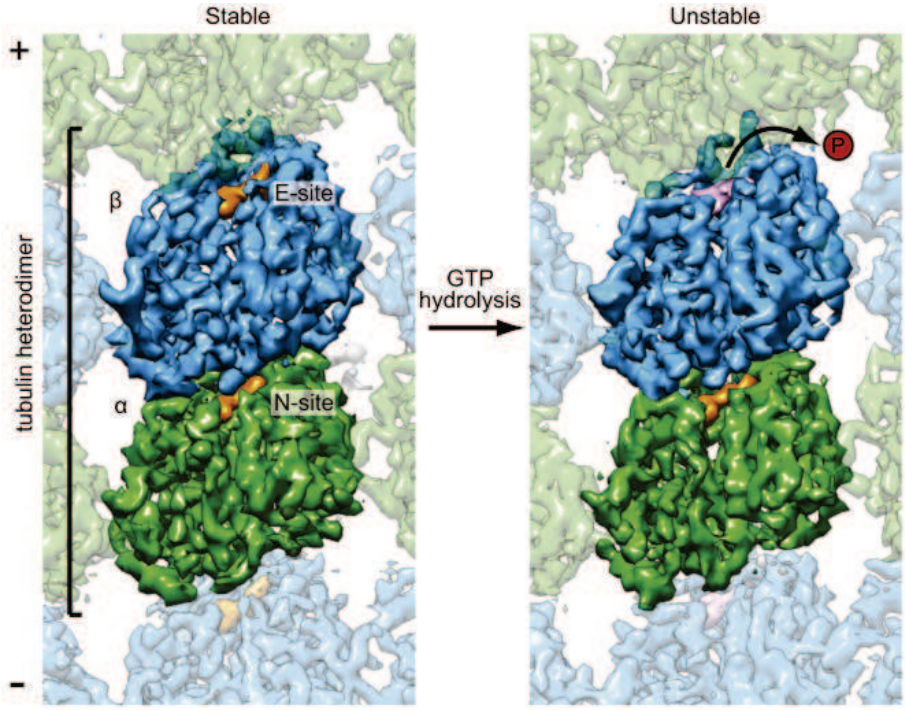


Figure 7: *Both alpha and beta tubulin have a GTP binding pocket, located at the longitudinal interface between neighboring subunits. The GTP bound to alpha tubulin is buried and non-exchangeable, whereas the GTP bound to beta tubulin is hydrolyzed to GDP as the dimer is incorporated into the microtubule. Upon hydrolysis, the dimer undergoes conformational changes and becomes more unstable in the lattice. (From Alushin et al., 2014)*

Therefore, the minus end of a tubulin subunit can be seen as GTPase activating protein (Choi *et al.*, 1998; Nogales *et al.*, 1998; Nogales *et al.*, 1999; Anders and Botstein, 2001). Hydrolysis of GTP bound to tubulin and subsequent phosphate release takes place after incorporation at a rate of about 0.25 $min^{-1}$ (Carlier *et al.*, 1981). At sufficiently high free GTP tubulin concentration, GTP hydrolysis is slower than the addition of new GTP tubulin at the growing end, creating a GTP tubulin cap (Carlier and Pantaloni 1981; Carlier *et al.*, 1987). After hydrolysis, the GDP nucleotide becomes locked in the E site until the dimer dissociates from the microtubule. Free tubulin dimers have a higher affinity for GTP than for GDP and therefore exchange hydrolyzed nucleotides rapidly.

For a long time free GTP tubulin dimers were thought to be straight, favoring their incorporation into the lattice, in contrast to free GDP tubulin dimers which where shown to be slightly curved (Kirschner *et al.*, 1974; Rice *et al.*, 2008). It was therefore hypothesized that hydrolysis of tubulin bound GTP is accompanied by a switch to a curved state. However, crystal structures of free GDP and GTP bound tubulin indicate that both GDP and GTP tubulin exhibit a similar intradimer curvature (Nawrotek *et al.*, 2011; Ayaz *et al.*, 2012; Pecqueur *et al.*, 2012) which is incompatible with the microtubule lattice, indicating that GTP tubulin dimers have to undergo conformational changes involving straightening upon incorporation into the lattice (Buey *et al.*, 2006; Rice *et al.*, 2008; Nawrotek *et al.*, 2011). Whether these conformational changes are strictly related to the nucleotide state of the dimer or whether they occur subsequently as a result of the interplay between the nucleotide state and the interactions with other dimers in the microtubule lattice is still under debate. However, it has been shown that GDP tubulin which is incorporated into the lattice changes microtubule dynamics compared to GTP tubulin that hydrolyses to become GDP tubulin after incorporation (Valiron *et al.*, 2010). In addition, Carlier *et al.* suggested that GTP hydrolysis is not strictly coupled to polymerization

and occurs in a subsequent step (Carlier *et al.*, 1981). How the hydrolysis rate is influenced by the conformational and nucleotide states of the neighboring dimers still has to be elucidated, but there is evidence that a coupled random model, where hydrolysis occurs randomly except for the terminal dimer which takes longer to hydrolyze due to lacking interactions with the GTP pocket at the E-site, is most likely (Bowne-Anderson *et al.*, 2013).

Upon hydrolysis, lattice bound tubulin dimers undergo structural changes involving a compaction of the interdimer interface, conformational changes especially in alpha tubulin and a weakening of the longitudinal bonds (Alushin *et al.*, 2014). Part of the energy released upon GTP hydrolysis is therefore used to deform the tubulin dimer, in a way that is believed to destabilize the dimer in the microtubule and induce mechanical stress while it is constrained by the lattice. Consequently, GDP tubulin is less tightly bound in the microtubule lattice; it easily falls off when it is not stabilized by more stably bound GTP tubulin dimers at the end of the microtubule. Microtubules made of GDP tubulin are therefore metastable structures; as soon as the protecting GTP tubulin cap is lost, depolymerization is initiated (Carlier *et al.*, 1987). The size of the GTP cap has been determined indirectly using EB1, a plus end tracking protein that seems to recognize the nucleotide state of lattice bound tubulin and to preferentially bind GTP tubulin (Zanic *et al.*, 2009). EB1 localizes to growing microtubule ends, and its signal decays exponentially with the distance from the tip (Bieling *et al.*, 2007). However, it doesn't reach the very tip of the microtubule (Maurer *et al.*, 2014). This suggests a 'patchwork' GTP cap that consists of dimers in different nucleotide and / or conformational states.

## 1.5 Microtubule dynamics

As longitudinal contacts between tubulin dimers occur between alpha and beta subunits, the resulting microtubule is polar: The end where beta tubulin is exposed tends to grow faster and is therefore called plus end, while the slower growing minus end exposes alpha tubulin. Microtubule polarity is used by plus and minus end directed molecular motor proteins for directional transport along microtubules.
In vitro, the rate-limiting step in microtubule polymerization is nucleation (see Fig. 8). Oligomerization of tubulin dimers is energetically unfavorable and therefore slow. Once a sufficiently large oligomer is formed, growth becomes favorable and faster. In the absence of co-factors, the critical tubulin concentration for spontaneous nucleation is 20 - 40 $\mu$M (Bré *et al.*, 1990; Kollman *et al.*, 2011; Wieczorek *et al.*, 2015). Cells therefore have nucleators like the gamma-tubulin ring complex (gamma-TuRC), which mimics the 13 protofilament architecture of the microtubule and accelerates nucleation.

Microtubule growth velocity depends on several factors, like free tubulin concentration, $Mg^{2+}$ concentration, pH, ionic strength (Olmsted and Borisy, 1975; Kuchnir Fygenson *et al.*, 1994) and microtubule associated proteins that assist polymerization (Akhmanova and Steinmetz, 2010). In general, for conditions used *in vitro*, microtubule growth rates are around a few $\mu$m/min and increase linearly with free tubulin concentration (Carlier *et al.*, 1987; Walker *et al.*, 1988; Kinoshita *et al.*, 2001). In vivo, growth rates are often substantially higher; They can range from 7 - 42 $\mu$m/min, depending on the cell type and the stage in the cell cycle (Cassimeris *et al.*, 1988; Kinoshita *et al.*, 2001; Piehl and Cassimeris, 2003; Srayko *et al.*, 2005; Komarova *et al.*, 2009). A possible explanation for the discrepancy in growth rates observed *in vivo* vs. *in vitro* are proteins that assist polymerization. For example, XMAP215 and EB1 have been shown to increase polymerization rates *in vitro* to physiological levels (Zanic *et al.*, 2013).

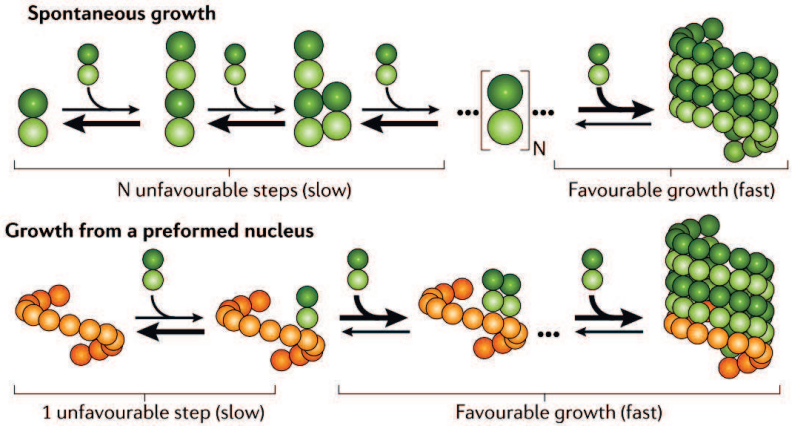


Figure 8: *Microtubule nucleation is a slow, energetically unfavorable process, but it can be accelerated considerably by the presence of a nucleus (e.g. a gamma-tubulin ring complex). (Adapted from Kollmann et al., 2011)*

During growth, some protofilaments are longer than others, creating differences in the number of lateral bonds (Chrétien *et al.*, 1995; Brouhard 2015); some protofilaments protrude up to 100-200 nm (Mandelkow *et al.*, 1991). It is therefore necessary to treat each protofilament separately to determine rate constants. In this '2D' model, GTP tubulin dimers are fast to bind to protofilament ends, with a rate constant of 4 $\mu\mathrm{M}^{-1}\mathrm{s}^{-1}$. However, they fall off rapidly if they are not stabilized by lateral bonds with other dimers. Each bond formed with neighboring dimers stabilizes the newly incorporated dimer a bit more (VanBuren *et al.*, 2005; Gardner *et al.*, 2011; Fig. 9).

The 2D model can explain some experimental observations like fluctuations in the growth dynamics of individual microtubules (Schek *et al.*, 2007). However, it fails to explain other phenomena, like the fact that paclitaxel, a drug known to stabilize interdimer bonds, slows down microtubule growth (Prota *et al.*, 2013; Zanic *et al.*, 2013). We lack taking into account intrinsic curvature of GTP tubulin and angles

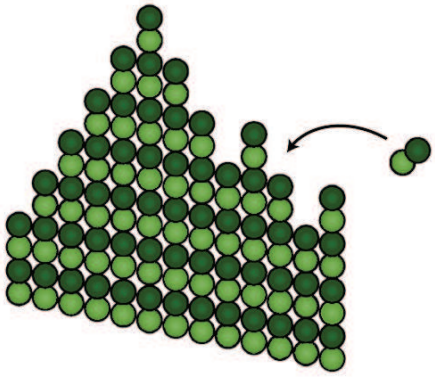

Figure 9: *According to the 2D model, tubulin dimers binding to the ends of protofilaments fall off rapidly unless they are stabilized by lateral bonds. (Adapted from Brouhard, 2015.)*

of alpha beta tubulin bonds (Brouhard 2015). Growing protofilaments are either straight or, especially when they extend far beyond others, slightly bent (0-5° per dimer); microtubule tips shift from a blunt to a more tapered appearance as the concentration of free tubulin increases (Chrétien *et al.*, 1995; see Fig. 10). Microtubules have been proposed to form sheets at growing ends which later close into tubes (Chrétien *et al.*; 1995); and a computational study proposed the existence of alternative lateral tubulin bonds during microtubule assembly that could explain the observation of sheet-like structures undergoing conformational changes to form a tube (Wu *et al.*, 2012). A pure chemical kinetics view of microtubule dynamic instability is therefore not sufficient; connecting mechanical and biochemical aspects seems a key to understand microtubule dynamics (Kueh and Mitchison, 2010).

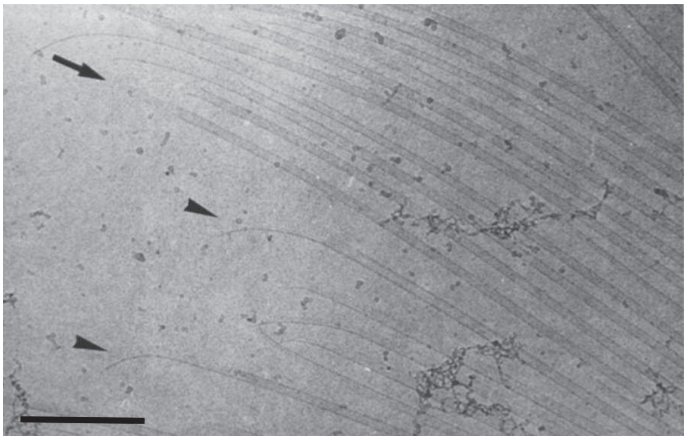

Figure 10: *Protofilaments at growing microtubule ends often look slightly curved. Microtubules have been proposed to form sheets which later close into tubes. Scale bar: 300 nm. (Adapted from Chrétien et al., 1995)*

Overall microtubule dynamic behavior is more complex than mere addition of subunits. Elongation phases are stochastically interrupted by sudden switches to depolymerization, called catastrophes. Depolymerizing microtubules on the other hand can switch back to growth by so-called rescue events. Together, these phenomena describe what is called 'dynamic instability' (see Fig. 11).

Catastrophes are thought to occur when the stabilizing GTP cap at the end of the microtubule is lost. Catastrophe frequency accordingly decreases with free tubulin concentration. It is generally higher for plus ends than for minus ends (Walker *et al.*, 1988). Interestingly, the probability that the plus end of a microtubule undergoes catastrophe increases with time, presumably because microtubule ends become more tapered and therefore more likely to switch to shrinking, a process called 'aging' (Gardner *et al.*, 2011; Coombes *et al.*, 2013). This shows that catastrophe of the plus end has to be viewed as a multistep process (Odde *et al.*, 1995).

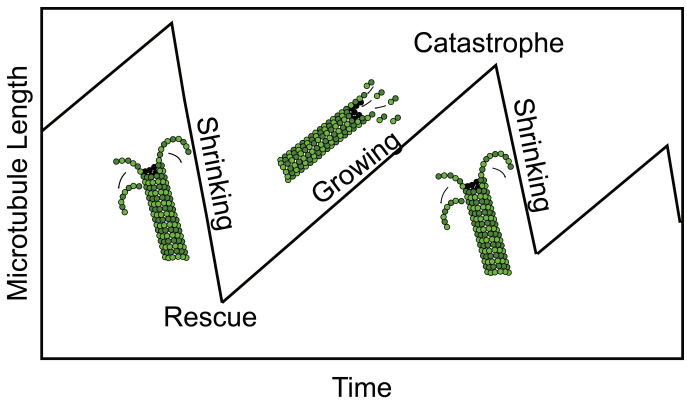


Figure 11: *Microtubule dynamic instability phases. (Adapted from Hawkins et al., 2010)*

Upon depolymerization, the elastic energy stored in the GDP tubulin dimers is released when the depolymerizing protofilaments break the lateral bonds between each other and curl into so-called ram's horns, with a curvature of around 12° per dimer (Chrétien *et al.*, 1995; see Fig. 12). Microtubules therefore can be used to do work not only during growth, but also during disassembly. Shortening rates *in vitro* are similar at the two ends and much faster than growth rates: They have been measured around 20 - 30 $\mu$m/min and are independent of the free tubulin concentration (Walker *et al.*, 1988; Kinoshita *et al.*, 2001).

Rescue is much less well understood than the other phases of dynamic instability (Brouhard 2015). It increases with free tubulin concentration, but it is much less sensitive to tubulin concentration than the catastrophe frequency, especially at the plus end which has a lower rescue frequency than the minus end (Walker *et al.*, 1988). This suggests that rescue is not a result of stochastic GTP-tubulin addition at the shrinking microtubule end, and that rather some features previously embedded in the lattice might disrupt depolymerization (Gardner *et al.*, 2013). Indeed, it has been suggested that non-hydrolyzed GTP-tubulin remnants in the lattice, so-called GTP islands, are responsible for microtubule rescue (Dimitrov *et al.*, 2008; see Fig. 13). How these islands are created and why they don't hydrolyze is, however, unknown.

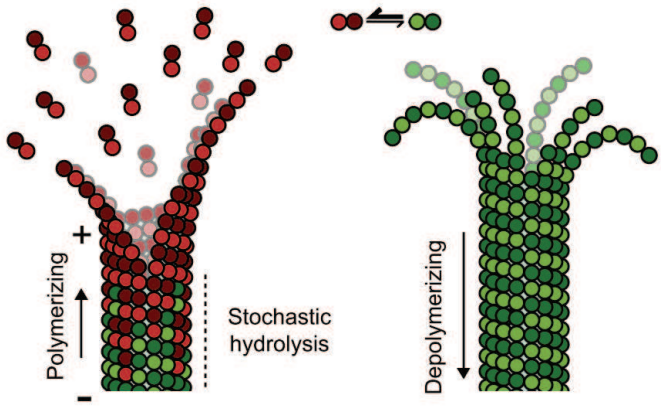


Figure 12: *Microtubule assembly and shrinkage. During microtubule growth, GTP tubulin dimers (red) add at the ends of protofilaments which slightly curve outward. Upon incorporation into the microtubule, the GTP is hydrolyzed (green), inducing mechanical stress in the lattice. The resulting metastable lattice that is stabilized by a cap of GTP tubulin dimers at the end of the microtubule. When the GTP cap is lost, the protofilaments curl outwards and the microtubule disassembles. (Adapted from Alushin et al., 2014)*

In vivo, linker proteins might locally promote rescue by halting depolymerization and assisting regrowth (Komarova *et al.*, 2002; Al-Bassam *et al.*, 2010).

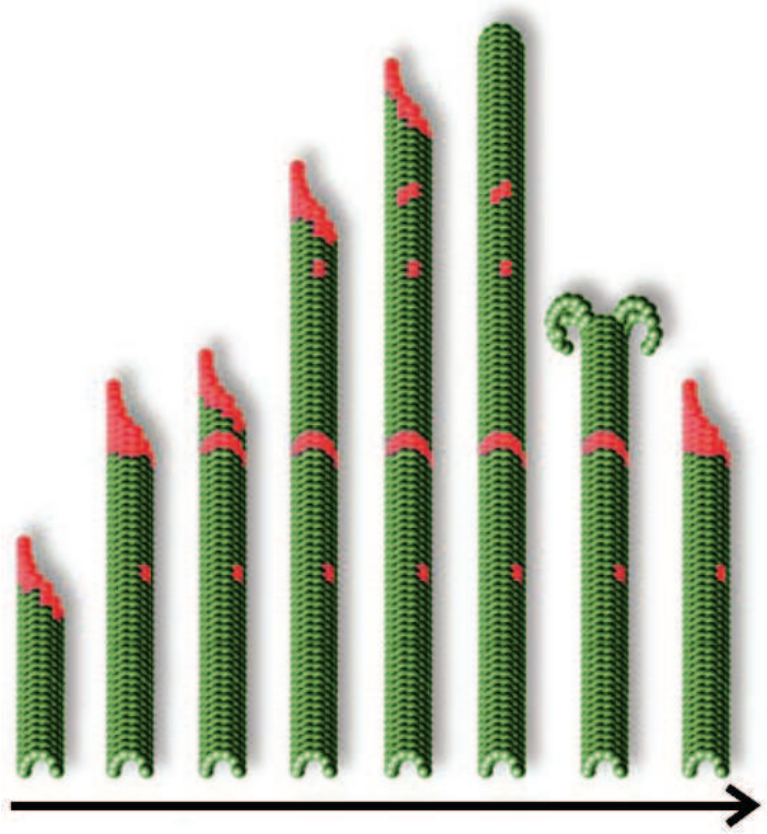

Figure 13: *GTP islands are hypothesized to be rescue sites. As a microtubule grows, islands of GTP tubulin are proposed to be excluded from hydrolysis. During depolymerization, the GTP remnants might stabilize the lattice, leading to regrowth of the microtubule. (Adapted from Dimitrov et al., 2008)*

## 1.6 Microtubule mechanical properties

Microtubules are very stiff biopolymers. Their flexural rigidity (or bending stiffness), defined as their resistance to bending, is comparable to carbon nanotubes (Hawkins *et al.*, 2010). If tubulin were a homogeneous and isotropic material, its Young's modulus would be around 1.2 GPa, similar to rigid plastic (Gittes *et al.*, 1993). However, due to the anisotropy of tubulin bonds, microtubules exhibit at the same time a high lateral deformability and a high longitudinal stiffness (Sui *et al*, 2010; Huber *et al.*, 2013). This property can be observed in other biological materials, such as bamboo and wood, which are also more rigid longitudinally in order to increase resistance to breaking by external forces (Hawkins *et al.*, 2010).
Due to difficulties to measure microtubule mechanical properties in living cells, most knowledge about microtubule mechanics comes from *in vitro* experiments. Many different groups measured *in vitro* microtubule bending stiffness with different techniques. Most techniques directly exert a force to measure microtubule stiffness, e.g. using flow, optical tweezers, atomic force microscopy or trajectories of microtubules transported by surface-attached kinesin molecules (Hawkins *et al.*, 2010; see Fig. 14). Thermal fluctuations are used as a passive way to probe microtubule stiffness, relying on slight bending induced by thermal energy only. Due to the inherent stiffness of microtubules, this approach is limited to long microtubules.

Surprisingly, the stiffness values found by the different groups vary substantially: Persistence length estimates range from 0.03 mm to 46.8 mm (Hawkins *et al.*, 2010). This variability is likely to reflect the influence of the measurement technique as well as the way microtubules are grown. Indeed mechanical properties of microtubules are influenced by a number of factors. For example, some neuronal MAPs are able to increase microtubule stiffness (Mickey and Howard 1995), while MAP65, which is associated to spindle formation and stabilization, promotes flexibility (Portran *et al.*, 2013). Taxol, a drug known to stabilize microtubules against depolymerization,

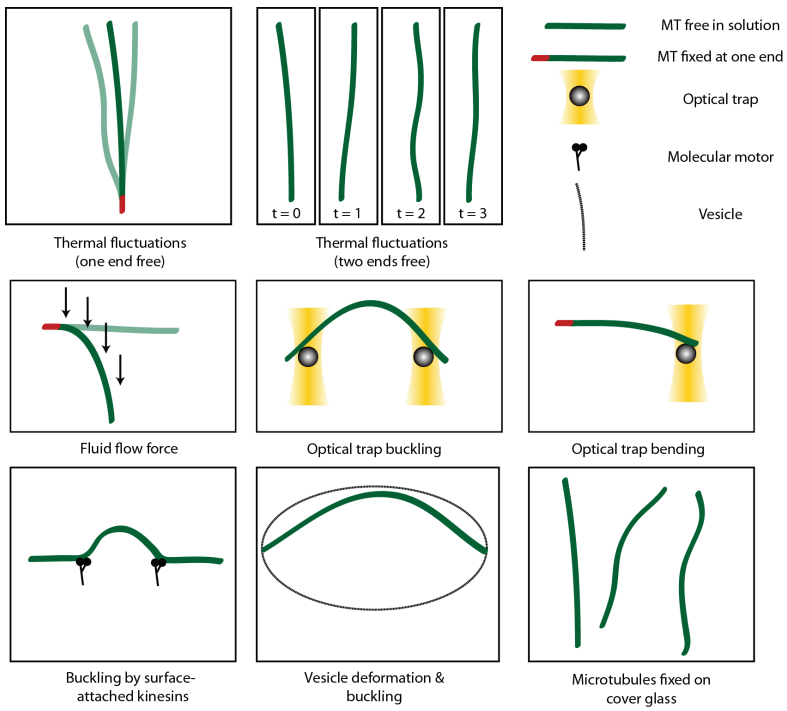


Figure 14: *Examples of microtubule persistence length measurement techniques.*

makes microtubules less rigid (Dye *et al.*, 1993). Even growth velocity has been shown to affect microtubule stiffness: Microtubules grown faster are more flexible, probably due to structural defects in the lattice which are more likely to occur during fast polymerization (Kurachi *et al.*, 1995; Janson and Dogterom 2004). These defects have been visualized with atomic force and electron microscopy, revealing different types of lattice irregularities: Protofilament mismatches, where a switch between different protofilament numbers occurs within a microtubule (Chrétien *et al.*, 1992; see Fig. 15a); missing tubulin dimers, corresponding to point defects in an otherwise perfect lattice, and separations between neighboring protofilaments (Schaap *et al.*, 2004; see Fig. 15b). The frequency of occurrence of these defects is largely unknown; only protofilament transitions have been characterized in this respect. Chrétien *et al.* showed that transitions occur with an average separation on the order of micrometers (Chrétien *et al.*, 1992).

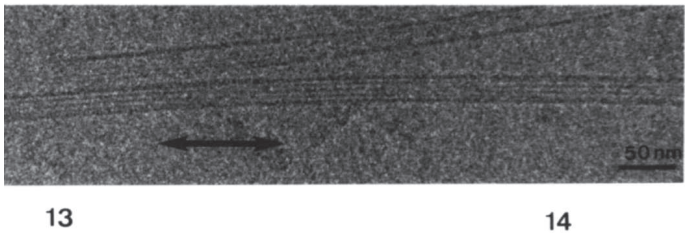


(a)

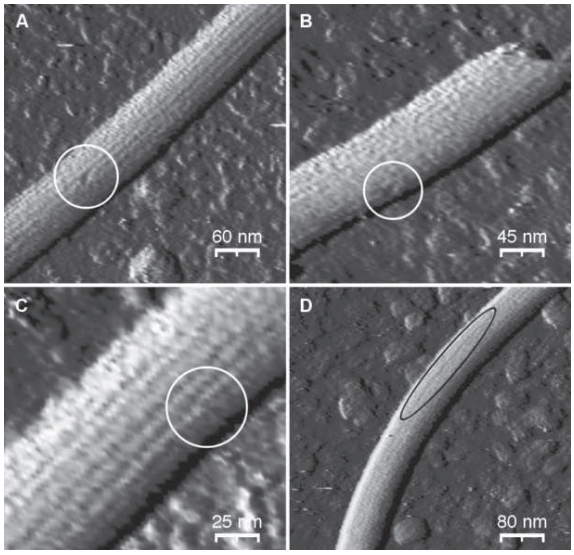


(b)

Figure 15: *Microtubule lattice defects. (a) Protofilament transitions, in this case a transition between 13 and 14 protofilaments indicated by the black arrow, can be observed in electron microscopy images. The number of protofilaments is inferred from characteristic contrast patterns. (From Chrétien et al., 1992) (b) Atomic force microscopy images of microtubules show point defects, with single missing tubulin dimers (A) and (B), lateral shifts in the lattice (C) and separations between protofilaments (D). (From Schaap et al., 2004)*

Interestingly, microtubules exhibit a length-dependent stiffness; short filaments are more flexible than longer ones (Pampaloni *et al.*, 2006; Taute *et al.*, 2008). The reason for this observation is not clear, but has been linked to the anisotropy of

tubulin bonds.

Microtubules can be laterally deformed, as shown by a study using a depletant to exert osmotic pressure (Needleman *et al.*, 2005), highlighting the flexibility of lateral bonds. Pointwise indentation with atomic force microscopy revealed that microtubules can deform elastically for up to 15% lateral deformation, before the lattice collapses (Schaap 2006). Taken together, these observations suggest that microtubules are inherently diverse and adaptable structures.

## 1.7 Microtubule mechanics in cells

### 1.7.1 Mechanical properties of cellular microtubules

In a living cell, unknown forces that vary temporarily and spatially throughout the cell make direct measurements of microtubule persistence length unaccessible. Different groups have studied cellular mechanics on the scale of entire cells, mostly describing them as a viscoelastic material (Haase *et al.*, 2015). However, as material properties are heterogeneous within a cell, it is difficult to deduce mechanical properties of single elements from observations of the overall response to a load. Therefore, to date, the only estimates of microtubule bending rigidity *in vivo* are derived from measurements of cellular structures mainly composed of microtubules, like cilia (e.g. Baba 1972). Information on microtubule mechanics *in vivo* is therefore sparse, and sometimes contradictory. For example, Battle *et al.* estimated the bending rigidity of microtubule doublets from the measured bending rigidity of entire cilia by bending them with an optical trap. They obtained a bending rigidity of $2\text{-}4{\cdot}10^{-24}$ $\mathrm{Nm}^2$, corresponding to a persistence length of approximately 0.5 - 1 mm (Battle *et al.*, 2015). However, they assumed weak coupling between the doublets to fit their data with *in vitro* estimations of microtubule rigidity, and simply treated the cilia as bundles of doublets where the total bundle rigidity equals the sum of the rigidities of the doublets. It is not clear whether this is a valid assumption;

there may be a moderate degree of coupling between doublets, which would mean that Battle *et al.* overestimated the rigidity of the doublets. Considering this, the stiffness values they obtained are surprisingly low compared to *in vitro* data.
Tolomeo *et al.* used a similar method to estimate single microtubule rigidity from pillar cells from the inner ear, where 1000-3000 microtubules grow in parallel and are linked by molecular crosslinkers. Tolomeo *et al.* inactivated the crosslinkers and estimated single microtubule bending rigidity to be around $7 \cdot 10^{-23}$ Nm$^2$ (corresponding to a persistence length of about 16 mm) - an order of magnitude higher than the result obtained by Battle *et al.* (Tolomeo *et al.*, 1997). The difference in the values obtained highlights the difficulty to extract reliable data on microtubule mechanics from *in vivo* data.

### 1.7.2 Forces on cellular microtubules

Microtubules produce forces which shape their environment *in vivo* and, at the same time, they experience forces which influence their behavior, leading to force-feedback and self-regulation. The forces exerted by - and on - microtubules can induce ordering of microtubules themselves and other cytoskeletal structures (Schaller *et al.*, 2010). Cells are densely packed: The total content of proteins, lipids and sugars amounts to up to 40 % of the total cytoplasmic volume (Fulton 1982). The mere presence of other proteins in the cytoplasm leads to molecular crowding which can induce microtubule bundling and change reaction kinetics (Ellis 2001; Hosek and Tang 2004).

Forces acting on microtubules *in vivo* often make them adopt highly bent or buckled shapes, with short wavelengths on the order of a few microns and curvatures well below 1 rad/$\mu$m (see Fig. 16). In addition, bent microtubule shapes appear dynamic and change on the order of seconds (Odde *et al.*, 1999; Brangwynne *et al.*,

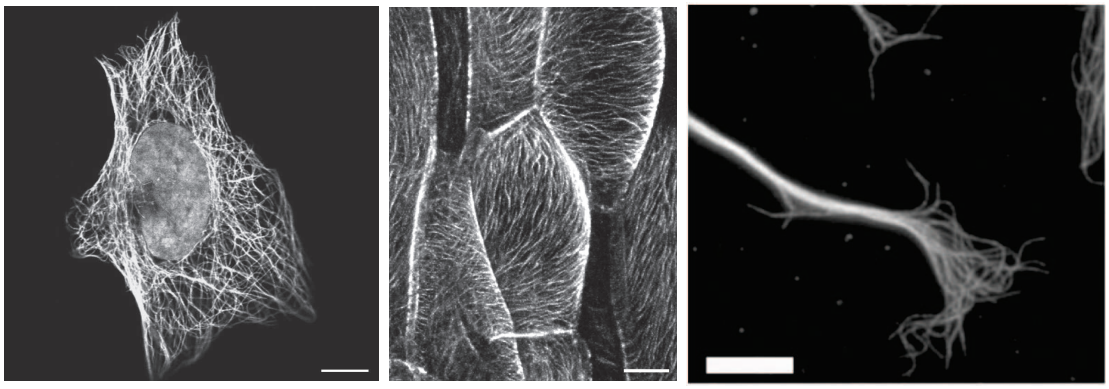

(a) (b) (c)

Figure 16: *Microtubules in different cell types. (a) Microtubules in human U-2 OS cells. Scale bar: 10 µm. (From* `http://www.proteinatlas.org/learn/dictionary/cell/cytoskeleton`*) (b) Microtubules in Arabidopsis hypocotyl cells. Scale bar: 10 µm. (From Lang et al., 2014) (c) Microtubules in cultured rat sympathetic neuronal growth cones. Scale bar: 6 µm. (From Jean et al., 2012)*

2006, 2007; see Fig. 17). During growth, the microtubule tips are often reoriented, leading to winding growth trajectories (Brangwynne *et al.*, 2007). This is in stark contrast to the straight, rigid appearance of unconstrained microtubule *in vitro*, and to the long-range, long-wavelength buckling behavior of microtubules buckling *in vitro* when growing against a rigid barrier (Dogterom and Yurke, 1997). The difference in buckling behavior has been attributed to the elastic network present in cells. A microtubule surrounded by an elastic cytoskeletal network has to displace the network upon buckling and is therefore constrained in its movement, which favors small wavelength buckling with high local curvature (Brangwynne *et al.*, 2006; see Fig. 18). The coupling of microtubules to an elastic network leads to a larger critical force for buckling: The minimum compressive force necessary to produce the observed shapes was estimated to be around 100 pN by Brangwynne *et al.*, who assumed microtubule stiffness in cells to be comparable to *in vitro* estimations.

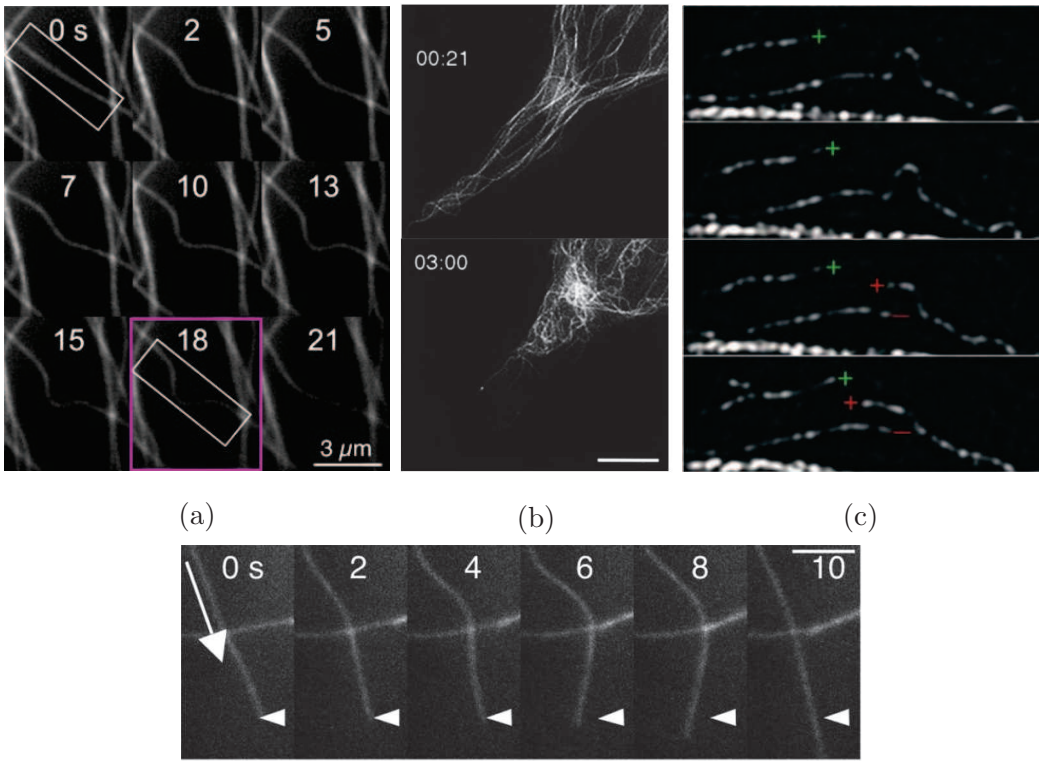


Figure 17: *Forces on cellular microtubules. (a) Some microtubules are observed to bend locally. (From Bicek et al., 2009) (b) Microtubule buckling in response to cell rounding. Scale bar: 10 µm. (From Heidemann et al., 1999) (c) Microtubule breaking in cells is often associated with high local curvature. (From Schaefer et al., 2002) (d) Microtubule transported along a second microtubule. Scale bar: 3 µm. (From Bicek et al., 2009)*

However, not all microtubules in the same cell are equally bent, even when they are close together: In cardiac myocytes, some microtubules buckle upon contraction, while other nearby microtubules stay straight, indicating that only some of the microtubules are actually coupled to elastic elements in the cell (Brangwynne *et al.*, 2006). In addition, in other cell types such as neurons, microtubules often grow as bundles where they are much less bent (Spedden *et al.*, 2012; see Fig. 16).
Sometimes, microtubules in cells are observed to break (Waterman-Storer and Salmon,

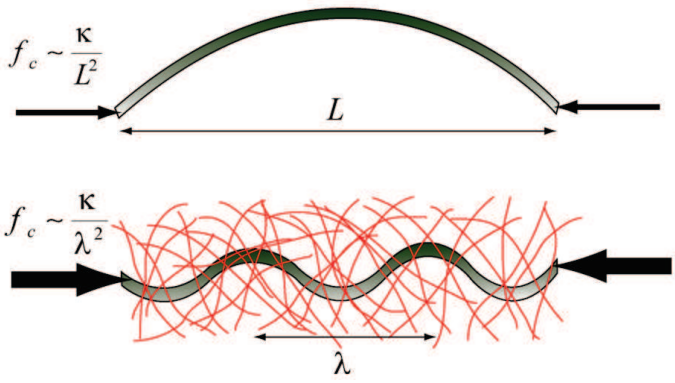


Figure 18: *Microtubule reinforcement by the surrounding elastic cytoskeletal network is thought to lead to an increased critical buckling force and short-wavelength, high-curvature buckling. Reinforcement might help microtubules bear compressive forces in cells. (From Brangwynne et al., 2006)*

1997; Odde *et al.*, 1999; Gupton *et al.*, 2002; see Fig. 17c); increased local microtubule curvature was shown to correlate with an increased probability of breaking (Odde *et al.*, 1999). Mostly however, microtubules are able to withstand even high curvatures without breaking.

Forces acting on or produced by microtubules in cells originate from different mechanisms. For example, assembly and disassembly are ways of direct force production by microtubules. In vitro, polymerizing microtubules can exert forces up to 4 pN when growing against barriers. At the same time, the opposing forces from the barriers decrease or stall polymerization (Dogterom and Yurke, 1997; Huber *et al.*, 2013). In cells, the actin cortex can be an effective barrier, as it is observed to be impenetrable for microtubules (Waterman-Storer and Salmon, 1997).
Depolymerizing microtubules can generate forces due to the energy stored from GTP hydrolysis in the lattice, as the outward curling protofilaments are no longer forced into a straight conformation by the constraints of the lattice. Forces produced during depolymerization can be ten times higher than the force generated by

a microtubule associated motor protein (Molodtsov *et al.*, 2005), and are important e.g. for chromosome segregation.

A key way of force production in cells is molecular motor activity. Three main types of motors are involved in cellular force generation: Kinesin, dynein and myosin. Cortical dynein, a microtubule associated motor protein, can capture microtubule ends at the cell periphery and pull on them, stabilizing them against depolymerization (Laan *et al.*, 2012). Microtubule associated motors can also transport microtubule segments towards stationary points ('pinning points'), and therefore transiently induce local bending until the pinning is released (Kent *et al.*, 2016). Teams of motors can exert forces up to 20 pN on microtubules (Hendricks *et al.*, 2012). Beside bending, motor proteins can also exert friction forces on microtubules: When kinesin-8, a processive plus end directed motor, is attached to a microtubule and is dragged by an optical trap, it exerts friction forces of several piconewtons on the microtubule (Bormuth *et al.*, 2009). Friction is also likely to occur between microtubules and other cellular components.
The cytoskeletal network in which microtubules are embedded is also known to exert forces on microtubules. For example, myosin II, an actin associated motor protein, can slide actin filaments against each other and thus generate contractile forces. Actin networks can push microtubules, or, when they act in an end-on fashion, lead to microtubule buckling (Wang *et al.*, 2001; Gupton *et al.*, 2002; Schaefer *et al.*, 2002). Even the polymerization of actin at the leading edge of a cell, not considering motor activity, can produce considerable forces that have been estimated to be on the order of nanonewtons per micron (Mogilner and Oster, 2003; Ananthakrishnan and Ehrlicher, 2007).

Due to the high degree of confinement in cells, fluctuations in microtubule shape caused by thermal forces have been discarded as a possible mechanism for microtubule bending. Yet, most groups found the distribution of local microtubule curvature to be thermal-like, leading to an apparent persistence length of about 20 $\mu$m (Brangwynne *et al.*, 2007; Pallavicini *et al.*, 2014). However, as this value is two orders of magnitude lower than what *in vitro* measurements suggest, it was concluded that microtubule bending in cells must be exclusively of non-thermal origin (Wang *et al.*, 2001; Brangwynne *et al.*, 2006). Still, as microtubule stiffness measurements *in vivo* are not accessible so far, thermal fluctuations might contribute to the bent shapes of microtubules in cells.

Apart from specialized microtubule structures such as cilia and flagella, the structural role of microtubules in cells is not yet entirely understood, as it is not clear to what degree microtubules contribute to cell mechanics. Lateral reinforcement might help microtubules to bear compressive loads and might help the cell to resist external forces, as proposed by Brangwynne *et al.*: An *in vitro* study showed increased stiffening of actin networks at high strains when even a low number of non-crosslinked is microtubules is present in the networks (Lin *et al.*, 2011). Microtubules have also been proposed to act as internal compression elements and balance prestress in the cell, counteracting e.g. actomyosin contraction and retaining bending energy (Buxbaum and Heidemann 1988; Wang *et al.*, 1993; Lin *et al.*, 2011). This would suggest that microtubule disruption in a surface adhered cell should cause a substantial part of the stress to be transmitted to the extracellular space. However, Wang *et al.* only observed a mean increase in traction of 13 % in human smooth muscle cells (Wang *et al.*, 2001); this seemingly contradicts the hypothesis of microtubules being a major element of balancing prestress.
In addition, AFM measurements of cell (visco-)elasticity performed by a substantial number of groups have shown a dominant effect of the actin cytoskeleton in different

cell types, whereas microtubules contribute much less to cell stiffness (Kirmizis and Logothetidis, 2010; Henderson *et al.*, 1992; Rotsch *et al.*, 1997; Wu *et al.*, 1998; Charras and Horton, 2002; Nawaz *et al.*, 2012; Haase *et al.*, 2015). Heidemann *et al.* concluded from their observations of microtubule buckling in cells (see Fig. 17b) that microtubules are too weak to resist large compressive forces and that microtubule buckling is a result of this weakness, rather than a consequence of large forces (Heidemann *et al.*, 1999). On the other hand, microtubules in neurons often grow as bundles and appear much less bent than in other cell types, and areas of high elastic modulus in the cell bodies of cortical neurons are associated with high microtubule density, rather than with F-actin (Spedden *et al.*, 2012).

## 1.8 Motivation

Overall, as explained in the previous chapters, microtubules in cells often appear surprisingly bent, which implies either the action of high forces, or an overestimation of microtubule stiffness. The apparently contradictory findings on the structural role of microtubules highlight the importance of estimating microtubule mechanical properties in a cellular context.

As a direct measurement of microtubule stiffness in cells is not accessible so far, a first step towards better understanding the structural role of microtubules is to assess their response to mechanical stimuli. So far, little is known about the impact of forces on microtubule mechanics. As a hint, an *in vitro* study on microtubules that are transported by surface-attached kinesins showed that protein friction between motors and microtubules can lead to loss of tubulin dimers at the microtubule ends, indicating molecular wear (Dumont *et al.*, 2015). What the consequences for microtubule structure and behavior might be, and if bending might lead to a similar response and has an impact on microtubule mechanics, still remain open questions.

In this thesis, the effect of mechanical stress, specifically of bending forces, on microtubule mechanics is studied. Three different possibilities are considered: Either microtubules indeed act as rigid structures, as suggested by stiffness measurements *in vitro*, and are unaffected by mechanical stress - in this case, bending would lead to a purely elastic response. This would confirm the role of microtubules as major load-bearing elements in the cell. Another possibility is that microtubules are affected by forces and experience material fatigue and, as a consequence, 'wear out' when repeatedly exposed to mechanical stress until they break or are deformed permanently. Thirdly, microtubules might be affected by forces and experience fatigue, but they might recover due to a 'repair' mechanism. In this case, it would be interesting to know how efficient and fast the repair is, what it requires and what other consequences it may have for microtubule behavior, in cells as well as *in vitro*.
Whichever of these possibilities is true, it will increase our understanding of the physical basis of microtubule mechanics in a context that is highly relevant for various cellular functions.

# 2 Results

## 2.1 Study 1. Schaedel *et al.*, Nature Materials, 2015

### 2.1.1 Introduction

As explained in the introductory chapters, microtubules in cells are continuously exposed to external forces. Bending has been identified as a major source of mechanical stress, and it is observed to vary considerably on the order of seconds in many cell types. To date it is not clear how repeated mechanical stress affects microtubule mechanics, *in vitro* as well as *in vivo*. Yet, mechanical properties of microtubules are important for cells, as many cellular functions depend on microtubule integrity. Considering the highly curved shapes that microtubules often adopt in cells on the one hand and their stiffness measured in *in vitro* experiments on the other hand, it is surprising that microtubules are rarely observed to break. Due to the difficulty to measure mechanical properties of microtubules in living cells, *in vitro* approaches offer a way to shed some light on this issue. The aim of this study was therefore to develop an *in vitro* setup to expose microtubules to well-defined, repeated bending stress and observe how this affects their mechanical properties.

To this end, it was necessary to exert forces on microtubules that could be precisely controlled on short time scales and to measure microtubule mechanical properties with the same setup. In the past, calibrated flow has often been used to determine microtubule bending rigidity *in vitro* (Hawkins *et al.*, 2010). At the same time, this technique provides a way to exert forces on microtubules. Specifically, microfluidic systems offer an excellent approach to exert well-defined forces on microtubules in the form of hydrodynamic bending stress, while also allowing fast exchange of the surrounding medium during an experiment. For this reason, and as basic microfluidic tools were available in the laboratory, microtubule bending by fluid flow using

a custom-made microfluidic device was chosen as a method to tackle the task.
The system developed by Portran *et al.* provided a good basis as it combined controlled grafting of microtubules at one end on an otherwise non-adhesive surface that minimized friction ('micropatterning') with bending induced by fluid flow (Portran *et al.* (*MBoC*), 2013). However, the system did not allow good control of flow velocities and repeated, reproducible bending of the same microtubule within short time scales was not possible. Therefore, a microfluidic setup was developed that permitted better flow control and that could be combined with the micropatterning technique developed by Portran *et al.* (Portran *et al.* (*Cytoskeleton*), 2013).

The microfluidic chip needed to allow grafting of microtubules on micropatterns on the one hand, and fluid flow perpendicularly to microtubules to induce bending on the other hand. It was therefore designed to consist of a central chamber with two inlet channels that are perpendicular to each other (see Fig. 19a). Liquid exited the chip through two outlet channels that are also perpendicular to each other and could be opened and closed as and when required. One inlet channel was used to graft short, pre-polymerized microtubule seeds, from which dynamic microtubules were grown. The advantage of using dynamic microtubules was that by avoiding stabilizing agents, important properties like the nucleotide state and bond energies were left unaltered, increasing the relevance of the results. The second inlet channel was used to deform microtubules by applying a fluid flow. Flow was controlled with a microfluidic pump that allowed good temporal control of flow velocities (see Fig. 19b).
A challenging task was to obtain reliable estimations of absolute persistence lengths. Microtubule persistence length was calculated from their bent shapes under flow and from the flow velocity. Flow velocity was estimated using fluorescent beads, whose displacement in the solution was monitored. However, the flow velocity that microtubules experienced did not correspond to the velocity of the beads, since the beads

were located further away from the surface than the microtubules. Boundary effects were likely to reduce flow velocity close to the surface. For this reason, microtubule persistence length was first calculated from thermal fluctuations, using the method described by Gittes *et al.* (Gittes *et al.*, 1993). The values obtained were then used to correct for the discrepancy in actual and measured flow velocity, by applying the same correcting factor to all measurements.

Overall, the microfluidic setup was used to study the effect of repeated bending stress on microtubule persistence length under various conditions.

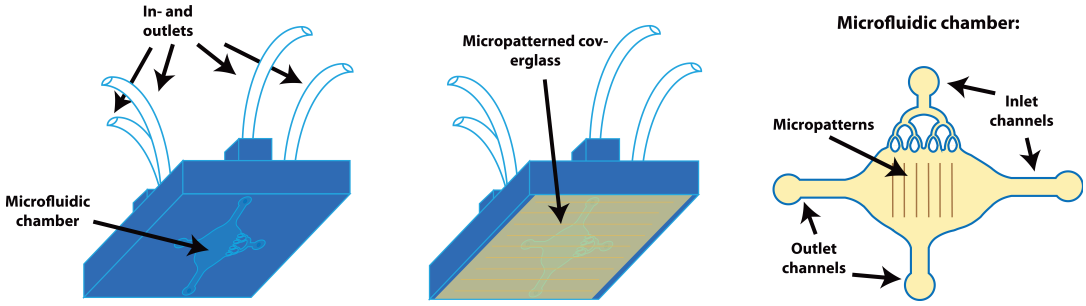


(a)

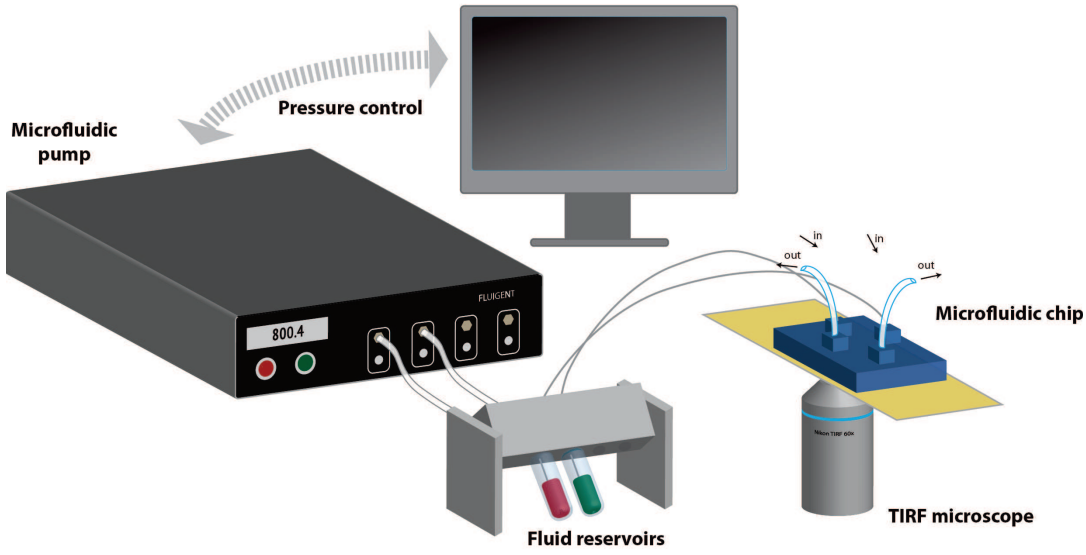


(b)

Figure 19: *Illustration of the microfluidic device. (a) A micropatterned coverglass is attached to the microfluidic chip. Microtubules are grafted on the coverglass. (b) A microfluidic pump allows precise flow control inside the chip.*

ARTICLES
PUBLISHED ONLINE: 7 SEPTEMBER 2015 | DOI: 10.1038/NMAT4396
nature materials

# Microtubules self-repair in response to mechanical stress

Laura Schaedel[1], Karin John[2], Jérémie Gaillard[1], Maxence V. Nachury[3], Laurent Blanchoin[1]* and Manuel Théry[1,4]*

**Microtubules—which define the shape of axons, cilia and flagella, and provide tracks for intracellular transport—can be highly bent by intracellular forces, and microtubule structure and stiffness are thought to be affected by physical constraints. Yet how microtubules tolerate the vast forces exerted on them remains unknown. Here, by using a microfluidic device, we show that microtubule stiffness decreases incrementally with each cycle of bending and release. Similar to other cases of material fatigue, the concentration of mechanical stresses on pre-existing defects in the microtubule lattice is responsible for the generation of more extensive damage, which further decreases microtubule stiffness. Strikingly, damaged microtubules were able to incorporate new tubulin dimers into their lattice and recover their initial stiffness. Our findings demonstrate that microtubules are ductile materials with self-healing properties, that their dynamics does not exclusively occur at their ends, and that their lattice plasticity enables the microtubules' adaptation to mechanical stresses.**

Microtubules are dynamic polymers that span the intracellular space. The self-organization of microtubule arrays defines the shape of axons, cilia, flagella and centrioles, as well as the structure of mitotic spindles and of intracellular transport networks[1]. Therefore, the growth dynamics and mechanical properties of microtubules, which determine network architecture, are central to cell physiology. The dynamics of microtubule growth has been exhaustively investigated and is now fairly well described[2,3] relative to microtubules mechanical properties, which are poorly understood despite their critical role in the regulation of microtubule network geometry[4–7].

The large and hollow cross-section of a microtubule's tubular shape confers it a high bending stiffness[8]. Microtubule persistence lengths—of a few millimetres—surpass by several orders of magnitude the stiffness of other cytoskeleton polymers[7,9]. The regular lattice of adjacent protofilaments has been an inspiring structure and the subject of various physical models of microtubule mechanics. Cracks, defects and holes in the lattice, as well as breathing or sliding of adjacent protofilaments, have all been proposed to modulate microtubule mechanical properties[8,10–17]. *In vivo*, microtubules are submitted to various types of external forces; produced by fluid flow in the case of cilia and flagella, or by molecular motors and deformation of other cytoskeleton networks in the cytoplasm[18–24]. Microtubules can move, bend or break in response to those constraints[25,26]. Yet, it is at present not known how microtubules respond to the vast forces exerted on them and if cracks and defects actually modulate this response.

Optical tweezers and fluid flow have been used to bend microtubules and estimate microtubule stiffness[7,27]. They revealed key microtubule features such as stiffness–length dependency and the softening effect of microtubule-stabilizing drugs[28,29]. However, investigations into the mechanical properties of dynamic microtubules in response to external forces are in urgent need of a new method that does not sacrifice throughput for accuracy and is compatible with high-quality imaging. Here we developed a device that can be used to apply controlled hydrodynamic constraints on arrays of dynamic microtubules and monitor their deformation.

## Microtubules soften under mechanical stress

To study the effect of mechanical stress on microtubules, we attached microtubule seeds onto micropatterns[30], grew dynamic microtubules and applied a calibrated (and locally quantifiable) flow orthogonal to the microtubule axis using microfluidics (Fig. 1a). When subjected to a transient hydrodynamic flow, microtubules bent and recovered their original straight shape with no apparent hysteresis (that is, microtubules demonstrated elastic deformation, Supplementary Movie 1 and Fig. 1b). Surprisingly, repeated bending cycles using identical flow revealed that microtubules bent further with each cycle. The maximal deflection increased incrementally with each mechanical cycle (Supplementary Movie 2 and Fig. 2a,b), suggesting that microtubules became softer—that is, exhibited material fatigue—under repeated mechanical stress. Microtubule persistence length, a direct correlate of microtubule stiffness, can be inferred from the microtubule shape and the velocity of the fluid exerting the hydrodynamic force on the microtubule[29] (see Methods). Although the initial persistence length varied from 2 to 4 mm, the majority of microtubules (60%, $n = 15$), which were assembled in the presence of 20 μM of tubulin, exhibited a progressive reduction of stiffness cycle after cycle (Fig. 2c). On average, those microtubules became twice as soft as their initial state after six bending cycles.

## Lattice defects promote microtubule softening

Material fatigue of highly ordered polymers and crystal-like structures is known to stem from pre-existing structural defects that concentrate stresses and spread into more extensive damage[31].

[1]Laboratoire de Physiologie Cellulaire et Végétale, Institut de Recherche en Technologie et Science pour le Vivant, UMR5168, CEA/INRA/CNRS/UGA, 38054 Grenoble, France. [2]Laboratoire Interdisciplinaire de Physique, CNRS/UGA Grenoble, 140 Rue de la Physique BP 87, 38402 Saint-Martin-d'Hères, France. [3]Department of Molecular and Cellular Physiology, Stanford University School of Medicine, California 94305, USA. [4]Unité de Thérapie Cellulaire, Hôpital Saint Louis, Institut Universitaire d'Hematologie, UMRS1160, INSERM/AP-HP/Université Paris Diderot, 75010 Paris, France.
*e-mail: laurent.blanchoin@cea.fr; manuel.thery@cea.fr

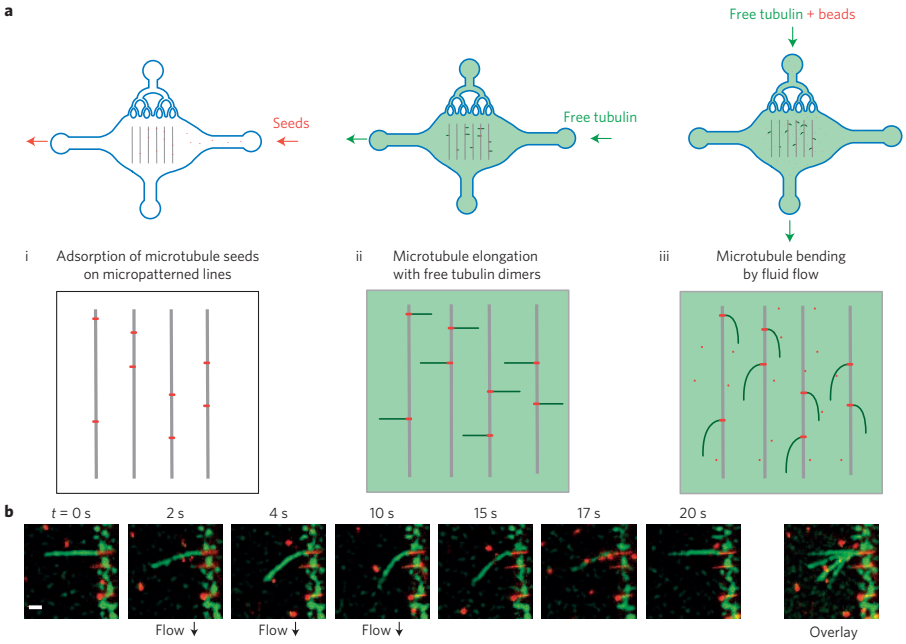


**Figure 1 | Microtubule bending device. a**, Illustration of the work flow. Red fluorescent microtubule seeds (short red lines) were flowed into the microfluidic device and grafted on micropatterned lines (grey lines) (step i). Free green fluorescent tubulin dimers were then added onto the seeds to grow microtubules (green lines) (step ii). The same mix was then flowed normal to the microtubules and used as a hydrodynamic constraint to bend microtubules (step iii). Red fluorescent beads were added to the mix to measure fluid flow next to microtubules. **b**, Time-lapse sequence of microtubule (green) bending in response to fluid flow. Scale bar is 3 μm. Overlay of images during the bending steps conveniently shows the magnitude of microtubule deformation (far right).

Pre-existing structural defects in the microtubules lattice, such as lack of dimers, abrupt variations of protofilament number, or of helix start number have been reported[32,33]. By altering the regularity of the lattice, defects introduce areas of weakness that concentrate stresses and undergo local protofilament disorganization and partial lattice disassembly. We use the term 'defect' to refer to initial lattice imperfections and the term 'damage' to refer to the lattice disorganization and destruction that results from stress accumulation on defects. Defects in the microtubule lattice have already been suggested as altering the mechanical properties, but this hypothesis remains untested[8,11,13,14]. Consistently, rapidly polymerized microtubules harbour a greater frequency of defects and tend to exhibit lower stiffness[32,34]. We confirmed that rapidly assembled microtubules are softer than slowly assembled microtubules (Fig. 2d). To test whether the amount of pre-existing defects is responsible for microtubule softening through the generation of more extensive damage, we subjected microtubules assembled at various speeds to repeated bending cycles. It emerged that the magnitude of microtubule fatigue in response to cyclic stress was indeed larger in rapidly assembled microtubules (Fig. 2e). All microtubules assembled at the highest tested concentration of free tubulin (26 μM) exhibited material fatigue, whereas softening was undetectable for microtubules assembled at the lowest concentration (14 μM; Fig. 2f and Supplementary Fig. 1). These results demonstrate that stress alone is not sufficient to fatigue microtubules and suggest that pre-existing lattice defects may be responsible for this mechanical property. Notably, highly curved microtubules in cells have long puzzled investigators considering the intrinsic stiffness of pure microtubules. Although microtubule curvature in cells may result from the large forces exerted by actin network contraction[35], the microtubule fatigue we describe here suggests that repeated mechanical constraints may soften microtubules in cells.

## Softened microtubules can self-repair

Some structures made of long-lived microtubules in sensory organelles, such as sensory cilia or axons, maintain their mechanical properties despite being continuously subjected to external constraints[24,36]. This raises the possibility that mechanisms may protect long-lived microtubules from material fatigue or allow them to recover from the effect of injurious bending. We tested this hypothesis by letting microtubules recover for long periods of time between the bending cycles (Fig. 3a). Microtubules were assembled at 20 μM of free tubulin. As the duration of the rest period increased from 10 to 100 s, the proportion of microtubules affected by fatigue was progressively reduced (Supplementary Fig. 2). Remarkably, when microtubules remained at rest for 100 s between the bending cycles, microtubule stiffness was unchanged from one cycle to another (Fig. 3b–c). Because microtubules were subjected to the same bending forces in all recovery experiments, the absence of softening when resting time is increased to 100 s suggests that microtubules underwent repair between the bending cycles. To further test whether microtubules recover their mechanical properties after being damaged, we induce softening with five rapid bending cycles followed by a 100 s rest (Fig. 3d). The majority of microtubules that had softened during the five bending cycles exhibited a significant stiffness increase during the rest period. Also, for most of the microtubules that did not soften, stiffness did

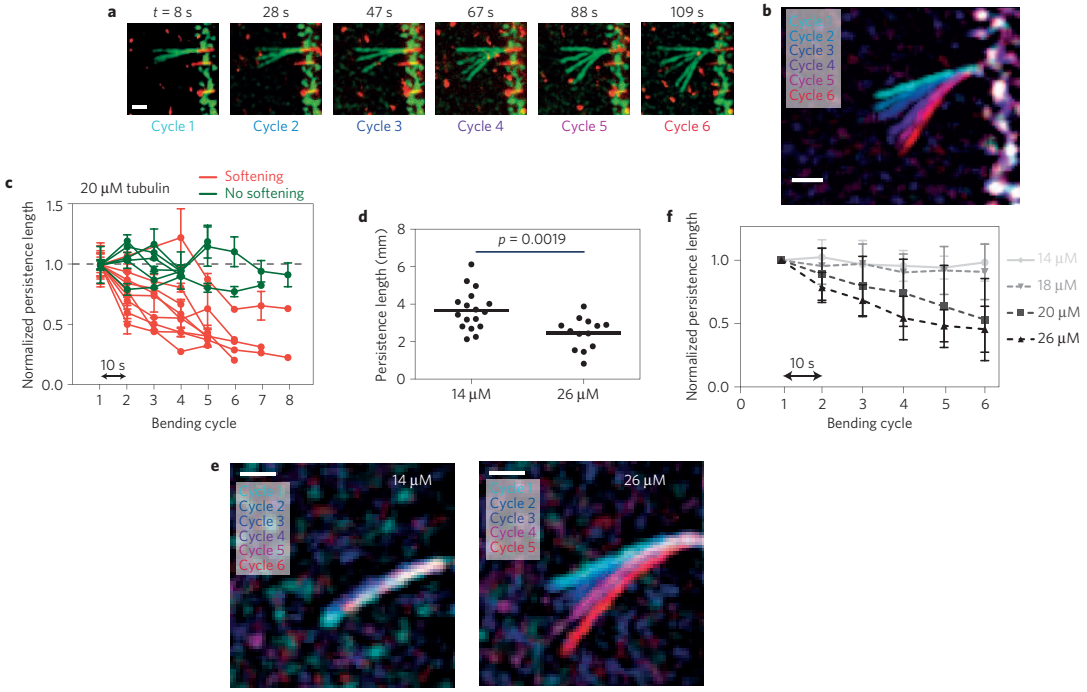


**Figure 2 | Microtubule softening on external constraint. a**, Sequence of bending cycles. Images show the overlay of microtubule deformations during each successive bending cycle. Bending flows were applied for a duration of 10 s, with a pause of 10 s between bending steps. Deformations appeared larger cycle after cycle. Scale bar is 3 µm. **b**, Overlay of microtubule maximal deformation during each bending cycle. Distinct colours have been attributed to each cycle. Scale bar is 3 µm. **c**, Measurements of microtubule persistence length evolution over the successive bending cycles. Delay between cycles was 10 s. Microtubule persistence lengths were normalized to their initial value. Error bars correspond to the standard deviation calculated from five consecutive frames for each cycle. As a test of tendency, Spearman correlation tests for persistence length values over the successive cycles were performed. Green curves show microtubules for which the persistence length was not significantly affected over the bending cycles, whereas red curves show those that had been softened during the cyclic stress. **d**, Comparison of initial microtubule persistence length for microtubules assembled in the presence of 14 µM or 26 µM of free tubulin dimers. Values were compared with an unpaired *t*-test (two-tailed). **e**, Overlay of microtubule maximal deformation during bending cycles for microtubules assembled in the presence of 14 µM or 26 µM of free tubulin dimers. **f**, Measurements of microtubule persistence length evolution over successive bending cycles for microtubules assembled in the presence of various concentration of free tubulin dimers (26 µM: $n=9$; 20 µM: $n=15$; 18 µM: $n=15$; 14 µM: $n=13$). Microtubule persistence lengths were normalized to their initial values. Values correspond to the average persistence length of individual measurements shown in Supplementary Fig. 1. Error bars show the standard deviation between distinct microtubule bending experiments. All curves were considered significantly different using a two-way ANOVA test, except for 14 and 18 µM. A *t*-test on the average persistence length showed all these differences became significant at the fourth bending cycle.

not increase during the rest period. These findings demonstrate that damaged microtubules have the ability to recover their stiffness through self-repair.

## Microtubules have self-healing properties

We propose two hypotheses for the recovery of mechanical properties during the pauses: incorporation of new tubulin to patch damage in the lattice and lateral realignment of protofilaments that underwent sliding or separation. In the former hypothesis, stiffness recovery should involve the incorporation of new dimers in the lattice. To test the possibility that tubulin incorporation can actually heal microtubules, we generated large, but locally and temporally controlled, structural damage to microtubules with laser pulses (Supplementary Movie 3 and Supplementary Fig. 4). To visualize possible tubulin incorporation into the microtubule lattice, red microtubules were bathed in a solution of green tubulin and damaged by laser pulses. On switching the solution back to red tubulin, it was apparent that the green tubulin had become incorporated not only at the end but also at the impact site on the red microtubule (Supplementary Movie 4 and Fig. 4a). This suggests that microtubule lattice repair can take place and be directly visualized in the case of large damage.

Incorporation of tubulin along the microtubule length has previously been hypothesized[37]. Stabilized, end-to-end annealed axonemes were shown to adopt curved shapes on removal of free tubulin dimers in solution and to resume their original straight shapes on dimer addition. This suggested that microtubule shape recovery depended on intra-lattice dimer incorporation[37]. To test whether bent microtubules heal by local incorporation of tubulin at areas of high stress, we subjected red-labelled microtubules to five bending cycles with prolonged recovery periods in the presence of green-labelled tubulin (Fig. 4b). Concentrates of green fluorescence were found along the red microtubules (Supplementary Movie 5 and Fig. 4c,d) in more than 80% ($n=24$) of microtubules that had been repeatedly bent. Green fluorescence peaks 1.5–4 times higher than the adjacent background were found in line scans (Fig. 4e and

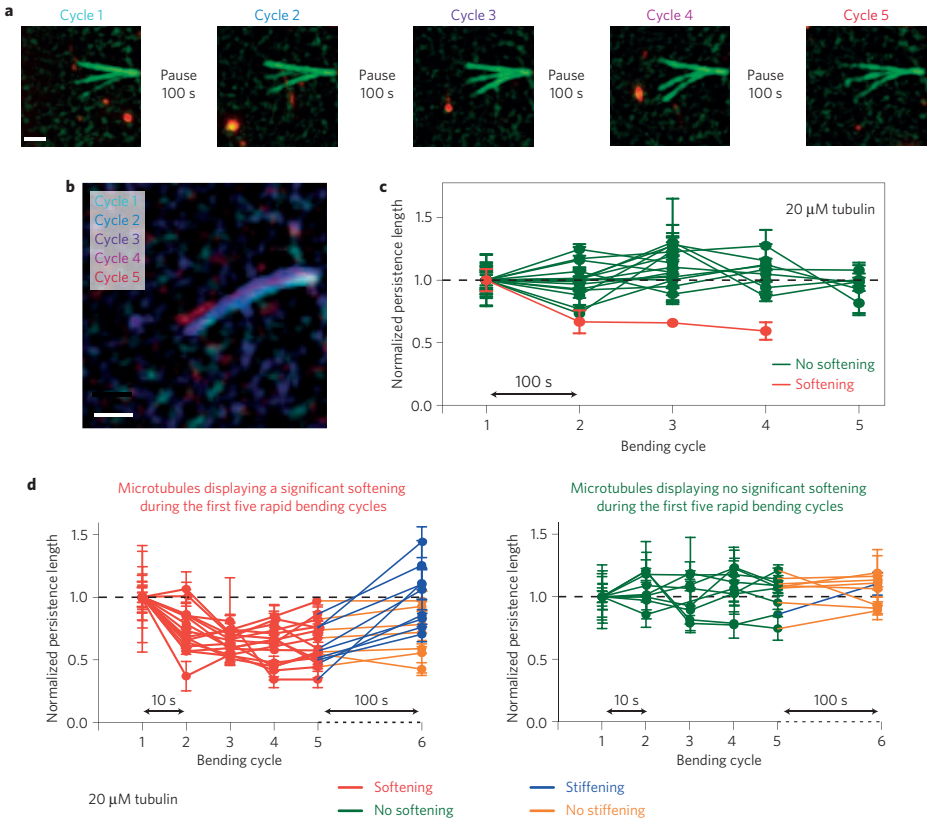


**Figure 3 | Microtubule mechanical recovery. a**, Sequence of bending cycles. Images show the overlay of microtubule deformations during each successive cycle. Bending flows were applied for a duration of 10 s, with a pause of 100 s between bending steps. Deformations appeared similar for all cycles. Scale bar is 3 µm. **b**, Overlay of microtubule maximal deformation during each bending cycle. Distinct colours have been attributed to each bending cycle. Scale bar is 3 µm. **c**, Measurements of microtubule persistence length evolution over the successive bending cycles. Delay between bending cycles was 100 s. Error bars correspond to the standard deviation calculated from five consecutive frames for each bending cycle. As a test of tendency, Spearman correlation tests for persistence length values over the successive cycles were performed. Green curves show microtubules for which the final persistence length was not significantly different from their initial one, whereas red curves show those that had been softened during the cyclic stress. **d**, Evolution of microtubule persistence length following five rapid bending cycles. The delay between the first five bending cycles was 10 s. To distinguish softening from non-softening microtubules, we used the distance between the minimum normalized persistence length and the persistence length during the first cycle (=1) as a parameter for a *k*-means clustering. The clustering algorithm found one group with a low distance, which corresponds to non-softening microtubules (shown on the left graph), and another group with a high distance, corresponding to softening microtubules (shown on the right graph). The recovery after a 100 s pause time was assessed by comparing the persistence length before and after the pause with a Wilcoxon matched-pairs test. Microtubules exhibiting significant recovery are shown in blue, the others are shown in orange.

Supplementary Fig. 5). The appearance of new tubulin along the microtubule length takes place preferentially in the proximal and most curved half of the microtubule (Fig. 4f), thus suggesting that the areas subjected to the greatest local stress underwent damage that was repaired by local tubulin incorporation. Furthermore, we detected no incorporation of green-labelled tubulin into red-labelled microtubules subjected to a longitudinal—rather than orthogonal—flow (Fig. 4g–j and Supplementary Movie 6 and Supplementary Fig. 6). In addition, slowly assembled microtubules (with 14 µM tubulin) that did not exhibit material fatigue (Fig. 2e) also failed to incorporate new tubulin into their lattice under repeated cycles of bending (Supplementary Fig. 7). Thus, free tubulin dimers incorporate systematically along the sidewall of microtubules, recovering their stiffness after having been damaged by external forces, but they do not incorporate in microtubules in which stiffness is unchanged (whether they had been bent or not). Therefore tubulin dimer incorporation along the lattice seems to be a key correlate of microtubule stiffness recovery.

Intriguingly, curvature seems to vary smoothly along the length of the bent microtubule even though the size of the tubulin incorporation area—that is, the repaired area—is rather limited (green fluorescent sites were 1.2 µm ± 1 µm long ($n = 26$)). Local damage should intuitively lead to localized kinks rather than homogeneous global deformation. As we could not measure experimentally the size of the softened regions, which seems to differ from the size of the repair region, we developed a method to estimate it by comparing the experimental deformation we measured to that of numerical microtubules of a known stiffness

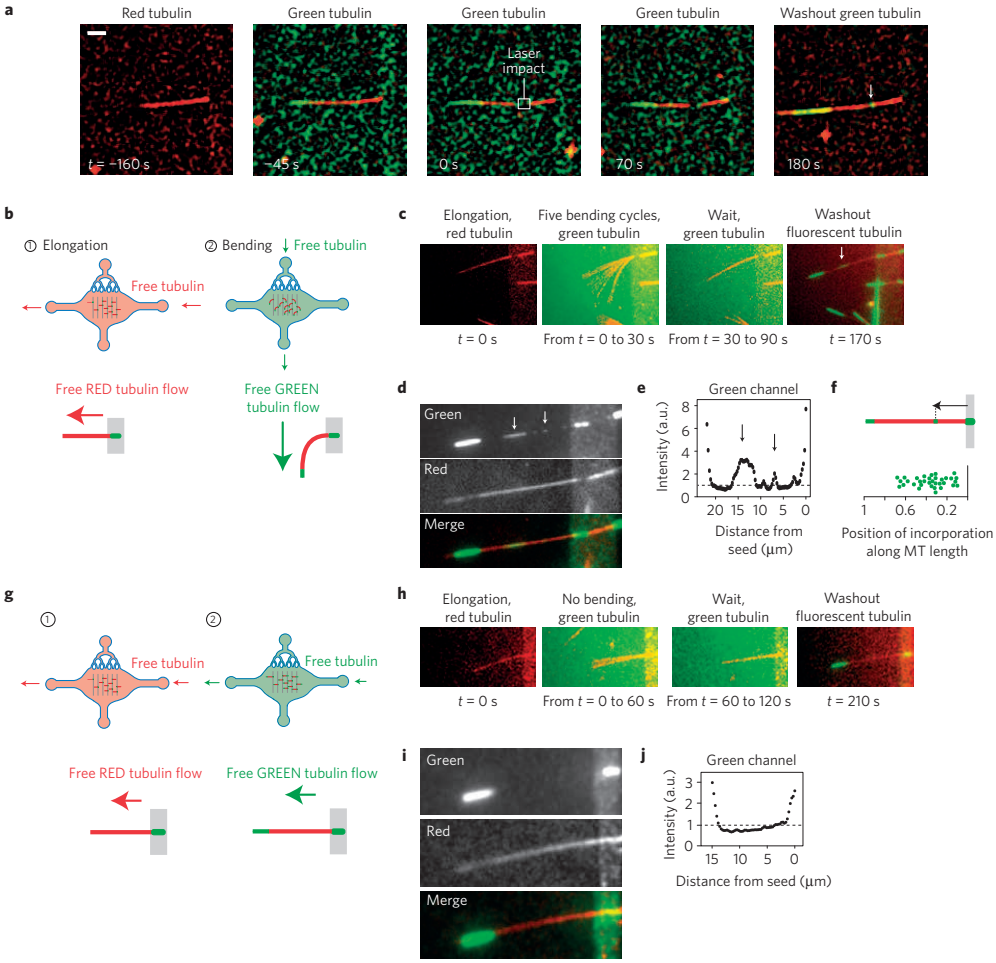


**Figure 4 | Microtubule self-healing. a**, Image sequence showing a microtubule assembled with red tubulin ($t = -160$ s), bathed in a solution of green tubulin ($t = -45$ s), damaged (but not cut) with laser pulses ($t = 0$) and left in the presence of green tubulin for 70 s. Green tubulin was then washed away and replaced by red tubulin. Removal of the green fluorescent background revealed incorporation of tubulin dimers at the damaged site (arrow). Scale bar is 5 μm. **b**, Experimental procedure to grow microtubules with red tubulin and bend them in the presence of green tubulin. **c**, Image sequence showing from left to right: a red microtubule, the overlay of five bending cycles in the presence of green tubulin, the 1-min-long pause, followed by the green tubulin washout revealing incorporation of tubulin dimers along the microtubule length (arrow). **d**, Averages of 30 images taken successively in the red and green channels at the end of the image sequence shown in **c** to improve the signal-to-noise ratio. Stretches of green tubulin along the red lattice become more visible (arrows). **e**, Green fluorescence intensity linescan along the microtubule length on the image shown in **d**. Arrows correspond to incorporation sites between the microtubule seed (right peak) and the growing end (left peak). **f**, Measurement of external tubulin incorporation site positions along the microtubule length. Distances were normalized with respect to the microtubule length. **g**, Experimental procedure to grow microtubules with red tubulin and flow green tubulin along their length without bending them. **h**, Image sequence showing from left to right: a red microtubule, the overlay of pictures taken during green tubulin flow along the microtubule length, the 1-min-long pause, followed by the green tubulin washout revealing the absence of incorporation of tubulin dimers along the microtubule length. **i**, Averages of 30 images taken successively in the red and green channels at the end of the image sequence shown in **h** to improve the signal-to-noise ratio. No stretch of green tubulin could be detected along the red lattice. **j**, Green fluorescence intensity linescan along the microtubule length on the image shown in **i**. Fluorescence linescans showed no fluorescence peak between the microtubule seed (right peak) and the growing end (left peak).

profile. We performed numerical simulations in which softening was limited to segments of defined length (Fig. 5a and Methods). In our simulations, both the width and the degree of local softening contributed to the deformation and the apparent average stiffness of the entire microtubule (Fig. 5b and Supplementary Fig. 8). Then, to characterize microtubule deviation from homogeneous deformation, we measured the distance $\omega$ between experimentally bent microtubules and numerical microtubules of constant stiffness showing similar deformation (Fig. 5c). Large distances corresponded to microtubules showing local kinks, whereas short

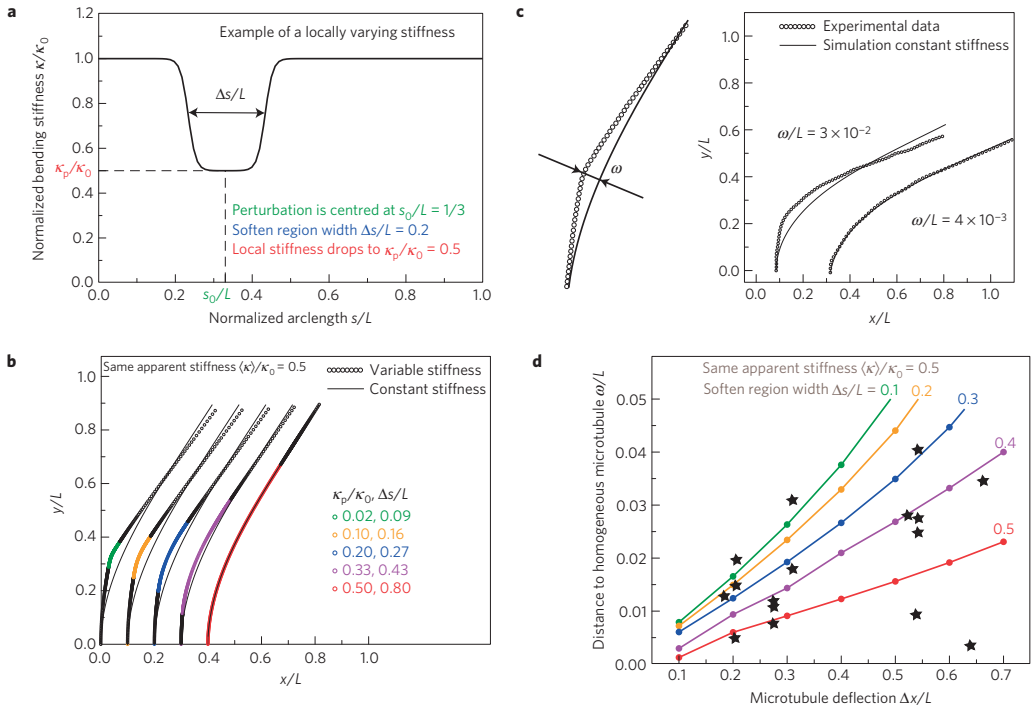


**Figure 5 | Numerical simulations of microtubule deformation in response to local or global stiffness reduction. a**, Graph representing the parameters used for the simulation. Microtubules had a length $L$ and a bending stiffness $\kappa_0$. Their stiffness was locally reduced to $\kappa_p/\kappa_0$ over a normalized length $\Delta s/L$ positioned at the arc length $s_0/L$. In this example, as well as in all simulations, $s_0/L = 0.33$. **b**, Examples of microtubule equilibrium shapes in response to distinct combinations of local softening parameters ($\kappa_p/\kappa_0$ and $\Delta s/L$) leading to the same apparent bending stiffness ($\langle\kappa\rangle/\kappa_0 = 0.5$). Also shown are the fits against a model with the constant stiffness 0.5 (full lines). **c**, Measurement of the distance $\omega/L$ between the shapes of experimental microtubules to shapes of microtubules with a constant rigidity, as explained in Methods. Two examples illustrate a high and low distance, suggestive of local and global softening processes, respectively. **d**, Comparison of distances to homogeneous microtubules between experimental observations and simulated microtubules. Coloured lines show the theoretical dependence of the distance $\omega/L$ on the microtubule deflection $\Delta x/L$ for different extents of the softened region $\Delta s/L$ (different colours) and the same given apparent stiffness $\langle\kappa\rangle/\kappa_0 = 0.5$. Stars correspond to experimental measurements of the distance $\omega/L$ and the deflection $\Delta x/L$ for different microtubules. Only values obtained from microtubules with an apparent stiffness between 0.4 and 0.6 after five bending cycles are shown.

distances corresponded to a more homogeneous deformation. We compared experimental values against those of numerically simulated microtubules with a variety of rigidity profiles but similar apparent stiffness (see Methods and Fig. 5d). Some experimental data points were close to numerical simulations of microtubules with small softened regions ($\Delta s/L = 0.1$), but others were closer to simulations of microtubules with long softened regions ($\Delta s/L = 0.5$). This showed that, in our experiments, the bending-induced damage was not always highly localized but often extended over a large portion of the microtubule. Thus, the two working hypotheses we formulated for microtubule repair—namely, local structure healing by incorporation of free dimers and lattice rearrangement over long distances—are both compatible with our experimental observations.

Here we report the softening and self-healing of microtubules in response to mechanical constraints. Although softening following repeated constraints, or fatigue, is common to all materials, self-healing is much less frequent[38,39] and appears here as the remarkable natural feature of a biological polymer. Defects in the microtubule lattice, such as variations of protofilament number[32,33], are likely to play a central role in microtubule fatigue and self-healing, because in the absence of defects microtubules deformed elastically with no fatigue and no repair (Fig. 2f and Supplementary Fig. 7). Exactly how the accumulation of stress at lattice defects alters microtubule architecture and bending stiffness remains a key question. Our data suggest that two processes may operate: a local disassembly spreading from the pre-existing defect (Fig. 4) and a long-range disorganization of the microtubule lattice (Fig. 5). We speculate that structural defects may initiate lattice disorganization by allowing a higher degree of freedom to adjacent protofilaments (Fig. 6). Protofilaments adjacent to the defect have fewer lateral interactions and are thus easier to separate, making their deformation less constrained (Fig. 6b). This favours the propagation of cracks in the lattice as well as protofilament rupture and disassembly (Fig. 6c). These effects contribute to global and local microtubule softening. They can be further amplified in repeated bending sequences, generating microtubule fatigue (Fig. 6c). As the microtubule recovers its original straight shape, owing to the remaining stiffness of the intact protofilaments, separated protofilaments spontaneously realign and progressively re-establish lateral interactions (Fig. 6d). Meanwhile, free tubulin in the medium binds to the newly generated protofilament ends

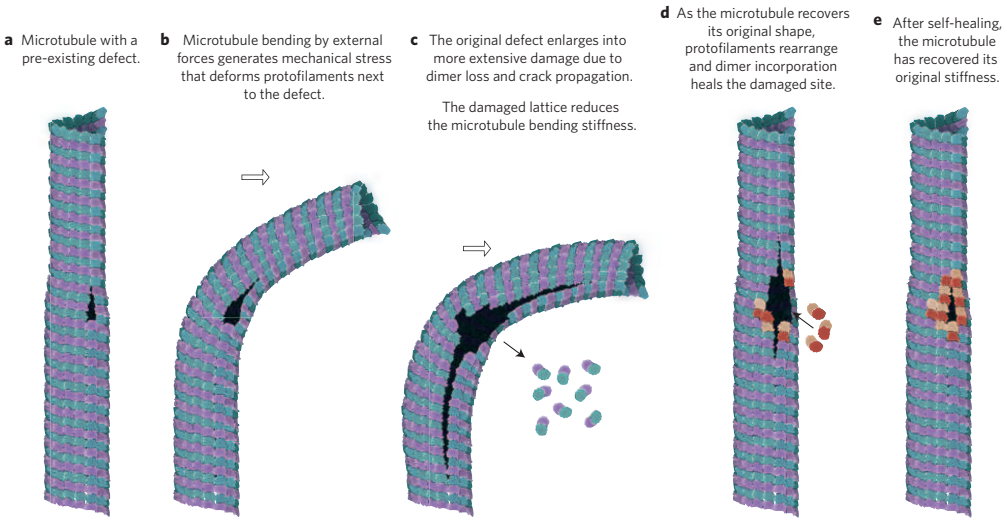


**Figure 6 | Model of microtubule softening and self-repairing under mechanical stress. a–e**, Speculative interpretation of the contribution of microtubule lattice defects to microtubule deformation, softening and self-healing under mechanical stress. Arrows indicate external force. Illustration by A. Kawska at IlluScientia.com.

and completes the healing of the structure (Fig. 6d). Thereby, the microtubule recovers its original stiffness (Fig. 6e).

These new properties of microtubule softening and self-repairing and the plasticity of the microtubule lattice profoundly change our appreciation of microtubule mechanics and dynamics. It should prompt us to revise our understanding of the regulation of microtubule network architectures.

## Methods

Methods and any associated references are available in the online version of the paper.

Received 11 December 2014; accepted 24 July 2015; published online 7 September 2015

## References


1. Mimori-Kiyosue, Y. Shaping microtubules into diverse patterns: Molecular connections for setting up both ends. *Cytoskeleton* **68,** 603–618 (2011).
2. Van der Vaart, B., Akhmanova, A. & Straube, A. Regulation of microtubule dynamic instability. *Biochem. Soc. Trans.* **37,** 1007–1013 (2009).
3. Schek, H. T., Gardner, M. K., Cheng, J., Odde, D. J. & Hunt, A. J. Microtubule assembly dynamics at the nanoscale. *Curr. Biol.* **17,** 1445–1455 (2007).
4. Dogterom, M. & Surrey, T. Microtubule organization *in vitro*. *Curr. Opin. Cell Biol.* **25,** 23–29 (2013).
5. Vignaud, T., Blanchoin, L. & Théry, M. Directed cytoskeleton self-organization. *Trends Cell Biol.* **22,** 671–682 (2012).
6. Howard, J. Elastic and damping forces generated by confined arrays of dynamic microtubules. *Phys. Biol.* **3,** 54–66 (2006).
7. Hawkins, T., Mirigian, M., Selcuk Yasar, M. & Ross, J. L. Mechanics of microtubules. *J. Biomech.* **43,** 23–30 (2010).
8. Mohrbach, H., Johner, A. & Kuli , I. M. Cooperative lattice dynamics and anomalous fluctuations of microtubules. *Eur. Biophys. J.* **41,** 217–239 (2012).
9. Gittes, F., Mickey, B., Nettleton, J. & Howard, J. Flexural rigidity of microtubules and actin filaments measured from thermal fluctuations in shape. *J. Cell Biol.* **120,** 923–934 (1993).
10. Hoey, D. A., Downs, M. E. & Jacobs, C. R. The mechanics of the primary cilium: An intricate structure with complex function. *J. Biomech.* **45,** 17–26 (2012).
11. Pampaloni, F. *et al.* Thermal fluctuations of grafted microtubules provide evidence of a length-dependent persistence length. *Proc. Natl Acad. Sci. USA* **103,** 10248–10253 (2006).
12. Sui, H. & Downing, K. H. Structural basis of interprotofilament interaction and lateral deformation of microtubules. *Structure* **18,** 1022–1031 (2010).
13. Mandelkow, E., Schultheiss, R., Rapp, R., Müller, M. & Mandelkow, E. On the surface lattice of microtubules: Helix starts, protofilament number, seam, and handedness. *J. Cell Biol.* **102,** 1067–1073 (1986).
14. Kis, A. *et al.* Nanomechanics of microtubules. *Phys. Rev. Lett.* **89,** 248101 (2002).
15. Díaz, J. F., Barasoain, I. & Andreu, J. M. Fast kinetics of Taxol binding to microtubules. Effects of solution variables and microtubule-associated proteins. *J. Biol. Chem.* **278,** 8407–8419 (2003).
16. Davis, L. J., Odde, D. J., Block, S. M. & Gross, S. P. The importance of lattice defects in katanin-mediated microtubule severing *in vitro*. *Biophys. J.* **82,** 2916–2927 (2002).
17. Mohrbach, H. & Kuli , I. M. Motor driven microtubule shape fluctuations: Force from within the lattice. *Phys. Rev. Lett.* **99,** 218102 (2007).
18. Yvon, A. M. C., Gross, D. J. & Wadsworth, P. Antagonistic forces generated by myosin II and cytoplasmic dynein regulate microtubule turnover, movement, and organization in interphase cells. *Proc. Natl Acad. Sci. USA* **98,** 8656–8661 (2001).
19. Gupton, S. L., Salmon, W. C. & Waterman-Storer, C. M. Converging populations of f-actin promote breakage of associated microtubules to spatially regulate microtubule turnover in migrating cells. *Curr. Biol.* **12,** 1891–1899 (2002).
20. Mandato, C. A. & Bement, W. M. Actomyosin transports microtubules and microtubules control actomyosin recruitment during *Xenopus* oocyte wound healing. *Curr. Biol.* **13,** 1096–1105 (2003).
21. Brangwynne, C. P., Mackintosh, F. C. & Weitz, D. A. Force fluctuations and polymerization dynamics of intracellular microtubules. *Proc. Natl Acad. Sci. USA* **104,** 16128–16133 (2007).
22. Bicek, A. D. *et al.* Anterograde microtubule transport drives microtubule bending in LLC-PK1 epithelial cells. *Mol. Biol. Cell* **20,** 2943–2953 (2009).
23. Laan, L. *et al.* Cortical dynein controls microtubule dynamics to generate pulling forces that position microtubule asters. *Cell* **148,** 502–514 (2012).
24. Goetz, J. G. *et al.* Endothelial cilia mediate low flow sensing during zebrafish vascular development. *Cell Rep.* **6,** 799–808 (2014).
25. Odde, D. J., Ma, L., Briggs, A. H., Demarco, A. & Kirschner, M. W. Microtubule bending and breaking in living fibroblast cells. *J. Cell Sci.* **3288,** 3283–3288 (1999).
26. Waterman-Storer, C. M. & Salmon, E. D. Actomyosin-based retrograde flow of microtubules in the lamella of migrating epithelial cells influences microtubule dynamic instability and turnover and is associated with microtubule breakage and treadmilling. *J. Cell Biol.* **139,** 417–434 (1997).
27. Bicek, A. D., Tüzel, E., Kroll, D. M. & Odde, D. J. Analysis of microtubule curvature. *Methods Cell Biol.* **83,** 237–268 (2007).
28. Kurachi, M., Hoshi, M. & Tashiro, H. Buckling of a single microtubule by optical trapping forces: Direct measurement of microtubule rigidity. *Cell Motil. Cytoskeleton* **30,** 221–228 (1995).

29. Venier, P., Maggs, A. C., Carlier, M. F. & Pantaloni, D. Analysis of microtubule rigidity using hydrodynamic flow and thermal fluctuations. *J. Biol. Chem.* **269,** 13353–13360 (1994).
30. Portran, D., Gaillard, J., Vantard, M. & Théry, M. Quantification of MAP and molecular motor activities on geometrically controlled microtubule networks. *Cytoskeleton* **70,** 12–23 (2013).
31. Sangid, M. D. The physics of fatigue crack initiation. *Int. J. Fatigue* **57,** 58–72 (2013).
32. Chrétien, D., Metoz, F., Verde, F., Karsenti, E. & Wade, R. H. Lattice defects in microtubules: Protofilament numbers vary within individual microtubules. *J. Cell Biol.* **117,** 1031–1040 (1992).
33. Schaap, I. T., de Pablo, P. J. & Schmidt, C. F. Resolving the molecular structure of microtubules under physiological conditions with scanning force microscopy. *Eur. Biophys. J.* **33,** 462–467 (2004).
34. Janson, M. E. & Dogterom, M. A bending mode analysis for growing microtubules: Evidence for a velocity-dependent rigidity. *Biophys. J.* **87,** 2723–2736 (2004).
35. Brangwynne, C. P. *et al.* Microtubules can bear enhanced compressive loads in living cells because of lateral reinforcement. *J. Cell Biol.* **173,** 733–741 (2006).
36. Krieg, M., Dunn, A. R. & Goodman, M. B. Mechanical control of the sense of touch by $\beta$-spectrin. *Nature Cell Biol.* **16,** 224–233 (2014).
37. Dye, R. B., Flicker, P. F., Lien, D. Y. & Williams, R. C. End-stabilized microtubules observed *in vitro*: Stability, subunit, interchange, and breakage. *Cell Motil. Cytoskeleton* **21,** 171–186 (1992).
38. Cordier, P., Tournilhac, F., Soulié-Ziakovic, C. & Leibler, L. Self-healing and thermoreversible rubber from supramolecular assembly. *Nature* **451,** 977–980 (2008).
39. Murphy, E. B. & Wudl, F. The world of smart healable materials. *Prog. Polym. Sci.* **35,** 223–251 (2010).

## Acknowledgements

We thank D. Chrétien for interesting discussions about microtubule defects and M. Dogterom and T. Salmon for bringing to our attention the seminal work of R. Williams. This work has been supported by an HFSP funding to M.T. and M.V.N. (RGY0088/2012) and ERC funding to M.T. (Starting Grant 310472).

## Author contributions

L.S. performed all experiments with the help of J.G. K.J. and L.S. conceived and performed microtubule stiffness measurements. K.J. performed numerical simulations. L.S., L.B. and M.T. designed the experiments. L.S., K.J., L.B. and M.T. analysed data. M.V.N., L.B. and M.T. wrote the manuscript.

## Additional information

Supplementary information is available in the online version of the paper. Reprints and permissions information is available online at www.nature.com/reprints. Correspondence and requests for materials should be addressed to L.B. or M.T.

## Competing financial interests

The authors declare no competing financial interests.

## Methods

**Tubulin purification and labelling.** Tubulin was purified from fresh bovine brain by three cycles of temperature-dependent assembly and disassembly in Brinkley Buffer 80 (BRB80 buffer; BRB buffer: 80 mM PIPES, pH 6.8, 1 mM EGTA and 1 mM $MgCl_2$ plus 1 mM GTP; ref. 40). MAP-free neurotubulin was purified by cation-exchange chromatography (EMD SO, 650 M, Merck) in 50 mM PIPES, pH 6.8, supplemented with 1 mM $MgCl_2$ and 1 mM EGTA (ref. 41). Purified tubulin was obtained after a cycle of polymerization and depolymerization. Fluorescent tubulin (ATTO-488 and ATTO-565-labelled tubulin) and biotinylated tubulin were prepared as previously described[42]. Microtubules from neurotubulin were polymerized at 37 °C for 30 min and layered onto cushions of 0.1 M NaHEPES, pH 8.6, 1 mM $MgCl_2$, 1 mM EGTA, 60% v/v glycerol, and sedimented by high centrifugation at 30 °C. Then microtubules were resuspended in 0.1 M NaHEPES, pH 8.6, 1 mM $MgCl_2$, 1 mM EGTA, 40% v/v glycerol and labelled by adding 1/10 volume 100 mM NHS-ATTO (ATTO Tec), or NHS-Biotin (Pierce) for 10 min at 37 °C. The labelling reaction was stopped using two volumes of 2X BRB80, containing 100 mM potassium glutamate and 40% v/v glycerol, and then microtubules were sedimented onto cushions of BRB80 supplemented with 60% glycerol. Microtubules were resuspended in BRB80, and a second cycle of polymerization and depolymerization was performed before use.

**Cover glass micropatterning.** The micropatterning technique was adapted from ref. 30. Cover glasses were cleaned by successive chemical treatments: 30 min in acetone, 15 min in ethanol (96%), rinsing in ultrapure water, 2 h in Hellmanex III (2% in water, Hellmanex), and rinsing in ultrapure water. Cover glasses were dried using nitrogen gas flow and incubated for three days in a solution of tri-ethoxy-silane-PEG (30 kDa, PSB-2014, Creative PEGWorks) 1 mg ml$^{-1}$ in ethanol 96% and 0.02% of HCl, with gentle agitation at room temperature. Cover glasses were then successively washed in ethanol and ultrapure water, dried with nitrogen gas, and stored at 4 °C. Passivated cover glasses were placed into contact with a photomask (Toppan) with a custom-made vacuum-compatible holder and exposed to deep ultraviolet (7 mW cm$^{-2}$ at 184 nm, Jelight) for 2 min 30 s. Deep ultraviolet exposure through the transparent micropatterns on the photomask created oxidized micropatterned regions on the PEG coated cover glasses.

**Microfluidic circuit fabrication and flow control.** The microfluidic device was fabricated in PDMS (Sylgard 184, Dow Corning) using standard photolithography and soft lithography[43]. The master mould was fabricated by patterning 50-μm-thick negative photoresist (SU8 2100, Microchem) by photolithography. A positive replica was fabricated by replica moulding PDMS against the master. Before moulding, the master mould was silanized (trichloro(1H,1H,2H,2H-perfluorooctyl)silane, Sigma) for easier lift-off. Four inlet/outlet ports were made in the PDMS device using 0.5 mm soft substrate punches (UniCore 0.5, Ted Pella). Connectors to support the tubing were made out of PDMS cubes (0.5 cm side length) with a 1.2 mm diameter through-hole. The connectors were bonded to the chip ports using still liquid PDMS as glue, which was used to coat the interface between the chip and the connectors, and was then rapidly cured on a hotplate at 120 °C. Teflon tubing (Tefzel, inner diameter: 0.03″, outer diameter: 1/16″, Upchurch Scientific) was inserted into the two ports serving as outlets. Tubing with 0.01″ inner and 1/16″ outer diameter was used to connect the inlets, via two three-way valves (Omnifit Labware) that could be opened and closed by hand, to a computer-controlled microfluidic pump (MFCS-4C, Fluigent). Flow inside the chip was controlled using the MFCS-Flex control software (Fluigent). For repeated bending experiments, a script was used that automatically set the flow to a defined value for 10 s, then turned off the flow for 10 s or 100 s, repeating this cycle up to ten times. Custom rubber pieces that fit onto the tubing were used to close the open ends of the outlet tubing when needed.

**Microtubule growth on micropatterns.** Microtubule seeds were prepared at 10 μM tubulin concentration (30% ATTO-488-labelled or ATTO-565-labelled tubulin and 70% biotinylated tubulin) in BRB80 supplemented with 0.5 mM GMP-CPP at 37 °C for 1 h. The seeds were incubated with 1 μM Taxotere (Sigma) at room temperature for 30 min and were then sedimented by high centrifugation at 30 °C and resuspended in BRB80 supplemented with 0.5 mM GMP-CPP and 1 μM Taxotere. Seeds were stored in liquid nitrogen and quickly warmed to 37 °C before use.

The PDMS chip was placed on a micropatterned cover glass and fixed on the microscope stage. The chip was perfused with neutravidin (25 μg ml$^{-1}$ in BRB80; Pierce), then washed with BRB80, passivated for 20 s with PLL-g-PEG (Pll 20K-G35-PEG2K, JenKem Technology) at 0.1 mg ml$^{-1}$ in 10 mM HEPES (pH = 7.4), and washed again with BRB80. Microtubule seeds were flowed into the chamber at high flow rates perpendicularly to the micropatterned lines to ensure proper orientation of the seeds. Non-attached seeds were washed out immediately using BRB80 supplemented with 1% BSA. Seeds were elongated with a mix containing 14, 18, 20 or 26 μM of tubulin (30% labelled) in BRB80 supplemented with 50 mM NaCl, 50 25 mM NaPi, 1 mM GTP, an oxygen scavenger cocktail (20 mM DTT, 2 mg ml$^{-1}$ glucose, 80 μg ml$^{-1}$ catalase and 0.67 mg ml$^{-1}$ glucose oxidase), 0.1% BSA, 0.025% methyl cellulose (1500 cp, Sigma) and 0.02% red fluorescent beads (Fluoro-Max polymer spheres, 0.52 μm diameter, Thermo Scientific). The same mix was used to subject microtubules to flow. For the experiments showing tubulin incorporation after bending, a mix was prepared with 100% labelled tubulin for bending the microtubules.

**Imaging.** Microtubules were visualized using an objective-based azimuthal ilas2 TIRF microscope (Nikon Eclipse Ti, modified by Roper Scientific) and an Evolve 512 camera (Photometrics). The microscope stage was kept at 37 °C by means of a warm stage controller (LINKAM MC60). Excitation was achieved using lasers with wavelengths of 491 and 561 nm (Optical Insights). Time-lapse recording was performed using Metamorph software (version 7.7.5, Universal Imaging). Movies were processed to improve the signal/noise ratio (smooth and subtract background functions of ImageJ, version 1.47n5). Images were typically taken every 150 ms.

**Laser-induced microtubule damage.** Laser-induced microtubule damage tests were performed using a Laser illuminator iLas2 (Roper Scientific) set up on an inverted microscope (Ti-E, Nikon) with a ×60 Nikon APO TIRF Oil-immersion objective. iLas2 is a dual-axis galvanometer-based optical scanner that focuses the laser beam on the sample (diffraction-limited spot size) over the whole field of view of the camera. Laser displacement, exposure time and repetition rate were controlled using Metamorph software (version 7.7.9.0, Universal Imaging). To damage Alexa-561-labelled microtubules, a 50 mW/561 nm laser was used at 90% power, performing 30 repetitions within a field size of approximately 4 μm × 4 μm. To merely photobleach microtubules, 20 repetitions were carried out at 80% laser power. To break microtubules, 50 repetitions at 100% laser power were used.

**Measurement of microtubule persistence length.** The microtubule is described as an inextensible slender filament with length $L$ and bending rigidity $\kappa$, which is bent in two dimensions by the fluid flow. Its elastic energy $E$ is given by

$$E[\mathbf{r}] = \int_0^L \left\{ \frac{\kappa}{2} \left( \frac{\mathrm{d}^2\mathbf{r}}{\mathrm{d}s^2} \right)^2 + \frac{\lambda}{2} \left[ \left( \frac{\mathrm{d}r}{\mathrm{d}s} \right)^2 - 1 \right] \right\} \mathrm{d}s \tag{1}$$

The vector $\mathbf{r}(s)$ denotes the position of the filament parameterized by the arc length $s$ and $\lambda$ denotes a Lagrange multiplier associated with the inextensibility condition $|\mathrm{d}\mathbf{r}/\mathrm{d}s| = 1$. The force exerted on the filament is given by the functional variation of the potential $E$ with respect to the filament position vector $\mathbf{r}$

$$\mathbf{F}_\mathrm{B} = -\frac{\delta E}{\delta \mathbf{r}} \tag{2}$$

The filament orientation is fixed by the seed orientation at $s = 0$, whereas the other end of the filament at $s = L$ is force-free. The hydrodynamic drag exerted by the fluid flow on a slender filament is given by

$$\mathbf{F}_\mathrm{H} = g\mu \left( \mathbf{I} - \frac{1}{2} \frac{\mathrm{d}\mathbf{r}}{\mathrm{d}s} \otimes \frac{\mathrm{d}\mathbf{r}}{\mathrm{d}s} \right) \mathbf{v}_\mathrm{b} \tag{3}$$

where $\mathbf{v}_\mathrm{b}$ denotes the velocity field measured by the bead displacements, $\mu$ denotes the viscosity of the fluid and $g$ denotes a geometrical factor of the order of 1, which depends on the distance of the filament from the surface, the radius of the filament and the distance of the beads from the surface. $\otimes$ denotes the outer product and $\mathbf{I}$ is the identity tensor. In mechanical equilibrium

$$\mathbf{F}_B + \mathbf{F}_\mathrm{H} = 0 \tag{4}$$

which determines the equilibrium shape of the filament subject to the appropriate boundary conditions. The filament rigidity was determined by solving equations (1)–(4) using the AUTO-07p software package[44] and by minimizing the function

$$\omega^2(\kappa) = \frac{1}{L} \int_0^L [\mathbf{r}_R(s) - \mathbf{r}(s)]^2 \mathrm{d}s \tag{5}$$

where $\mathbf{r}_R(s)$ denotes the measured position of the filament. The persistence length is then given by $L_p = \kappa/(k_\mathrm{B}T)$. $\omega$ is a measure for the distance between the shapes of two microtubules. In the fitting routine for the experimentally measured microtubule shapes, $\omega$ denotes the distance between the shape of the experimental snake and an inextensible flexible filament subjected to the same flow as the experimental snake.

We assumed that the origin of the microtubule was clamped in the direction of the seed. To correct for a measurement error of the microtubule origin, we optimized equation (5) also for the position of the microtubule origin.

The analytic determination of the geometrical factor $g$ is difficult, because the distance of the filament from the surface is not known, but is <100 nm (the depth of the evanescent wave field), the fluid velocity is determined by imaging of beads with a radius of 250 nm, which are visible with TIRF and the velocity field close to the surface is distorted by the PEG brush. We assume that $g$ is approximately constant for all experiments. From an independent measurement of microtubule

persistence length based on thermal fluctuations[9] we have calculated $g = 0.27 \pm 0.11$.

**Modelling of microtubule softening.** Using numerical simulations we tested whether the observed bending-induced softening of microtubules was localized or extended over a larger portion of the microtubule. To that end we calculated theoretically the shapes of microtubules with a spatially dependent rigidity of the form

$$\kappa = \kappa_p + \frac{\kappa_0 - \kappa_p}{2}\left\{2 + \tanh\left[\frac{2(s-s_0)-\Delta s}{\varepsilon}\right] - \tanh\left[\frac{2(s-s_0)+\Delta s}{\varepsilon}\right]\right\} \quad (6)$$

where $\kappa_0$ ($\kappa_p$) denotes the microtubule rigidity in the unsoftened (softened) region, $s_0$ and $\Delta s$ denote the centre position and the width of the softened region and $\varepsilon$ denotes the width of the transition region between the softened and unsoftened part of the microtubule. The shapes of microtubules with an inhomogeneous rigidity (equation (6)) were fitted to the shapes of microtubules with a homogeneous rigidity to obtain an apparent average stiffness $\langle\kappa\rangle$, as we did for experimentally obtained microtubules shapes using equation (5). For the calculations all lengths were scaled by the length $L$ of the microtubule and the forces were scaled by the hydrodynamic drag force per cross-section $g\eta v$. The shape of a microtubule with homogeneous stiffness then depends on a single dimensionless parameter $\langle\tilde{\kappa}\rangle = \langle\kappa\rangle/(L^3 g\eta v)$.

Apparent stiffness ($\langle\kappa\rangle/\kappa_0$) is the stiffness of an homogeneous microtubule whose shape best fits the observed (or simulated) deformation. It is higher than the stiffness of the soft part, except when this part gets long enough and the two values match.

In Fig. 5d, we worked with numerical microtubules with an apparent stiffness of $\langle\kappa\rangle/\kappa = 0.5$. We calculated the scaled fit parameter $\omega/L$ for microtubules with varying parameters of the perturbation $\Delta s/L$ and $\kappa_p/\kappa_0$ and different ratios $\kappa_0/L^3 g\eta v$, corresponding to different deflections of the unsoftened microtubule. All other parameters were kept constant, that is, $s_0/L = 0.33$ and $\varepsilon/L = 0.02$.

To match experimentally obtained scaled fit parameters $\omega/L$ to theoretical ones, we picked bending cycles where microtubules showed a scaled effective rigidity ratio $\langle\tilde{\kappa}_n\rangle/\langle\tilde{\kappa}_1\rangle \approx 0.4$–$0.6$. (The subscript denotes the number of the bending cycle.) We then matched the deflection of the first bending cycle $x/L$ and the experimental fit quality parameter $\omega_n/L_n$ to the theoretical curves to obtain an estimation of the width of the softened region (see Fig. 5d). Experimental points were spread between $\Delta s/L = 0$ and 0.6, which supports the hypothesis that the bending-induced damage was not always highly localized, but often extended over a larger portion of the microtubule.

## References


40. Shelanski, M. L. Chemistry of the filaments and tubules of brain. *J. Histochem. Cytochem.* **21,** 529–539 (1973).
41. Malekzadeh-Hemmat, K., Gendry, P. & Launay, J. F. Rat pancreas kinesin: Identification and potential binding to microtubules. *Cell. Mol. Biol. (Noisy-le-grand)* **39,** 279–285 (1993).
42. Hyman, A. *et al.* Preparation of modified tubulins. *Methods Enzymol.* **196,** 478–485 (1991).
43. Duffy, D. C., McDonald, J. C., Schueller, O. J. & Whitesides, G. M. Rapid prototyping of microfluidic systems in poly(dimethylsiloxane). *Anal. Chem.* **70,** 4974–4984 (1998).
44. Doedel, E. J. *AUTO-07p: Continuation and Bifurcation Software for Ordinary Differential Equations* (2007); http://www.macs.hw.ac.uk/~gabriel/auto07/auto.html

nature materials

SUPPLEMENTARY INFORMATION

DOI: 10.1038/NMAT4369

# Microtubules self-repair in response to mechanical stress

Laura Schaedel[1], Karin John[2], Jérémie Gaillard[1], Maxence V. Nachury[3], Laurent Blanchoin[1,*] and Manuel Théry[1,4*]

1 – Laboratoire de Physiologie Cellulaire et Végétale, Institut de Recherche en Technologie et Science pour le Vivant, UMR5168, CEA/INRA/CNRS/UGA, Grenoble, France.
2- Laboratoire Interdisciplinaire de Physique, CNRS / UGA Grenoble140 Rue de la Physique BP 87 - 38402 Saint-Martin-d'Hères, France
3- Department of Molecular and Cellular Physiology, Stanford University School of Medicine, CA 94305, USA.
4 - Unité de Thérapie Cellulaire, Hôpital Saint Louis, Institut Universitaire d'Hematologie, UMRS1160, INSERM/AP-HP/Université Paris Diderot, Paris, France.

Correspondence : laurent.blanchoin@cea.fr, manuel.thery@cea.fr

## Supplementary information

Supplementary figure S1 – S8
Supplementary video 1 – 6 legends

DOI: 10.1038/NMAT4369

## Supplementary Figures

Supplementary Figure S1 - Measurements of microtubule persistent length evolution over the successive bending cycles.
a, Microtubules were grown in the presence of 14, 18, 20 or 26 μM of tubulin and bent several times. Error bars correspond to the standard deviation calculated from 5 consecutive frames for each bending cycle. As a test of tendency, Spearman correlation tests for persistent length values over the successive cycles were performed. Green curves show microtubules for which the persistent length was not significantly affected over the bending cycles, whereas red curves show those that have been soften during the cyclic stress.
b, Same as a excepted that microtubule persistent lengths over bending cycles were normalized to their initial value.

Figure S1

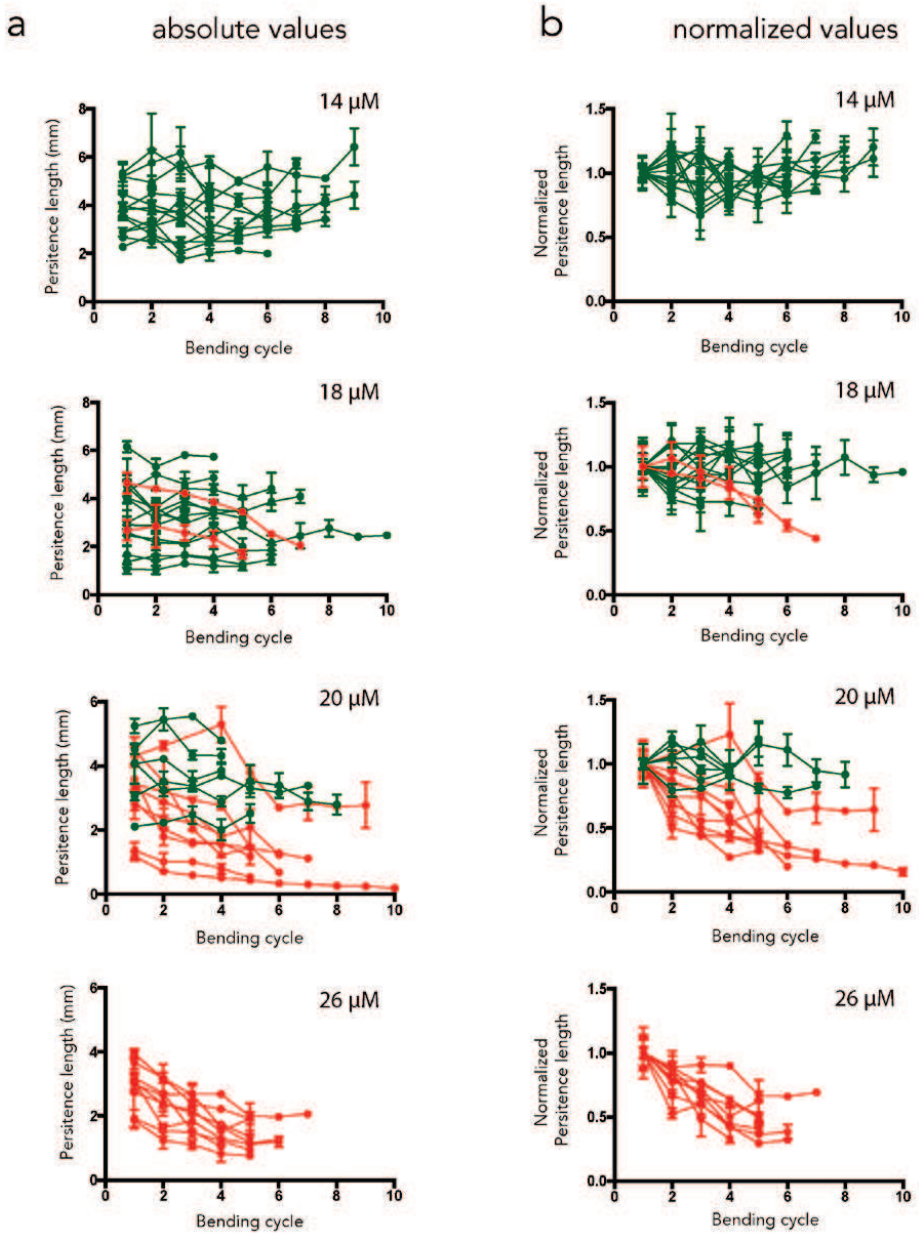

DOI: 10.1038/NMAT4369

Supplementary Figure S2 – Impact of the delay between bending cycles on the evolution of microtubule persistent length.
Microtubules were grown in the presence 20 μM of tubulin and bent several times. Delay between bending cycles was varied between 10 s (top line) and 100 s (bottom line). Microtubule persistent length was measured over the successive bending cycles. Microtubule persistent lengths were normalized to their initial value. Error bars correspond to the standard deviation calculated from 5 consecutive frames for each bending cycle. As a test of tendency, Spearman correlation tests for persistent length values over the successive cycles were performed. Green curves show microtubules for which the persistent length was not significantly affected over the bending cycles, whereas red curves show those that have been soften during the cyclic stress. The proportion of microtubules for which the persistent length decreased over the bending cycles reduced as the delay between the cycles was increased.

Figure S2

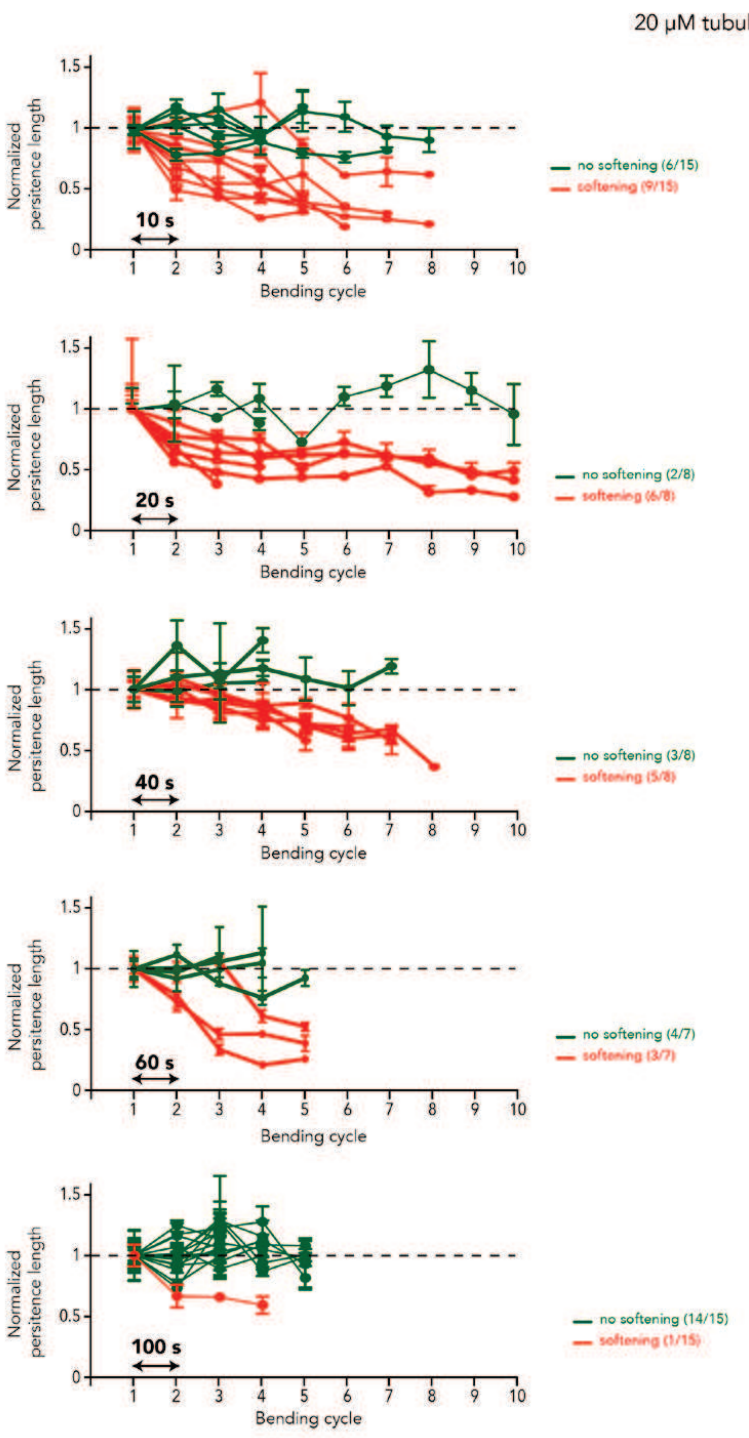

DOI: 10.1038/NMAT4369

Supplementary Figure S3 - Evolution of microtubule persistent length following five rapid bending cycles.

Microtubules were grown in the presence 20 μM of tubulin and bent five times with 10 s delay between the bending cycles. Then microtubules were not stimulated during 100 s. Stiffness recovery was measured by a last bending cycle after this rest period. To first distinguish softening from non-softening microtubules during the first bending cycles, we used the distance between the minimum normalized Lp and the Lp during the first cycle as a parameter for a k-means clustering. The clustering algorithm found one group with a low distance, which corresponds to non-softening microtubules (a, b), and another group with a high distance, corresponding to softening microtubules (c ,d). The recovery after a 100 s pause time was assessed by comparing Lp before and after the pause with a Wilcoxon matched-pairs test. Microtubules displaying significant recovery are shown in blue, the other in orange.

No stiffness change could be observed in the group displaying no softening during the first bending cycles (a, b) whereas a significant stiffness increased was measured in a majority of microtubule that have been soften during the first bending cycles (c ,d).

a, c, individual microtubule persistent length evolution during the five first bending cycles and the 100 s rest period.

b, d, average microtubule persistent length evolution during the five first bending cycles and the 100 s rest period.

Figure S3

20 µM tubulin

a Microtubules displaying NO significant softening during the 5 first rapid bending cycles

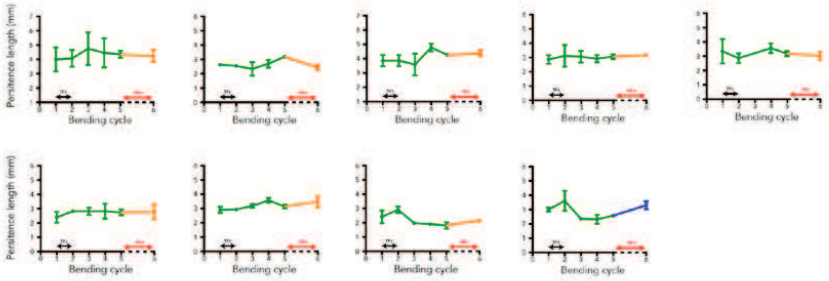


b

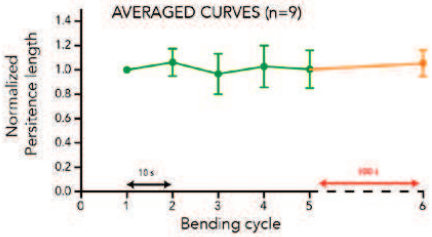


c Microtubules displaying a significant softening during the 5 first rapid bending cycles

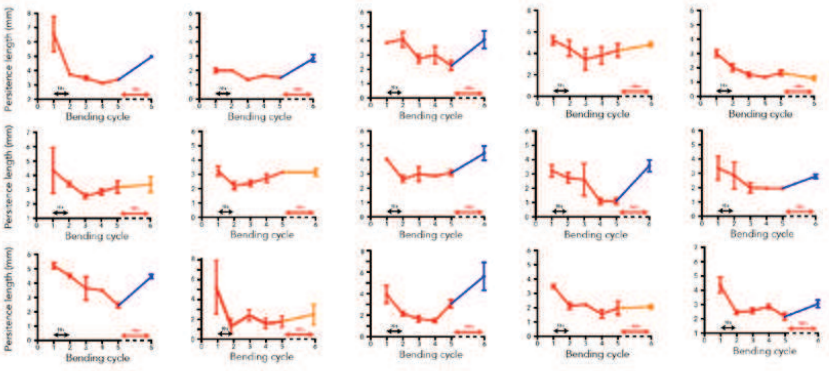


d

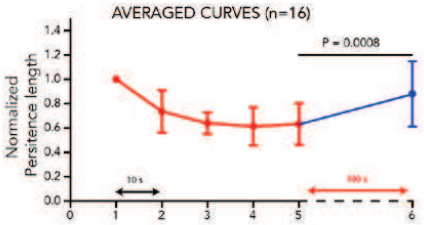


Cycle 5: <Lp> = 0.63 ± 0.17 (mean± sd)
Cycle 6: <Lp> = 0.88 ± 0.26

Wilcoxon two-tailed matched-pairs test
between cycle 5 and cycle 6:
p = 0.0008

softening stiffening
no softening no stiffening

DOI: 10.1038/NMAT4369

Supplementary Figure S4 – Laser-induced damages in microtubule lattice.
A laser emitting pulses at 561 nm was used to damage microtubule lattice. The total energy was modulated by varying laser repetition rate.
a, at low energy, microtubules were bleached but not damaged as revealed by the regular curved shapes they adopted when submitted to external flow.
b, at medium energy, microtubules were physically damaged, as shown by the kinked shape they displayed when submitted to flow. Microtubules were not severed and recovered their original straight shape as flow was stopped.
c, at high energy, microtubules were cut by the light pulses.

Figure S4

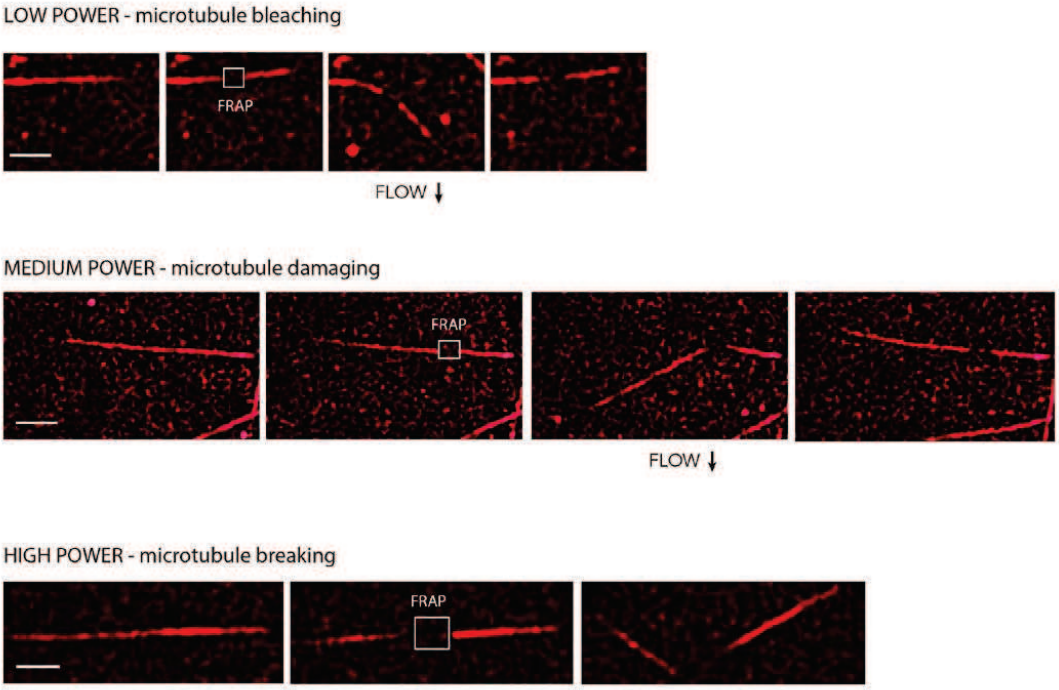

DOI: 10.1038/NMAT4369

Supplementary Figure S5 – Examples of intra-lattice dimer incorporation in bent microtubules.
Seventeen examples of red fluorescent microtubules after five successive bending cycles in the presence of green tubulin. Upper pictures show red fluorescent channel, lower pictures show the green channel after fluorescent tubulin washout. Arrows point at incorporation sites of green dimers into the red lattice between the microtubule seed on the right and the growing end on the left. Graphics display the corresponding green fluorescence intensity linescan along microtubule length.

Figure S5

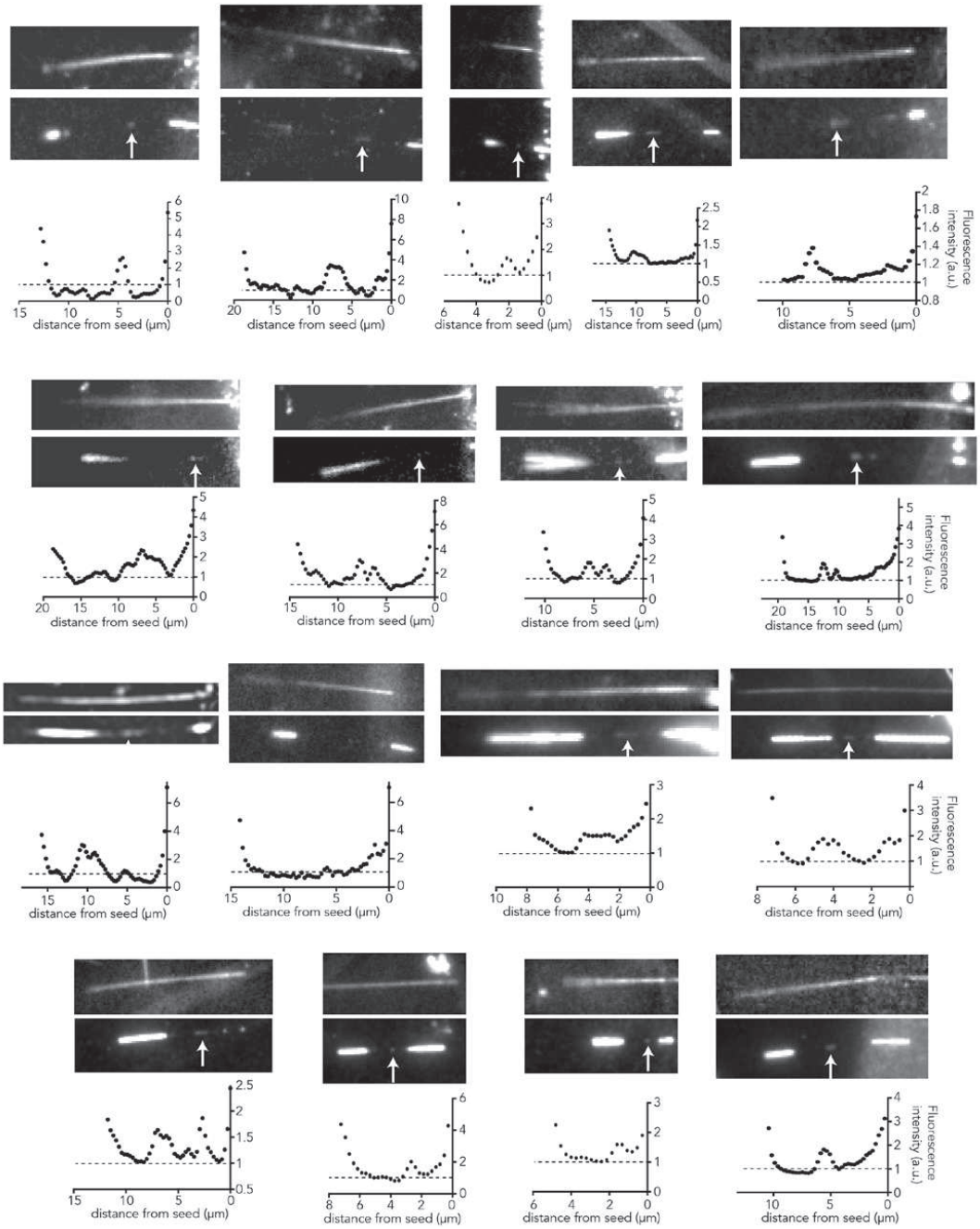

DOI: 10.1038/NMAT4369

Supplementary Figure S6 – Examples of absence of intra-lattice dimer incorporation in non-bent microtubules.
a, Experimental procedure to grow microtubules with red tubulin and flow green tubulin along their length.
b, Nine examples of red fluorescent microtubules submitted to green tubulin flow along their length. Upper pictures show red fluorescent channel, lower pictures show the green channel after fluorescent tubulin washout. Graphics display the corresponding green fluorescence intensity linescan along microtubule length and show no intra-lattice incorporation along microtubule length.

Figure S6

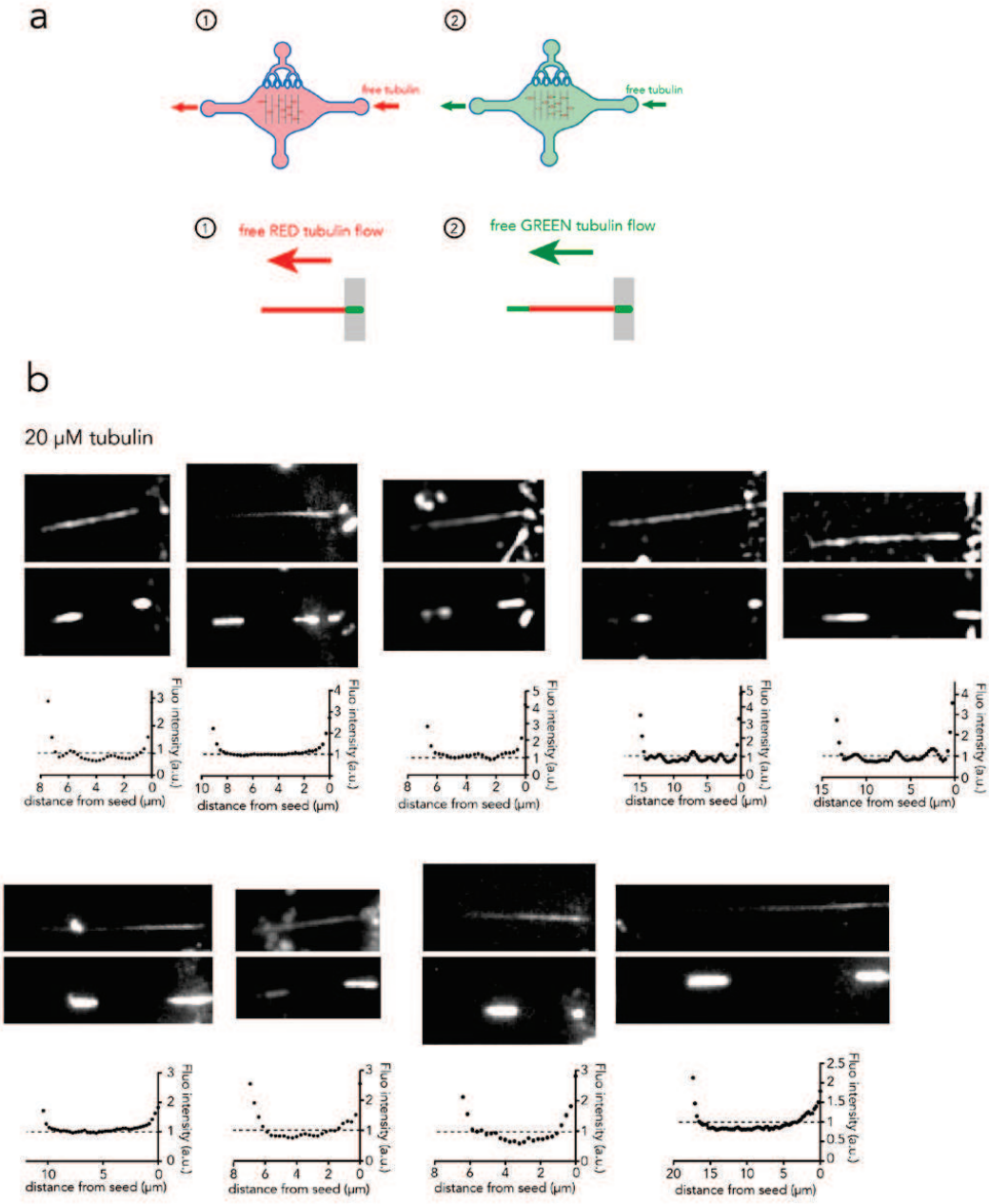

DOI: 10.1038/NMAT4369

Supplementary Figure S7 – Examples of absence of intra-lattice dimer incorporation in slowly-assembled microtubules after successive bendings.
a, Experimental procedure to grow microtubules with 14 μM of red tubulin and bend them in the presence of 20 μM of green tubulin.
b, two examples of slowly-assembled red fluorescent microtubules after five successive bending cycles in the presence of green tubulin. Upper pictures show red fluorescent channel, lower pictures show the green channel after fluorescent tubulin washout. Graphics display the corresponding green fluorescence intensity linescan along microtubule length and show no intra-lattice incorporation along microtubule length.

Figure S7

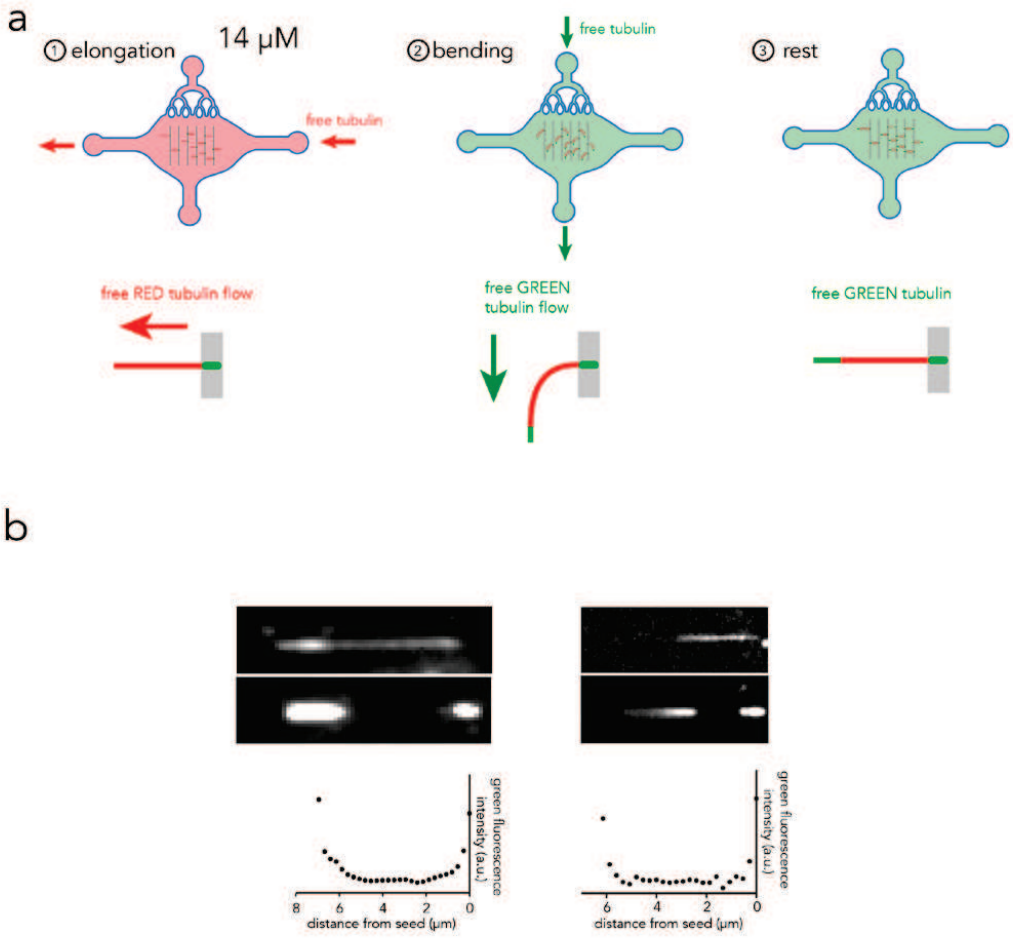

DOI: 10.1038/NMAT4369

Supplementary Figure S8 – Numerical simulations of microtubule bent shapes.
a, The graph shows the variations in the microtubule equilibrium shapes in response to a given hydrodynamic flow upon varying the stiffness reduction $\kappa_p/\kappa_0$ over a short (10%) portion of the microtubule.
b, The graph shows the variations in the microtubule equilibrium shapes in response to a given hydrodynamic flow upon varying the width of the portion whose stiffness has been reduced 10 times.
c, The graph shows the variations of apparent average stiffness depending on the degree of local softening ($\kappa_p/\kappa_0$) and the width on which it is applied ($\Delta s/L$). A given effective rigidity can be obtained for distinct degrees ($\kappa_p/\kappa_0$) and width ($\Delta s/L$) of local softenings (as shown with dotted lines).
d, Comparison of the distances to numeric homogeneous microtubules for experimental observations of microtubules assembled at low and high concentrations of tubulin. The distance ($\omega/L$) was plotted against microtubule deflection ($\Delta s/L$) (see Figure 5c). Hollow stars correspond to microtubules assembled in the presence of 14 μM of free tubulin. Full stars correspond to microtubules assembled in the presence of 20 μM of free tubulin. Both were submitted to five bending cycles. Microtubules assembled in the presence of 14 μM of free tubulin, and presumably with less lattice defects showed lower deviation to numeric and homogenous microtubules than microtubules assembled more rapidly in the presence of 20μM of free tubulin.

Figure S8

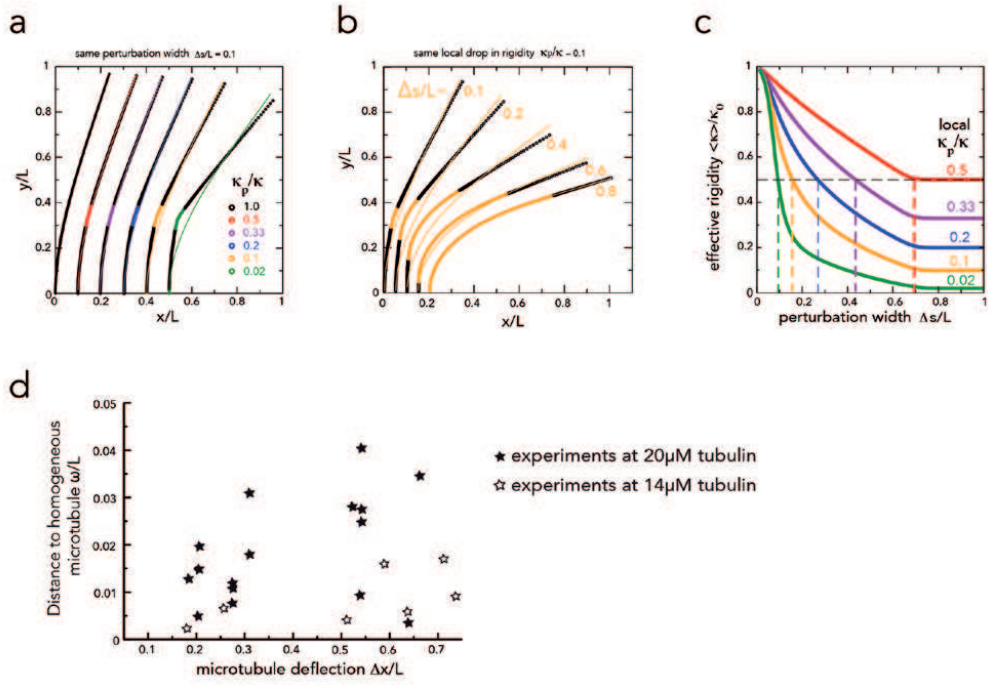

DOI: 10.1038/NMAT4369

## Supplementary Videos

Supplementary video 1
Time lapse sequence of microtubule (green) bending in response to fluid flow. Flow was applied during 10s (from t=10 to t=20s). Red beads were added to the medium to measure fluid flow. Images were taken every 150 ms. Time display is min:sec.

Supplementary video 2
Time lapse sequence of microtubule (green) bending in response to ten successive applications of fluid flow.
Flow sequences were applied during 10s every 20s. Red beads were added to the medium to measure fluid flow. Images were taken every 150 ms. Time display is min:sec.

Supplementary video 3
Time lapse sequence illustrating microtubule lattice damaging with a pulsed laser. Microtubule was assembled from a micropatterned line and damaged with a laser pulse (red disc 1s after movie start) whose location was indicated with a red arrow in the few following images. Damaged microtubule was then submitted to a bending cycle after which it recovered its original straight shape; thereby confirming it was neither severed nor heavily damaged.

Supplementary video 4
Time-lapse sequence illustrating a red microtubule damaged with a pulsed laser in the presence of green tubulin.
The microtubule was assembled from a micropatterned line with red tubulin, bathed in a solution of green tubulin (t=-3:20), damaged (but not cut) with laser pulses (t=0) and let in the presence of green tubulin (until t=1:30). Green tubulin was washed away and replaced by red tubulin. Removal of the green fluorescent background revealed incorporation of tubulin dimers at the damaged site. The light excitation of the green fluorescence was increased at t=2:45 to improve the visualization of the incorporated green tubulin. The light excitation of the red fluorescence was increased at t=3:15 to highlight the red microtubule shaft.

Supplementary video 5
Time-lapse sequence showing a red microtubule (red channel shown on the right) bent 5 times in the presence of green tubulin (green channel shown on the left). Green tubulin was washed out after 90 s and replaced by red tubulin. The light excitation of the green fluorescence was increased at t=171 s to improve the

visualization of the incorporated green tubulin. Several sites of green tubulin incorporation were visible along microtubule length.

Supplementary video 6
Time lapse sequence showing a red microtubule (red channel shown on the right) submitted to flow along it in the presence of green tubulin (green channel shown on the left). Green tubulin was washed out after 140 s and replaced by red tubulin. The light excitation of the green fluorescence was increased at t=210 s to improve the visualization of the incorporated green tubulin. No incorporation could be visualized along the microtubule length in those conditions.

### 2.1.2 Conclusions and perspectives

One of the most striking conclusions of the study is that microtubules, which get damaged by repeated bending forces such as they act in cells, are able to recover their mechanical properties even in the absence of other molecular players. This finding is important for understanding the structural role of microtubules in cells, as a repair mechanism may help microtubules bear mechanical loads. Besides, material self-repair is a rare property, and has attracted a lot of attention in the material science field due to its possible applications (Cordier *et al.*, 2008; Murphy *et al.*, 2010). Understanding the molecular mechanisms of microtubule self-repair might therefore be of interest not only for cell biology, but also for the development of new functional materials.

The bending force exerted on microtubules in the present study is on the order of piconewtons, and therefore rather low compared to the amount of forces that microtubules may experience in cells. At first sight, it therefore seems surprising that bending of microtubules is sufficient to provoke damages and repair of the lattice. Yet, the GDP tubulin lattice is known to be a metastable structure ready to disassemble, implying internal strains that lead to a high lattice energy. Bending further increases the lattice energy, which might favor the dissociation of tubulin dimers from the lattice. This is especially true at structural defect sites, where bonds between dimers are strained or lacking, as is the case at protofilament transitions. At a transition, one dimer misses a longitudinal contact, and at least two dimers lack one lateral contact each (see Fig. 20), though it is not clear from the literature how a protofilament transition looks like on the molecular scale - the separation between protofilaments might as well extend over a longer distance. In addition, lateral contacts are likely to be strained at the point where they close the gap above the transition. Due to the lack of precise information on the nature of the transition, it is not certain which dimer is least stable in the lattice around the defect and

therefore most likely to dissociate. However, as longitudinal bonds are considerably stronger than lateral ones and therefore more efficient in stabilizing a dimer in the lattice, a lacking longitudinal contact decreases dimer stability more than a missing lateral bond. In the scheme shown in Fig. 20, the dimer on the bottom of the transition would thus be most unstable. Bending might also lead to an opening of the lattice, as shown in Fig. 15 in the introduction. This could preferentially happen above the transition shown in Fig. 20, where lateral contacts between dimers are strained. While dimer loss at a protofilament transition (or another, less well described defect type, see Fig. 15 in the introduction) would lead to a local softening of the microtubule and therefore a visible deviation from the calculated bent shapes based on a homogeneous stiffness, openings between protofilaments might extend much further along the lattice, causing more global softening of the microtubule. Both local and global softening were observed (see Fig. 5 of the study), so the two mechanisms might play a role in microtubule softening.

Interestingly, tubulin incorporation into the lattice of a bent microtubule is only roughly correlated with local curvature. This suggests that stress is transmitted over a long distance along the lattice. Microtubules are often considered to be inextensible (Gittes *et al.*, 1993; Kent *et al.*, 2016), so that protofilaments would have to slide past each other as microtubules are bent. Indeed protofilament sliding has been proposed to facilitate microtubule bending (Pampaloni *et al.*, 2006; Sui *et al.*, 2010), and might explain how lattice regions far from locally high curvature are affected by bending.

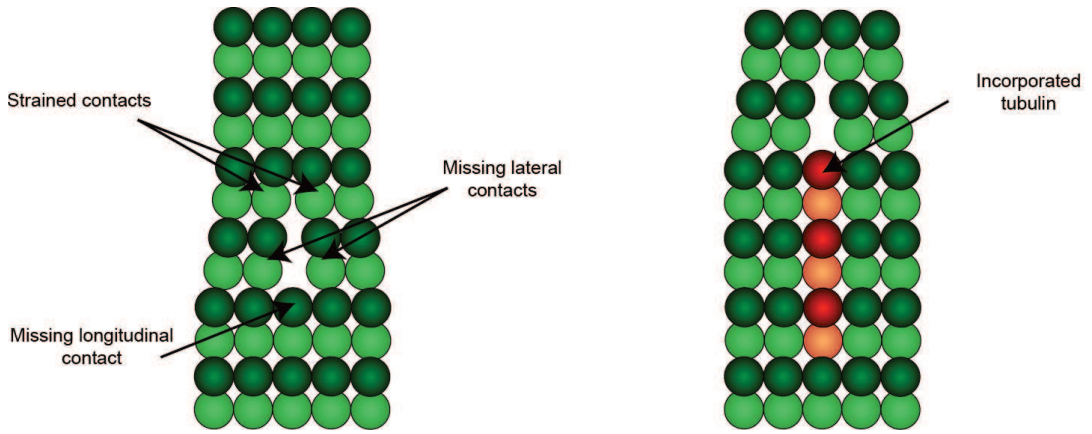


Figure 20: *Possible structure of a protofilament transition and incorporation site. The absence of lateral or longitudinal contacts for certain dimers as well as the strained configuration of the bonds may favor dimer dissociation at transition sites. Subsequent incorporation could preferentially take place by protofilament elongation.*

Of note, the incorporation of new tubulin from the solution leads to a (transient) presence of GTP tubulin in the lattice. This might explain the observation of GTP tubulin stretches along the lattice by Dimitrov *et al.* (Dimitrov *et al.*, 2008). It is tempting to hypothesize that the presence of GTP tubulin might have further consequences for microtubules. Importantly, proteins that specifically recognize the GTP tubulin state, such as +TIPs, might be recruited to the repair site. On the other hand, GTP tubulin itself has been proposed to be an efficient rescue factor (Dimitrov *et al.*, 2008; Tropini *et al.*, 2012). Tropini *et al.* demonstrated that stretches of GMPCPP (a slowly hydrolyzable GTP analog) in a GDP microtubule lattice are able to favor microtubule rescue. It would therefore be interesting to investigate the effects of GTP tubulin incorporation in response to damage on microtubule rescue. Besides, the influence of the nucleotide state on incorporation would be an interesting study subject: Does tubulin have to be in the GTP state in order to be incorporated into the lattice at the damage site? How fast does tubulin incorporate? How fast is incorporated GTP tubulin hydrolyzed? Based on tubulin association constants

at the ends, the repair of damaged microtubules seems rather slow. What limits repair? How big does the damage have to be in order to overcome repair and lead to microtubule breakage? High curvature might increase the tubulin off-rate to a point where it cannot be compensated any more by incorporation. It would also be interesting to further characterize the local distribution of incorporated tubulin to see e.g. if incorporation occurs via elongating protofilaments, as shown in Fig. 20.

The exact role and origin of lattice defects remains to be demonstrated. For example, it is necessary to understand how they form, and if (and if yes, why) they depend on the growth rate and other assembly conditions. This could be accomplished by electron microscopic studies of defect frequencies under different conditions. To visualize single protofilament transitions in greater detail, other techniques such as atomic force microscopy may be useful. Molecular players known to influence the protofilament number could be studied, such as doublecortin, which is known to reinforce 13 protofilament lattice configurations (Bechstedt and Brouhard, 2012). Microtubules with a perfect lattice structure may be less susceptible to bending induced damage. On the other hand, MAPs that are sensitive to microtubule lattice architecture could be used to distinguish between microtubules with different protofilament numbers, and indirectly help to visualize protofilament transitions in fluorescence assays (e.g. Bechstedt and Brouhard, 2013).

Last but not least, the importance of the present findings for microtubule mechanics in cells should be further investigated. Of course, it is possible that microtubule repair in cells is assisted by other proteins, selectively altering repair efficiency. Microtubules in cells grow much faster than *in vitro*, which might favor the occurrence of lattice defects. On the other hand, cells might do a 'quality inspection' of microtubules to avoid defects in the first place. An electron microscopic study of microtubule structure in cells could provide an answer to the question whether

defects occur in cells. As a first hint, Chrétien *et al.* found protofilament transitions in cell-free extract from *Xenopus* eggs, though they seemed to be less frequent than *in vitro* (Chrétien *et al.*, 1992).

Even in the absence of microtubule defects generated during assembly, forces on microtubules in cells could be large enough to induce extensive damage, so a perfect lattice may not guarantee the absence of molecular wear. The study performed by Dimitrov *et al.* suggests that GTP tubulin incorporation occurs *in vivo* as well as *in vitro* (Dimitrov *et al.*, 2008).

Apart from bending, other forces may lead to microtubule molecular wear in cells, notably nonspecific friction between microtubules and other cytoskeletal components, or molecular motors / crosslinkers. Though certainly challenging, an estimation of the relative contribution of the different forces could help to better understand microtubule mechanics *in vivo*. To this end, tubulin incorporation could be visualized in cellular microtubules, and specific subsets of microtubules could be studied. For example, bundled microtubules in neurons are much less likely to experience bending forces than microtubules in cilia.

To further elucidate the structural role of microtubules in cells, and to find out whether microtubule softening in response to mechanical stress occurs *in vivo* similarly to what was found in this study, it would be necessary to estimate microtubule stiffness in cells. Though not a simple task, there are several possibilities to achieve more reliable results than by simply relying on *in vitro* measurements, or on estimations based on bending whole cilia: One could introduce a microtubule-like object of known mechanical properties, like a carbon nanotube, into a cell and deactivate microtubule-specific motors and crosslinkers. From the bending and buckling response of the nanotubes due to intracellular forces one could at the same time measure the amount of force acting on the nanotubes and, by comparison with microtubule bending and buckling, estimate microtubule rigidity. One might also disrupt the cell membrane and extract single microtubules to measure their rigidity

with common *in vitro* techniques. For a less invasive approach, one could try to visualize microtubule motors and / or crosslinkers in living cells and observe local microtubule bending or buckling due to these proteins. Given that the stall force of the motors or the maximum force that crosslinkers can endure before detaching is known, this would allow a local estimation of microtubule mechanical properties.

In summary, the study shows that microtubules are non-homogeneous, and that microtubule dynamics is not limited to the ends of the microtubule, challenging a well-established paradigm of the field. In addition, once more, it is apparent that microtubule behavior and properties depend on the history of the microtubule, as has been proposed before (Janson and Dogterom, 2004; Gardner *et al.*, 2011; Coombes *et al.*, 2013): In this case, microtubule mechanics depend on the growth rate and on previous exposure to mechanical stress.

### 2.1.3 Limitations of the study

As with all experimental approaches, the presented study has some limitations. Specifically, as mentioned in the introduction, estimating the absolute persistence length of microtubules was challenging. However, as the way to analyze microtubule curvature and flow velocity and subsequent persistence length calculation was identical for all microtubules, relative differences and changes in the persistence length could be detected with higher accuracy. The differences in persistence length between different microtubules therefore certainly reflect inherent differences between the mechanical properties of the microtubules themselves, rather than imprecise measurements. To reduce the influence of small fluctuations in curvature of bent microtubules, five successive frames were analyzed and averaged when the microtubule had reached its equilibrium position.

In order to visualize microtubules, tubulin was labeled fluorescently. As intense light exposure is known to break microtubules *in vitro* (Guo *et al.*, 2006), illumination was kept at a minimum. Concerning the setup, though microtubule seed and flow orientation could be reasonably well controlled, the angle between the microtubule and the fluid flow often slightly differed form 90°. Although this was taken into account in the analysis, it could be observed that microtubules tended to fluctuate more around their equilibrium bent positions at small angles. Also, not all microtubules were subjected to exactly the same hydrodynamic force, as differences in microtubule lengths and flow velocities lead to different amounts of force. In addition, the quality and homogeneity of the surface coating with antifouling agents and the resulting degree of friction between microtubules and substrate are likely to change microtubule bending in response to a given force. To reduce the impact of these factors, only microtubules within a small range of lengths that were exposed to similar flow velocities and did not get visibly stuck on the substrate were considered for analysis.

Some parts of the setup were not passivated against protein adsorption (e.g. the PDMS surface of the chip and the tubing). To ensure reproducibility of the results, microtubule growth rate rather than tubulin concentration was used as a reference. The growth rate was monitored before each experiment and the tubulin concentration in the solution was slightly adjusted when necessary.

In spite of these technical limitations, the results presented in the study are without much doubt reliable, as differences could be observed e.g. between microtubules grown at different concentrations that could not be explained by technical factors, which were kept identical for all sets of parameters.

Describing microtubules which locally incorporate tubulin and might therefore exhibit local softening using a constant persistence length is certainly a simplification. It was, however, not possible to measure persistence lengths locally with the given

setup. The presence of slight local 'kinks' in the lattice could sometimes be inferred from a substantial deviation of the bent microtubule shape from the expected curvature based on a homogeneous stiffness. Still, the precision of these observations was limited by the imaging resolution on the one hand, and natural fluctuations in shape of the bent microtubules on the other hand.

Finally, the basic conditions chosen for the experiments might also have an influence on the results, as is the case for all *in vitro* experiments. For example, the pH and ionic strength of the buffer solution are known to influence bimolecular interactions (Spitzer and Poolman, 2009). In addition, the source of the tubulin could be an important factor, as e.g. posttranslational modifications depend on it. Even the way of preparing tubulin has been shown to alter microtubule mechanics, specifically when small quantities of MAPs were present (Hawkins *et al.*, 2012). Microtubule response to bending stress might therefore quantitatively depend on the chosen tubulin source, purification conditions and buffer.

## 2.2 Study 2. Aumeier / Schaedel *et al.*, Nature Cell Biology, 2016

### 2.2.1 Introduction

An important conclusion of the previous study is that GTP tubulin is not only present at microtubule ends, but also, most likely, along the lattice (though probably only transiently), and that this happens in response to mechanical stress which seems to locally favor subunit exchange between the lattice and the medium. The presence of GTP tubulin along the microtubule lattice is in line with the findings of Dimitrov *et al.*, who observed GTP tubulin 'islands' in the lattice using an antibody that recognizes the conformation of GTP tubulin (Dimitrov *et al.*, 2008). As they found a correlation between antibody localization along the lattice and rescue events, they proposed that GTP islands function as rescue sites. GTP is known to be more stably bound in the lattice than GDP tubulin (Alushin *et al.*, 2014) and might therefore stabilize the lattice enough for regrowth to occur. Confirming this hypothesis, a later study showed that the local presence of GMPCPP, a slowly hydrolyzable GTP analog, can promote microtubule rescue (Tropini *et al.*, 2012). These findings were a significant advance in the attempt to better comprehend microtubule rescue, which so far is poorly understood.
However, it is still unclear how stretches of GTP tubulin are generated along the lattice. Dimitrov *et al.* proposed that not all GTP tubulin dimers hydrolyze, and that GTP islands are therefore remnants that are generated during assembly. This hypothesis remains untested, and it seems difficult to justify that some dimers should be exempt from hydrolysis.

The findings of the previous study might provide the missing link between observations of GTP tubulin along the lattice on the one hand and rescue events on the other hand. It was tempting to assume that mechanical stress, leading to GDP

tubulin dissociation and subsequent incorporation of GTP tubulin during repair, could indirectly cause microtubule rescue.

This might be of particular interest for understanding microtubule dynamics *in vivo*: Dynamic instability in cells differs substantially from what is observed *in vitro*. Microtubules often grow persistently to the cell border and then show fast switches between catastrophe and rescue, while shrinking back towards the centrosome is not persistent (Komarova *et al.*, 2002; Gundersen and Bulinski, 1988). Therefore, dynamic instability in cells is likely to be regulated by mechanisms that are distributed non-homogeneously throughout the cell. While associated proteins might favor rescue in certain areas of the cell (Komarova *et al.*, 2002; Arnal *et al.*, 2004; Al-Bassam *et al.*, 2010), GTP tubulin incorporation in response to mechanical stress could be part of the answer to the riddle how microtubule rescue is regulated in cells: Microtubules are often observed to be more bent close to the cell margin than in the interior of the cell (Bicek *et al.*, 2009; Brangwynne *et al.*, 2006), indicating higher mechanical stress and therefore possibly increased GTP tubulin incorporation into the lattice.

The aim of this study was therefore to find out if repair in response to damage could induce rescue events. For this purpose, a method to create damage in a controlled way at a known location was needed. While bending is a physiological way of inducing microtubule damage, the localization of incorporation cannot be predicted: As shown in the first study, though it was more likely to occur in highly bent regions, it did not strictly correlate with the regions of highest curvature (see Fig. 4f of the first study). In addition, the amount of damage induced by bending varied between microtubules.

A way of generating damage at a precise position is by using photo damage, which leads to substantial tubulin incorporation (see Fig. 4a of the first study). In this study, photo damage was therefore chosen as the main way of producing local dam-

age.

The experiments were carried out *in vitro* as well as in cells; the two approaches are complementary as *in vitro* experiments offer controlled environments that allow testing different parameters in a minimal system and easier quantification, while *in vivo* observations directly test the relevance of the findings for cells. In this study, *in vivo* experiments were carried out by Charlotte Aumeier.

nature cell biology

# Self-repair promotes microtubule rescue

Charlotte Aumeier[1,4], Laura Schaedel[1,4], Jérémie Gaillard[1], Karin John[2], Laurent Blanchoin[1,3,5] and Manuel Théry[1,3,5]

**The dynamic instability of microtubules is characterized by slow growth phases stochastically interrupted by rapid depolymerizations called catastrophes. Rescue events can arrest the depolymerization and restore microtubule elongation. However, the origin of these rescue events remains unexplained. Here we show that microtubule lattice self-repair, in structurally damaged sites, is responsible for the rescue of microtubule growth. Tubulin photo-conversion in cells revealed that free tubulin dimers can incorporate along the shafts of microtubules, especially in regions where microtubules cross each other, form bundles or become bent due to mechanical constraints. These incorporation sites appeared to act as effective rescue sites ensuring microtubule rejuvenation. By securing damaged microtubule growth, the self-repair process supports a mechanosensitive growth by specifically promoting microtubule assembly in regions where they are subjected to physical constraints.**

Oriented growth of the microtubule network is a key process in the establishment of cell polarity[1]. The asymmetry of microtubule-network organization exists in various forms and usually involves differences in the protection of microtubules against depolymerization. Examples include the selective stabilization and orientation of microtubules during neuronal axon determination[2–4]; the selective stabilization of microtubules toward the leading edge of migrating cells[5–7] or the basal pole of epithelial cells[8]; the selective bundling of microtubules toward the immune synapse[9]; and the stabilization of a specific subset of microtubules for spindle assembly and orientation[10,11]. Most attention has been paid to the role of components such as Par3[12], mDia/APC[13], GSK3[14], IQGAP[15] or Lis1[16] that promote microtubule capture and stabilization in specific subcellular regions containing defined actin-network compositions. In particular, at the leading edge of migrating cells, microtubules appear to be protected from disassembly that could potentially be induced by the physical barrier of the plasma membrane[17]. The rescuing of microtubules from depolymerization is frequent in such regions where actin retrograde flow is active[5,6,18,19], and thus the rescue events could actively contribute to local differences in microtubule-network growth. However, the mechanisms controlling the occurrence and modulation of those rescue events are still poorly understood[20].

The frequency of rescue events increases with the concentration of free tubulin[21] and in the presence of MAP2, CLIP170 or CLASP[22–24]. Their locations appear to be correlated with the presence of short GTP-tubulin stretches along the microtubule shaft[25,26], but the origin of these stretches is still debated[20]. Recently, in response to bending arising from mechanical perturbations, microtubules have been shown to be capable of self-repair by the incorporation of free tubulin dimers into fractured points of the microtubule lattice[27]. This process of self-repair generates stretches of new tubulin dimers along the microtubule length reminiscent of those GTP-tubulin stretches described previously[25]. It is therefore tempting to hypothesize that microtubule repair sites act as rescue sites. However, microtubule self-repair has not yet been described *in vivo* and the mechanism by which it could promote microtubule rescue, alone[28] or with the help of microtubule-associated proteins[23,24,29,30] (MAPs), still needs to be investigated.

## RESULTS

### Microtubule repair in living cells

The investigation of microtubule repair requires free tubulin dimers to be distinguishable from polymerized dimers so that their incorporation into the microtubule lattice can be detected. Local photo-conversion of mEOS2-tubulin was used to convert some of the green-fluorescent dimers into red-fluorescent dimers (Fig. 1a; where red fluorescence is depicted as magenta). These red-fluorescent dimers rapidly diffused through the cell cytoplasm and became available for incorporation throughout the entire cell. A few minutes after photo-conversion (Supplementary Video 1), spots of red-fluorescent tubulin could be observed at the growing tips of microtubules, as well as along the shafts of pre-existing microtubules (Fig. 1a-I and Supplementary Video 2). Microtubules often grow along pre-existing ones. Therefore,

[1]CytoMorpho Lab, Biosciences & Biotechnology Institute of Grenoble, UMR5168, CEA/INRA/CNRS/Université Grenoble-Alpes, 38054 Grenoble, France. [2]Laboratoire Interdisciplinaire de Physique, CNRS/Université Grenoble-Alpes, 38402 Saint-Martin-d'Hères, France. [3]CytoMorpho Lab, Hopital Saint Louis, Institut Universitaire d'Hematologie, UMRS1160, INSERM/Université Paris Diderot, 75010 Paris, France. [4]These authors contributed equally to this work.
[5]Correspondence should be addressed to L.B. or M.T. (e-mail: laurent.blanchoin@cea.fr or manuel.thery@cea.fr)

Received 16 March 2016; accepted 4 August 2016; published online 12 September 2016; DOI: 10.1038/ncb3406

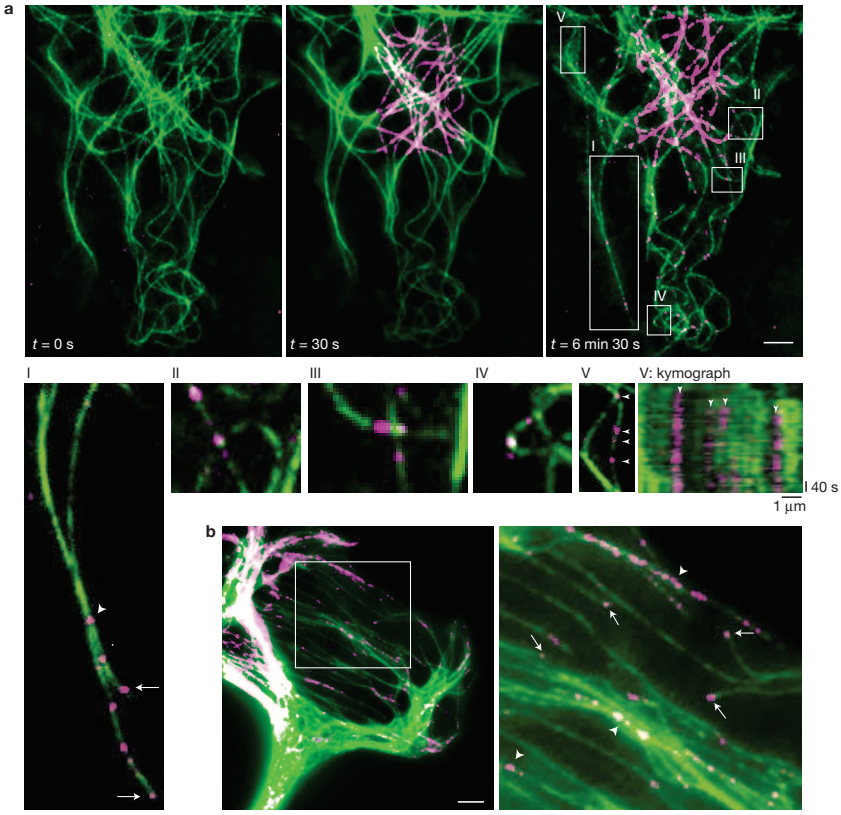


**Figure 1** Microtubule self-repair in living cells. (**a**) A PtK2 cell expressing mEos2 pre- and post-conversion. Converted free tubulin dimers (magenta) diffused through the cytoplasm. The signal of converted dimers (magenta) was observed at the growing tips as well as in spot-like structures along the length of pre-existing microtubules (green). *t*, time. (I–V) Enlarged regions of **a** according to the boxes in the upper right panel. (I) Bundled microtubules with photo-converted tubulin spots within the bundle (arrowhead) and at the growing tip (arrow). Image taken 1 min 35 s after photo-conversion. (II,III) Incorporation of converted dimers (magenta) in pre-existing microtubules (green) at microtubule crossing sites. Images taken respectively 6 min 38 s or 6 min 30 s after photo-conversion, respectively. (IV) Incorporation of converted dimers (magenta) in pre-existing microtubules (green) at bent sites. Image taken 6 min 38 s after photo-conversion. (V) Incorporation along pre-existing microtubules (arrowheads, 3 min after photo-conversion) with the corresponding kymograph. Bottom white arrowhead in (V) is represented by the first left arrowhead of the kymograph in (V - kymograph). (**b**) After photo-conversion the magenta tubulin signal was observed at growing microtubule tips (arrows). True incorporation was not distinguishable from growing tips within bundled microtubules (arrowheads). Arrows indicate growing microtubule tips after photo-conversion; arrowheads indicate sites of incorporation of converted tubulin dimers (magenta) in pre-existing microtubules. Images are representative of five independent experiments. Scale bars, 5 µm.

a local patch of red tubulin along a green microtubule shaft may correspond to a growing secondary microtubule rather than a site of red-tubulin incorporation into the green primary microtubule. However, in the former case, fluorescence intensity should increase over time along the original microtubule, concomitantly with the local incorporation of red tubulin at the growing tip. By observing microtubule fluorescence over several minutes before and after the appearance of red patches, we considered that no change in the fluorescence at the site of the initial red-fluorescent patch implied that tubulin was incorporated into the pre-existing lattice (Fig. 1a-V and V-kymograph). From this analysis, most of the tubulin-incorporation sites were located at microtubule crossovers (Fig. 1a-II, a-III) or in highly curved regions (Fig. 1a-IV). Interestingly, microtubule crossovers are known to recruit katanin[31,32], which has a strong affinity for sites of damaged lattice[33,34], suggesting that the incorporation sites were genuine repair sites. Incorporation sites were also frequently observed along microtubules forming bundles (Fig. 1a-I,1b), although in those cases, it was hard to confirm that the sites did not correspond to growing plus ends.

### Microtubule rescue at repaired sites in living cells

When following microtubule dynamics next to the repair sites, we found that with a microtubule undergoing catastrophe, depolymerization was arrested and regrowth was initiated precisely at the location of the repair site (Fig. 2a and Supplementary Video 3). Unfortunately, it was experimentally challenging to repeat these observations in regions where the network was sufficiently sparse

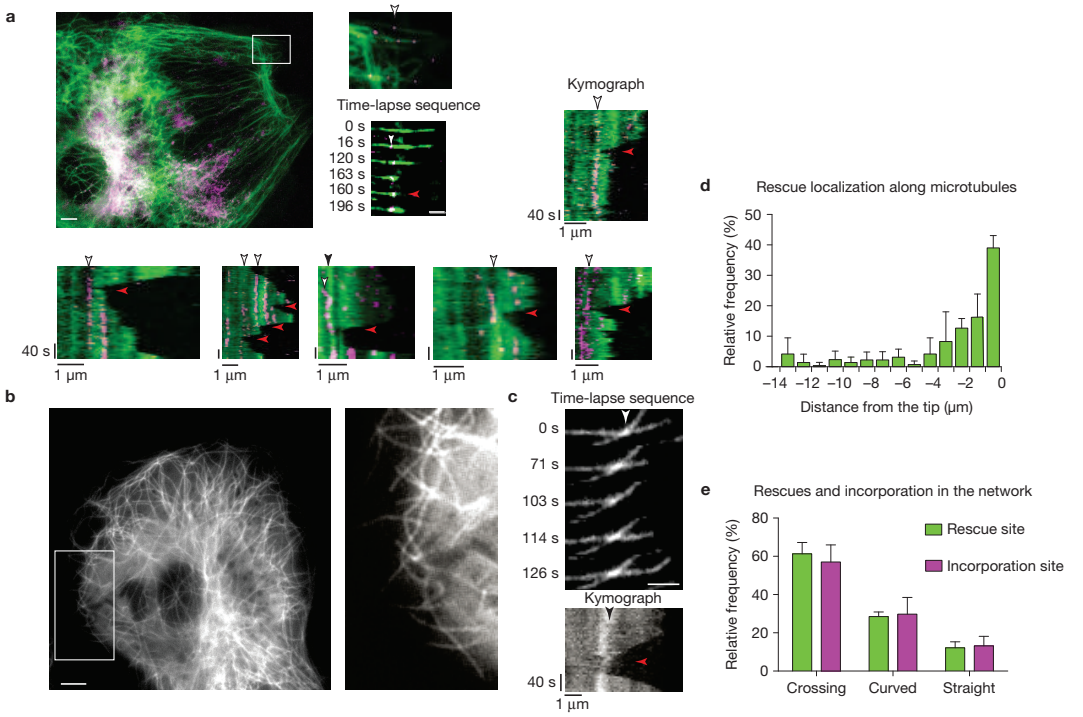


**Figure 2** Self-repair sites are rescue sites in living cells. (**a**) Photo-converted tubulin dimers (magenta) in pre-existing microtubules (green). The white arrowhead in the inset points to a repair site along a single microtubule. Scale bar, 5 µm. The time-lapse sequence shows the occurrence of a rescue event (red arrowhead) at the indicated site of incorporation with the corresponding kymograph (right panel). Scale bar, 2 µm. The kymographs at the bottom show additional examples of repair sites (white arrowheads) associated with rescue events (red arrowheads). The kymograph in the third panel shows an incorporation (white arrow head) and rescue event (red arrowhead) at a microtubule crossing site (black arrowhead). Images are representative of five independent experiments. (**b**) The localization of rescue events was analysed within the cell margin of PtK2 cells stably expressing GFP-tubulin. Enlarged region (white rectangle) of a representative analysed area. Scale bar, 5 µm. (**c**) Representative time-lapse sequence of a rescue event at a microtubule crossing site (white arrowhead) with the corresponding kymograph. The black arrow indicates the crossing site within the kymograph; the red arrow points to the rescue event. The images in **b**,**c** are representative of five independent experiments. Scale bar, 2 µm. (**d**) Histogram of the distance of rescue events with respect to the growing tip (set to zero) in PtK2 GFP-tubulin cells. Data represent mean ± s.d., $n=148$ rescue events from 4 cells. (**e**) Correlation of the site of rescue with the site of incorporation. Relative frequency of the localization of the rescue event, and of the incorporation, with respect to crossing sites, curved sites and straight microtubules. Incorporation was analysed in fixed cells 2 min after photo-conversion. Data represent mean ± s.d., $n=79$ rescue events from 4 cells, and $n=113$ incorporation events from 4 cells.

to follow single microtubules, and in regions where rescues were likely to occur[18]. Alternatively, we decided to record the locations of microtubule rescue events near the cell margin where microtubules show a high rescue frequency[26] (Fig. 2b–d) and compare the locations of rescue sites with those of incorporation sites (Fig. 2e). We found that most rescues occurred close to the microtubule tip (Fig. 2d) at microtubule crossovers (60%) (Supplementary Video 4) or at curved regions (30%) (Fig. 2e). Strikingly, the relative frequencies of microtubule rescues with respect to three different types of microtubule structure (crossover, curved and straight) precisely matched the relative frequencies of incorporation sites (Fig. 2e).

### Microtubule rescue at laser-induced photodamaged sites

To further validate this correlation at the single-microtubule level, and more directly, to test whether the repair of structural damage in the microtubule lattice was responsible for the rescue events, we selected a method to modulate microtubule damage and repair in space and time. This method used focused laser light, which was above the power required for bleaching but below the severing threshold, and can induce local damage and promote further self-repair of microtubules[27,35] (Supplementary Fig. 1a). The method both ensured the genuine occurrence of lattice damage on targeted sites and allowed the monitoring of potential consequential changes in microtubule dynamics at the same sites. We first confirmed that laser-induced photodamage could trigger lattice self-repair by photo-converting mEOS2-tubulin and then focusing the laser on a straight and central section of the microtubule, more than 2 µm away from the microtubule end, where rescues were unlikely (Supplementary Fig. 1b). Photo-converted free tubulin was rapidly incorporated at the photodamaged sites, confirming the effectiveness of the laser to

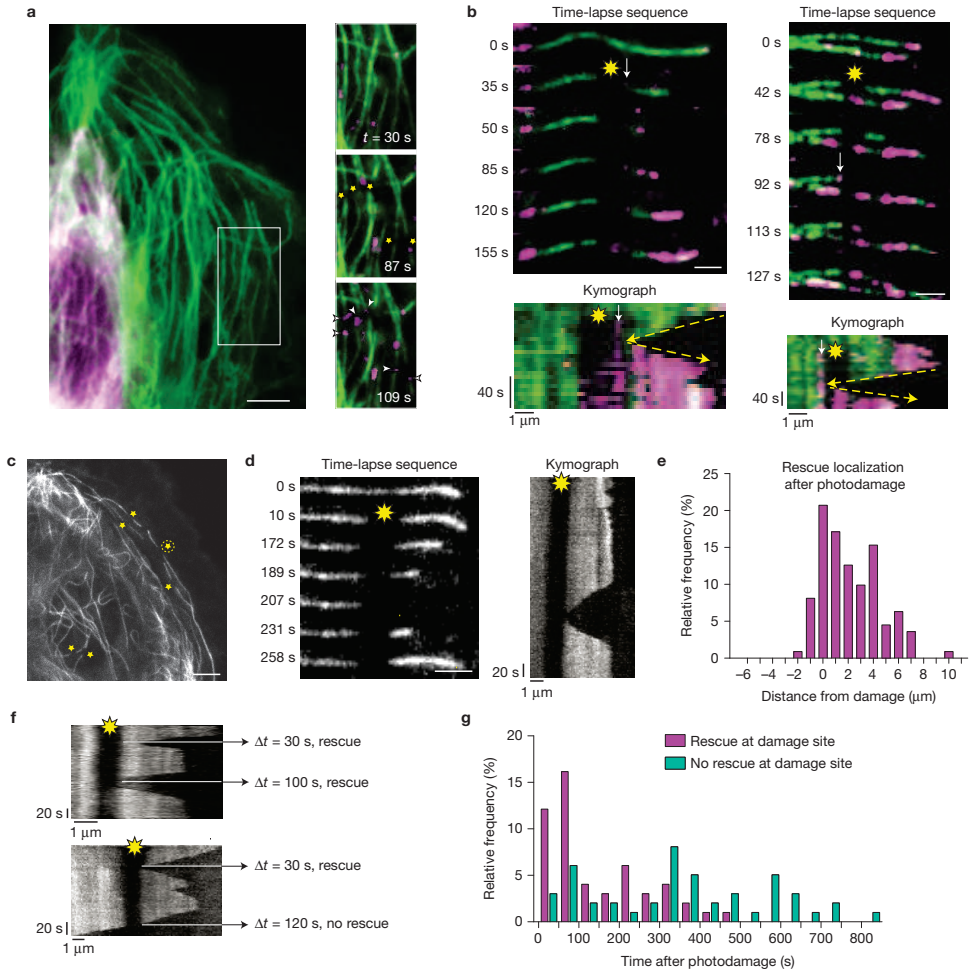


**Figure 3** Photodamaged sites are repair and rescue sites in living cells. Yellow stars indicate photodamage sites; white arrows indicate sites of incorporation of photo-converted tubulin dimers (magenta). Yellow arrows track the depolymerization, rescue and growth events. (**a**) Laser-induced photodamage sites get repaired (arrowheads) by converted tubulin dimers over time. Scale bar, 5 µm. (**b**) Time-lapse sequence with corresponding kymographs of microtubules after laser-induced photodamage. Incorporation of converted tubulin dimers occurs at the photodamage sites and these act as rescue sites. Note within the kymographs that rescue occurs at the exact position of the repair site, highlighted by yellow arrows. Scale bar, 2 µm. (**c**) Representative sites of laser-induced photodamage within the cell margin and near the nucleus of PtK2 GFP-tubulin cells. Time-lapse sequence and kymograph of the rescue event of the microtubule labelled with an encircled star is shown in **d**. Scale bar, 5 µm. (**d**) Representative time-lapse sequence and corresponding kymograph of an analysed microtubule after photodamage. Microtubule rescues at the photodamage site. Images are representative of 5 independent experiments. Scale bar, 2 µm. (**e**) Histogram of the localization of the 111 rescue events with respect to the 51 photodamage sites in 20 PtK2 GFP-tubulin cells. All rescue events occurring along the microtubule were taken into account. The centre of the photodamage site is $x =$ zero; average size of photodamage was 1.2 µm. Fifty per cent of the rescues occurred within the damage site. Only one rescue event was observed a short distance outside the damage site. The other 50% of rescues were observed along the microtubule closer to the tip, where the frequency of rescue is reported to be high. (**f**) Multiple rescues at a photodamage site were observed occasionally. Microtubules depolymerized eventually over the photodamage site after rescue events (bottom image). $\Delta t$, elapsed time after photodamage. (**g**) Histogram of the time between the induction of photodamage ($t = 0$ s) and observation of the rescue or depolymerization event in 10 cells showing 52 rescues at damaged sites and 47 absences of rescue at damaged sites. Rescue events are most frequent within 250 s after photodamage. No rescue was observed after 550 s.

induce microtubule damage and repair (Fig. 3a). Furthermore, we observed rescue events at the incorporation sites that were subsequent to microtubule depolymerization events (Fig. 3b). This behaviour was further quantified by recording the location of the rescue sites with respect to the damaged site (Fig. 3c–e and Supplementary Videos 5 and 6). Photodamaged microtubules rescued more frequently

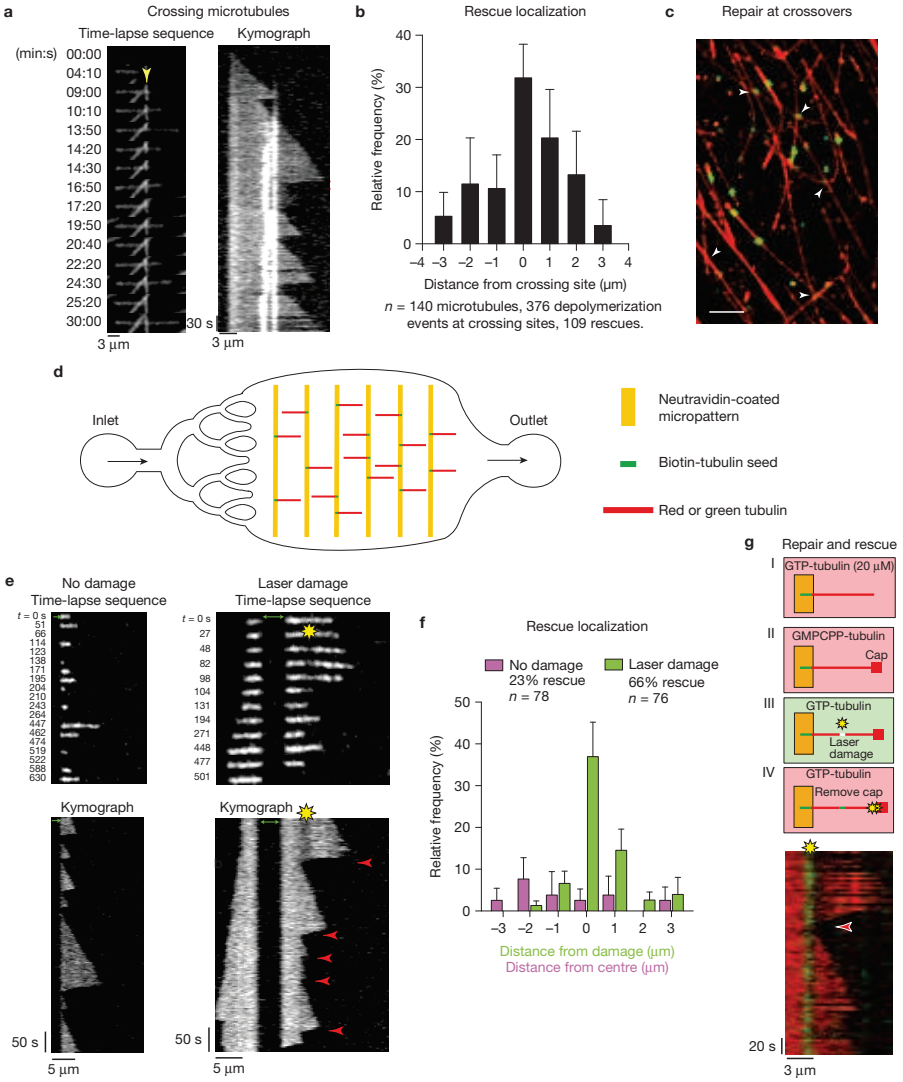


**Figure 4** Microtubule self-repair induces rescue events *in vitro*. (**a**) Rescue at crossing microtubules. Time-lapse sequence of three microtubules crossing each other. The kymograph highlights the crossing sites (yellow arrowhead pointing at the bright white vertical lines) and the occurrence of multiple rescue events at this site (red arrowheads). (**b**) The graph shows the frequency of rescue events for crossing microtubules as a function of distance from the crossing site. Data represent mean ± s.d. from $n=8$ independent experiments. (**c**) Repair at crossing microtubules. Observation of the incorporation of green tubulin dimers along red microtubules. White arrowheads point to crossing sites where accumulation of green tubulin was detected. The image is representative of three independent experiments. Scale bar, 5 µm. (**d**) Illustration of the microfluidic device. Short biotinylated microtubule seeds were fixed on neutravidin-coated micropatterns and elongated using red or green free tubulin. To exchange or remove the solution of free tubulin, a flow was induced parallel to the microtubules. (**e**) Photodamage sites can induce rescue. The time-lapse sequences and kymographs show microtubule dynamics with (right) and without (left) laser-induced damage (yellow star). The green arrows indicate the seed. Red arrowheads indicate rescue events. (**f**) The graph shows the frequency of rescue events for photodamaged microtubules as a function of distance from the centre of the damage (green bars) and for microtubules without damage, as distance from the centre of the observed microtubule (magenta bars). Data represent mean values ± s.d. from $n=4$ independent experiments. (**g**) Tubulin incorporation at photodamaged sites is associated with rescue. Green microtubule seeds were elongated with red free tubulin (step I). A GMPCPP cap was grown at the microtubule tip to avoid spontaneous depolymerization (step II). Photodamage was induced in the presence of green tubulin (step III). Depolymerization was initiated by removing the GMPCPP cap with a laser pulse at high intensity (step IV). The kymograph shows rescue (red arrowhead) at the damaged site (yellow star) where green tubulin was incorporated. GMPCPP, Guanosine-5′-[(α,β)-methyleno]triphosphate, sodium salt. The image is representative of four independent experiments.

(75%, 41/55, Fig. 3g) within a time frame of 4 min than non-photodamaged microtubules (39%, 24/62). The increased frequency is due to additional rescue events occurring next to the photodamaged site, regardless of its position along the microtubule (Fig. 3d,e and Supplementary Videos 5 and 6). It is noteworthy that repair by incorporation of new dimers was tightly focused and did not occur over the entire length of the targeted region, but rescues systematically occurred at the exact position of the repair site either on the right or on the left of the targeted region (Fig. 3b). These results clearly showed that microtubule damage and repair provided the microtubule with protection from depolymerization. Interestingly, some observations suggested that the protective effect did not last indefinitely (Fig. 3f). More quantitative experiments of longer duration further revealed that protection was quite effective within a two-minute period after photodamage. However, protection was progressively less effective from 2 to 8 min after photodamage (Fig. 3g). This effect of time showed that the microtubule repair and rescue events were not due to permanent structural changes and suggested that additional biochemical regulation was involved at longer timescales.

### Microtubule self-repair and rescue *in vitro*

At the repair site, newly incorporated dimers were certainly associated with GTP-tubulin, as is the case for dimer assembly at the growing end of the microtubule. Hence, the subsequent rescue event could have depended on intrinsic structural factors, such as the specific conformation of GTP-tubulin dimers[36], and extrinsic factors, such as the numerous proteins preferentially interacting with GTP-tubulin dimers[23,24,29,30]. To elucidate the mechanism of microtubule rescue after damage and repair events, and to identify the minimal conditions sufficient to support the mechanism, we performed *in vitro* experiments based on purified tubulin dimers that self-assembled to form microtubules on glass slides. This set-up provided more defined conditions than *in vivo* and could be used to challenge the role of MAPs during rescue at incorporation sites.

We first investigated the rescue events in networks of dynamic microtubules. They appeared preferentially localized at crossing sites (Fig. 4a,b and Supplementary Video 8, see Methods) confirming our observations *in vivo* (Fig. 2c,e). To test whether these sites corresponded to self-repair events based on free tubulin incorporation, we screened long microtubules, assembled from red tubulin and stabilized with a GMPCPP cap, in a medium containing free green tubulin dimers. Self-repair indeed occurred at crossing sites (Fig. 4c). Half of the 300 crossing sites (from 3 independent experiments) displayed incorporation of free tubulin in the seven minutes following free tubulin exchange.

To further quantify the repair and rescue events in single dynamic microtubules in a controlled environment, microtubules were assembled in a microfluidic device. Short microtubule fragments were adsorbed onto micropatterned lines and used as seeds to induce microtubule polymerization. Micropatterned lines were surrounded with PEG to minimize microtubule interactions with the glass-slide surface[37]. The micropatterned glass coverslips were mounted on a microfluidic circuit to modulate the addition and removal of soluble components without moving the microtubules under observation[27] (Fig. 4d). Laser light was used to generate photodamage on dynamic microtubules. As expected from our previous work[27], photodamaged microtubules self-repaired by incorporating free tubulin in the damaged site (Supplementary Fig. 2). In the absence of photodamage, rescue events were occasional (in 18 out of 78 microtubules) and randomly dispersed along the microtubule (Fig. 4f). By contrast, most photodamaged microtubules underwent depolymerization that was subsequently rescued (50 out of 76 microtubules, Fig. 4e,f and Supplementary Fig. 3 and Supplementary Video 7). These rescue events were precisely located at the sites of damage (Fig. 4e) where self-repair occurred (Fig. 4g) showing that damage/repair sites could protect microtubules from depolymerization independently of the presence of MAPs or any other cellular compound.

### Incorporation and hydrolysis of free tubulin

We then tested whether repair was actually required for rescue or whether damage in the lattice was sufficient to block microtubule depolymerization. Microtubules were photodamaged in the absence of free tubulin to prevent lattice self-repair. We ensured that the laser power and frequency were appropriate and did not induce microtubule breakage or lattice cauterization (Supplementary Fig. 4). Elongated microtubules were capped with non-hydrolysable GMPCPP-tubulin to protect the ends from initiating depolymerization that would otherwise occur in the absence of free tubulin (Fig. 5a). After a microtubule was photodamaged, the laser power was increased to sever the cap from the microtubule and trigger microtubule depolymerization (Methods). Under these conditions, no rescue events, pauses or arrests in depolymerization were observed at the damaged and non-repaired sites (Fig. 5a). This showed that lattice self-repair by the incorporation of free tubulin dimers was essential to protect the microtubule from depolymerization. Moreover, this dependency on free tubulin could account for the observations that rescue frequency also depends on the concentration of free tubulin[21,24]. Interestingly, it appeared that the protective capacity provided by the repair site, in the presence of free tubulin, was limited by time, similar to what was observed *in vivo*. Rescue events were frequent within 3 min after the damage/repair event (73%, 38/52), but less frequent from 3 to 20 min after the damage/repair event (30%, 14/47) (Fig. 5b). Nucleotide hydrolysis following tubulin polymerization at the microtubule tip effects the conformation and stability of the lattice structure[38]; we therefore tested whether hydrolysis of incorporated GTP tubulin was involved in rescue regulation. We compared the rescuing frequency at repair sites depending on the insertion of free tubulin dimers in the presence of control (GTP) and non-hydrolysable (GMPCPP) nucleotide 5 to 10 min after damaging microtubules with the laser (Fig. 5b). As tubulin bound to GMPCPP formed numerous seeds, the rescue effect had to be tested in the presence of a sub-critical concentration of free tubulin dimers to prevent the growth of too many additional microtubules next to our observation region. The pauses at the laser-damage site, following cap removal and microtubule depolymerization, were twice more frequent when microtubules were repaired with tubulin dimers bound to GMPCPP (Fig. 5c), confirming that nucleotide hydrolysis was limiting the rescue lifetime.

### Recruitment of MAPs with affinity for GTP-tubulin

At the microtubule growing tip, newly incorporated tubulin dimers together with specific proteins that have high affinity for GTP-bound tubulin form a cap that protects microtubules from

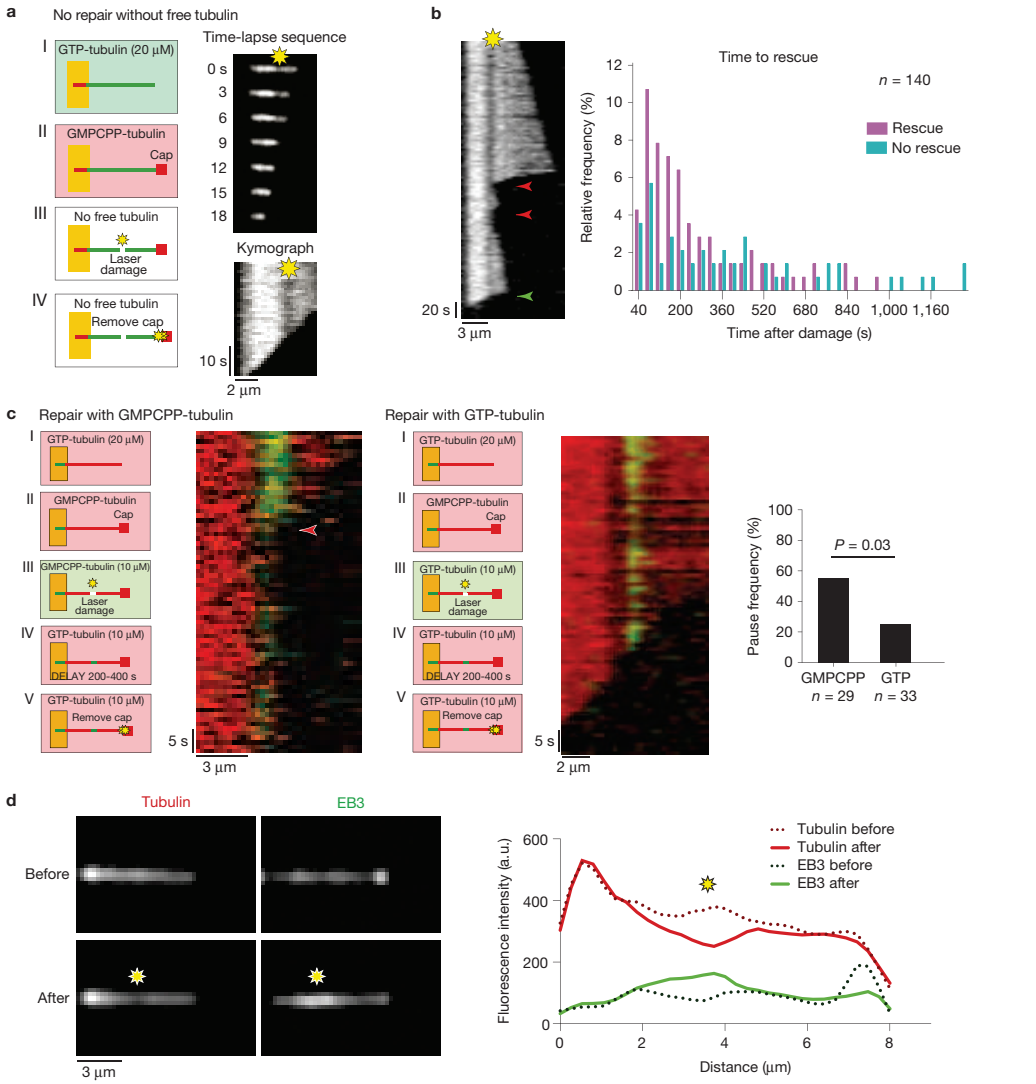


**Figure 5** Incorporation and hydrolysis of free tubulin. (**a**) Damage without repair. Red microtubule seeds were elongated with green free tubulin (step I). A GMPCPP cap was grown at the microtubule tip to avoid spontaneous depolymerization (step II). Photodamage was induced in the absence of free tubulin (step III). Depolymerization was initiated by removing the GMPCPP cap with a laser pulse at high intensity (step IV). The time-lapse sequence and kymograph show no rescue nor pause at the damaged (yellow star), and non-repaired, site. See quantification in Supplementary Fig. 4. (**b**) Rescue lifetime. The kymograph shows multiple rescues (red arrowheads) at a photodamage site (yellow star) eventually followed by microtubule depolymerization (green arrowhead). The graph represents the time between inducing the damage and observation of the rescue or depolymerization event. Rescue events become less frequent as the time after damage increases. No rescue could be observed 17 min after inducing the damage. (**c**) Hydrolysis of incorporated tubulins. Red microtubules were laser damaged and repaired with non-hydrolysable (GMPCPP, left panels) or hydrolysable (GTP, right panels) tubulin. After an additional delay of 3 to 6 min, the cap was removed in the presence of a sub-critical concentration of free tubulin. The graph shows the frequency of pauses (highlighted in the left panel with a red arrowhead) in both cases. Non-hydrolysable tubulins increased the lifetime of repair and rescue sites. A chi-square test was used to compare pause frequencies for GTP and GMPCPP. *n* represents the number of microtubules that were allowed to repair in the presence of GTP and GMPCPP, respectively. (**d**) EB3 recruitment at repair sites. Red microtubules were photodamaged in the presence of red-fluorescent free tubulin dimers and EB3-GFP. The images show microtubule fluorescence in the red (left) and green (right) channels, before (top) and after (bottom) the laser-induced damage. The graph shows fluorescent linescans along this microtubule before and after the damage. The yellow star represents the damaged site. More examples are shown in Supplementary Fig. 5 as well as absence of EB3 recruitment in the absence of free tubulin. Images are representative of five independent experiments.

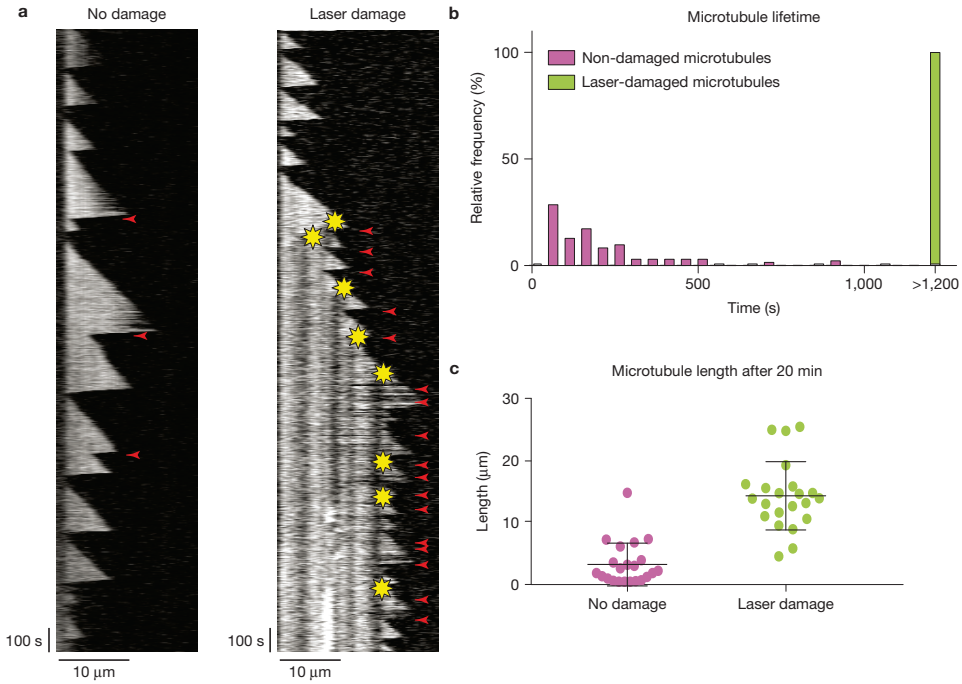


**Figure 6** Self-repair biases microtubule dynamic instability *in vitro*. (**a**) The kymograph on the left shows a typical non-damaged microtubule with infrequent rescue events. On the right, the microtubule was damaged several times close to the tip as soon as it grew out long enough. Although catastrophe events were frequent, this microtubule was protected from complete depolymerization by the photodamage. The yellow stars indicate the photodamage sites. The red arrowheads indicate rescue events. (**b**) Damage increases microtubule lifetime. The graph shows the distribution of 28 laser-damaged (green) and 133 non-damaged (magenta) microtubule lifetimes. Damaged microtubule lifetime was found to be considerably longer than the lifetime of non-damaged microtubules. (**c**) Damage increases microtubule length. The graph shows the length of laser-damaged (green) and non-damaged (magenta) microtubules after 20 min. Error bars show mean ± s.d. for $n=22$ microtubules per condition, pooled from 4 independent experiments.

depolymerization[39]. These proteins could then be recruited to repair sites, which are also made of GTP-tubulin, and form some cap-like structures that could act as rescue factors[23,24,29,30]. To test this hypothesis, we grew red-fluorescent microtubules and followed microtubule repair after laser-induced damage, in the presence of red-fluorescent tubulin and GFP-tagged end-binding protein 3 (EB3). We found that lattice damage, which we could visualize by the reduction of fluorescent tubulin along the lattice, was associated with a specific recruitment of EB3 at the repair site (Fig. 5d). Interestingly, this recruitment was firmly dependent on the incorporation of free tubulin at the damaged site since it could not be detected in the absence of free tubulin (Supplementary Fig. 5). Therefore, the self-repair process induced GTP islands resembling cap structures along the microtubule lattice that are able to recruit proteins with high affinity for GTP-tubulin. Although we could not detect such recruitment in cells following laser-induced damage because of the high background of cytoplasmic EBs, this cap could contribute to the rescue process *in vivo*[23,24,29,30]. However, our previous data *in vitro* showed that the incorporation of free tubulin was necessary (Fig. 5a) and sufficient (Fig. 4b,c) to promote microtubule rescue. Microtubule repair by free tubulin incorporation conditioned the recruitment of EBs and associated proteins, which may contribute but did not appear to be required to promote microtubule rescues.

## Repeated damage lengthens microtubule protection from depolymerization

*In vitro*, a single event of microtubule repair had a time-limited effect on microtubule dynamics. We reasoned that *in vivo* the duration of protection against depolymerization could be extended in situations when repair events occur frequently, for example, at the cell margin where microtubules often crossover their neighbours, form bundles and are repeatedly bent by the retrograde flow of actin[6]. Indeed, repeated photodamage near the tip of microtubules growing *in vitro* in the presence of 12 µM of tubulin could prevent catastrophic depolymerization for more than 20 min, whereas, in the absence of damage, depolymerization frequently occurred within 5 min (Fig. 6a,b and Supplementary Fig. 6 and Supplementary Video 9). Therefore, damaged microtubules became much longer (Fig. 6c). Remarkably, the targeting of individual microtubules using the same approach *in vivo* had similar consequences. We focused on peripheral cell parts where microtubules were sparse. To compare the effects of laser-induced damage on microtubules with the nonspecific damage the laser may

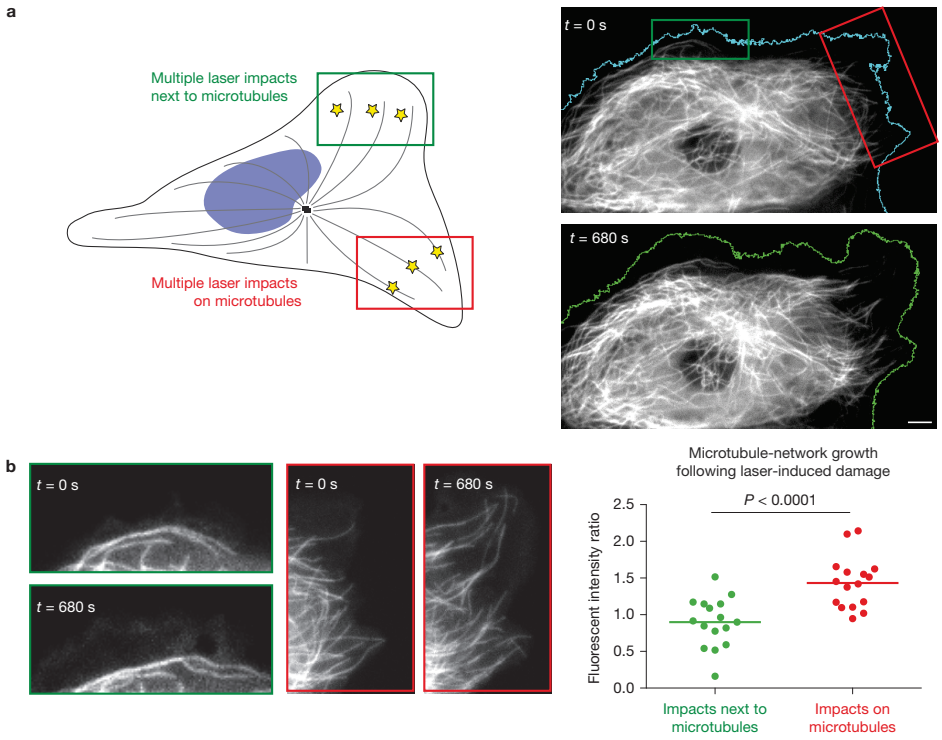


**Figure 7** Self-repair biases microtubule dynamic instability *in vivo*. (**a**) Repeated microtubule shooting 'on-' and 'off-target'. Laser-induced photodamage was targeted either on the microtubules, in the red region, or next to the microtubules, in the green region. The images show the cell before (top) and after (bottom) the shooting. A comparison of the left and right cell margin pre- and post-photodamage is shown. Scale bar, 5 μm. (**b**) Preferential microtubule-network growth in damaged regions. Images show the microtubule network in the 'on-target' (red) and 'off-target' (green) regions before ($t = 0$ s) and after ($t = 680$ s) the shooting. The graph shows the after/before ratio of the mean microtubule fluorescence intensity in each region. Lines represent mean values from $n = 16$ cells from 4 independent experiments. The $P$ value was generated by a Wilcoxon paired test. The total microtubule length increased in the regions where the laser impacts were targeted on the microtubules.

cause to all surrounding components, pulses were simultaneously sent to two distinct subcellular regions. In one the laser impacts targeted the microtubules, in the other they were focused next to microtubules (Fig. 7a). The evolution of the microtubule network was followed over 10 to 15 min during which both regions were subjected to repeated laser pulses (Fig. 7a and Supplementary Video 10). Laser-induced photodamage of every microtubule that approached the cell margin robustly protected those microtubules from depolymerization and promoted their elongation whereas no net extension of the network was seen when impacts were off-target (Fig. 7b and Supplementary Video 10). The damaged microtubules underwent multiple rescue events, continued to grow and eventually aligned parallel to the cell edge (Supplementary Fig. 7 and Supplementary Video 10). These effects were quantified by measuring the ratio of fluorescent tubulin before and after the laser-induced damage on the two windows of laser pulses. No net growth was detected when laser impacts were off-target whereas an average of 50% increase was measured when impacts were focused on microtubules (Fig. 7b). Strikingly, cells then tend to move toward this newly defined leading edge (Fig. 7a and Supplementary Fig. 8 and Supplementary Videos 10 and 11). These observations were consistent with the known enhancement of cell motility in response to microtubule overgrowth following downregulation of microtubule severing enzymes[40,41]. Therefore, damage and self-repair appeared capable of sustaining microtubule polymerization in cells and affect higher-order processes such as modulating the polarity of a motile cell.

## DISCUSSION

Our results have revealed a mechanical and structural mechanism by which a damaged microtubule can acquire a capacity to prevent its catastrophic depolymerization through the incorporation of new dimers of tubulin.

Incorporation could be directly visualized thanks to the monitoring of photo-converted tubulin dimers. It occurred not only at microtubule ends but also along the microtubule shaft. It was not randomly distributed along the microtubule length but preferentially located in regions where the lattice is likely to be submitted to geometrical and mechanical constraints such as microtubule crossover, bundle and bending sites (Fig. 8a). Solid friction between adjacent

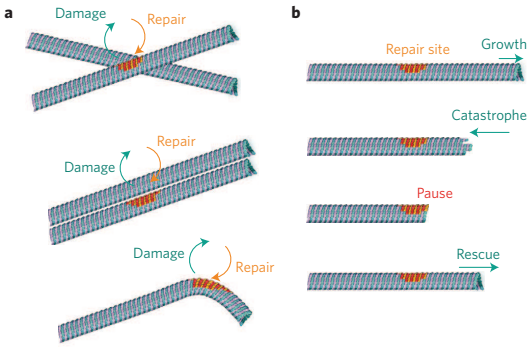


**Figure 8** Microtubule self-repair and rescue. (**a**) Microtubule self-repair. The schemes show the preferential conformation of microtubules in which free tubulin incorporation (orange–red) was observed along pre-existing microtubules (green–blue) in living cells. (**b**) Microtubule rescue at self-repair sites. The schemes show the interruption of microtubule depolymerization at the repaired site (shown with orange–red dimers) and the induction of microtubule regrowth.

microtubules[42] and microtubule bending by guiding motors[43] or surrounding networks[6] are general sources of mechanical stress in the lattice that could promote protofilament peeling and dimer removal. Although our observations of lattice turnover at microtubule crossover *in vitro* did not involve any additional component than the physical constraints on microtubules[27], proteins with specific affinity for these network conformations, such as bundling proteins, may contribute to the lattice turnover via their binding to tubulin dimers[44]. In return, the appearance of new protofilament ends and the incorporation of new tubulin dimers at damaged sites may promote the local recruitment of specific proteins, such as EB3 in our observations. Katanin for example, which is known to localize at microtubule crossovers[32], may be recruited according to its affinity for the damaged lattice and further benefit from the open structure to sever microtubules. Similarly, doublecortin, which recognizes plus ends and bent regions, may benefit from lattice damage and turnover for its targeting[45]. The high degree of microtubule lattice plasticity revealed by our data opened many interesting perspectives in the regulation of MAPs.

Microtubule lattice plasticity also impacts microtubule dynamics, since the incorporation of new dimers rejuvenates the lattice. Our observation of red tubulin stretches along green microtubule length, which had already been indirectly observed with antibodies directed against the GTP conformation of tubulin dimers[25], signed the implication of external tubulin incorporation for lattice repair, rather than internal lattice remodelling, at damaged sites. As was reported for the GTP-stretch[25], we found that the newly incorporated dimers were responsible for microtubule rescue (Fig. 8b). Hence, the repair sites appear to act as plus-end-like 'mini caps' that can protect the microtubule from depolymerization and support subsequent elongation. Importantly, our *in vitro* experiments show that the incorporation of new tubulin dimers in the absence of MAPs is sufficient to rescue microtubule depolymerization. However, we documented the ability of newly incorporated dimers to recruit EB3. Additional MAPs with high affinity for GTP-tubulin, such as CLASP, could also be recruited and further contribute to the rescue mechanism in cells[23,24,29,30]. Thus, microtubule rejuvenation by incorporation of new tubulin dimers could synergize with MAPs recruitment to enhance the autonomous rescuing capacities of repair sites.

Finally, the repair and rescue mechanism we described biases the dynamic instability of the microtubule in a direction where the lifespan and maximal length are greater than would have occurred in a stochastic process without damage. What is also notable is that the repair process provides a mechanosensitive feedback loop that specifically promotes microtubule extension in intracellular regions where network entanglement and physical constraints are higher, and hence supports the directed growth of the microtubule network within the cell. □

## METHODS

Methods, including statements of data availability and any associated accession codes and references, are available in the online version of this paper.

*Note: Supplementary Information is available in the online version of the paper*

ACKNOWLEDGEMENTS

We thank G. Montagnac for sharing his unpublished data on tubulin photoactivation in cells; and F. Perez and C. Poüs for sharing their unpublished data on the microtubule rescue by CLIP170. This work has been supported by HFSP (RGY0088/2012), ANR funding (ANR-12-BSV5-0014) and ERC (Starting Grant 310472).

AUTHOR CONTRIBUTIONS

C.A. performed experiments in cells. L.S. and J.G. performed the experiments *in vitro*. L.B. and M.T. directed the work. C.A., L.S., K.J., L.B. and M.T. analysed the data. M.T. wrote the paper.

COMPETING FINANCIAL INTERESTS

The authors declare no competing financial interests.

Published online at http://dx.doi.org/10.1038/ncb3406
Reprints and permissions information is available online at www.nature.com/reprints

1. Mimori-Kiyosue, Y. Shaping microtubules into diverse patterns: Molecular connections for setting up both ends. *Cytoskeleton* **68,** 603–618 (2011).
2. Hammond, J. W. *et al.* Posttranslational modifications of tubulin and the polarized transport of kinesin-1 in neurons. *Mol. Biol. Cell* **21,** 572–583 (2010).
3. Winans, A. M., Collins, S. R. & Meyer, T. Waves of actin and microtubule polymerization drive microtubule-based transport and neurite growth before single axon formation. *ELife* **5,** 1–22 (2016).
4. Stiess, M. *et al.* Axon extension occurs independently of centrosomal microtubule nucleation. *Science* **327,** 704–707 (2010).
5. Wadsworth, P. Regional regulation of microtubule dynamics in polarized, motile cells. *Cell Motil. Cytoskeleton* **42,** 48–59 (1999).
6. Waterman-Storer, C. M. & Salmon, E. D. Actomyosin-based retrograde flow of microtubules in the lamella of migrating epithelial cells influences microtubule dynamic instability and turnover and is associated with microtubule breakage and treadmilling. *J. Cell Biol.* **139,** 417–434 (1997).
7. Gundersen, G. G. & Bulinski, J. C. Selective stabilization of microtubules oriented toward the direction of cell migration. *Cell* **85,** 5946–5950 (1988).
8. Akhtar, N. & Streuli, C. H. An integrin-ILK-microtubule network orients cell polarity and lumen formation in glandular epithelium. *Nat. Cell Biol.* **15,** 17–27 (2012).
9. Yi, J. *et al.* Centrosome repositioning in T cells is biphasic and driven by microtubule end-on capture-shrinkage. *J. Cell Biol.* **202,** 779–792 (2013).
10. Sampath, S. C. *et al.* The chromosomal passenger complex is required for chromatin-induced microtubule stabilization and spindle assembly. *Cell* **118,** 187–202 (2004).
11. Grill, S. W., Go, P. & Hyman, A. A. Polarity controls forces governing asymmetric spindle positioning in the *Caenorhabditis elegans* embryo. *Nature* **409,** 630–633 (2001).
12. Labbe, J. *et al.* PAR proteins regulate microtubule dynamics at the cell cortex in *C. elegans*. *Curr. Biol.* **13,** 707–714 (2003).
13. Wen, Y. *et al.* EB1 and APC bind to mDia to stabilize microtubules downstream of Rho and promote cell migration. *Nat. Cell Biol.* **6,** 820–830 (2004).
14. Etienne-manneville, S. & Hall, A. Cdc42 regulates GSK-3 b and adenomatous polyposis coli to control cell polarity. *Nature* **421,** 753–756 (2003).
15. Fukata, M. *et al.* Rac1 and Cdc42 capture microtubules through IQGAP1 and CLIP-170. *Cell* **109,** 873–885 (2002).

16. Dujardin, D. L. *et al.* A role for cytoplasmic dynein and LIS1 in directed cell movement. *J. Cell Biol.* **163,** 1205–1211 (2003).
17. Janson, M. E., de Dood, M. E. & Dogterom, M. Dynamic instability of microtubules is regulated by force. *J. Cell Biol.* **161,** 1029–1034 (2003).
18. Komarova, Y. A., Vorobjev, I. A. & Borisy, G. G. Life cycle of MTs: persistent growth in the cell interior, asymmetric transition frequencies and effects of the cell boundary. *J. Cell Sci.* **115,** 3527–3539 (2002).
19. Shelden, E. & Wadsworth, P. Observation and quantification of individual microtubule behavior *in vivo*: microtubule dynamics are cell-type specific. *J. Cell Biol.* **120,** 935–945 (1993).
20. Gardner, M. K., Zanic, M. & Howard, J. Microtubule catastrophe and rescue. *Curr. Opin. Cell Biol.* **25,** 14–22 (2013).
21. Walker, R. A. *et al.* Dynamic instability of individual microtubules analyzed by video light microscopy: rate constants and transition frequencies. *J. Cell Biol.* **107,** 1437–1448 (1988).
22. Kowalski, R. J. & Williams, R. C. Microtubule-associated protein 2 alters the dynamic properties of microtubule assembly and disassembly. *J. Biol. Chem.* **268,** 9847–9855 (1993).
23. Komarova, Y. A., Akhmanova, A., Kojima, S. I., Galjart, N. & Borisy, G. G. Cytoplasmic linker proteins promote microtubule rescue *in vivo*. *J. Cell Biol.* **159,** 589–599 (2002).
24. Al-Bassam, J. *et al.* CLASP promotes microtubule rescue by recruiting tubulin dimers to the microtubule. *Dev. Cell* **19,** 245–258 (2010).
25. Dimitrov, A. *et al.* Detection of GTP-tubulin conformation *in vivo* reveals a role for GTP remnants in microtubule rescues. *Science* **322,** 1353–1356 (2008).
26. Tropini, C., Roth, E. A., Zanic, M., Gardner, M. K. & Howard, J. Islands containing slowly hydrolyzable GTP analogs promote microtubule rescues. *PLoS ONE* **7,** e30103 (2012).
27. Schaedel, L. *et al.* Microtubules self-repair in response to mechanical stress. *Nat. Mater.* **14,** 1156–1163 (2015).
28. Billger, M. A., Bhatacharjee, G. & Williams, R. C. Dynamic instability of microtubules assembled from microtubule- associated protein-free tubulin: neither variability of growth and shortening rates nor 'rescue' requires microtubule-associated proteins. *Biochemistry* **35,** 13656–13663 (1996).
29. Vitre, B. *et al.* EB1 regulates microtubule dynamics and tubulin sheet closure *in vitro*. *Nat. Cell Biol.* **10,** 415–421 (2008).
30. Arnal, I., Heichette, C., Diamantopoulos, G. S. & Chrétien, D. Clip-170/tubulin-curved oligomers coassemble at microtubule ends and promote rescues. *Curr. Biol.* **14,** 2086–2095 (2004).
31. Wightman, R. & Turner, S. R. Severing at sites of microtubule crossover contributes to microtubule alignment in cortical arrays. *Plant J.* **52,** 742–751 (2007).
32. Zhang, Q., Fishel, E., Bertroche, T. & Dixit, R. Microtubule severing at crossover sites by Katanin generates ordered cortical microtubule arrays in *Arabidopsis*. *Curr. Biol.* **23,** 2191–2195 (2013).
33. Davis, L. J., Odde, D. J., Block, S. M. & Gross, S. P. The importance of lattice defects in katanin-mediated microtubule severing *in vitro*. *Biophys. J.* **82,** 2916–2927 (2002).
34. Díaz-Valencia, J. D. *et al.* Drosophila katanin-60 depolymerizes and severs at microtubule defects. *Biophys. J.* **100,** 2440–2449 (2011).
35. Walker, R. A., Inou, S. & Salmon, E. D. Asymmetric behavior of severed microtubule ends after ultraviolet-microbeam irradiation of individual microtubules *in vitro*. *Cell* **108,** 931–937 (1989).
36. VanBuren, V., Cassimeris, L. & Odde, D. J. Mechanochemical model of microtubule structure and self-assembly kinetics. *Biophys. J.* **89,** 2911–2926 (2005).
37. Portran, D., Gaillard, J., Vantard, M. & Théry, M. Quantification of MAP and molecular motor activities on geometrically controlled microtubule networks. *Cytoskeleton (Hoboken)* **70,** 12–23 (2013).
38. Alushin, G. M. *et al.* High-resolution microtubule structures reveal the structural transitions in αβ-tubulin upon GTP hydrolysis. *Cell* **157,** 1117–1129 (2014).
39. Bowne-Anderson, H., Zanic, M., Kauer, M. & Howard, J. Microtubule dynamic instability: a new model with coupled GTP hydrolysis and multistep catastrophe. *BioEssays* **35,** 452–461 (2013).
40. Zhang, D. *et al. Drosophila* katanin is a microtubule depolymerase that regulates cortical-microtubule plus-end interactions and cell migration. *Nat. Cell Biol.* **13,** 361–370 (2011).
41. Charafeddine, R. A. *et al.* Fidgetin-like 2: a microtubule-based regulator of wound healing. *J. Invest. Dermatol.* **135,** 2309–2318 (2015).
42. Ward, A. *et al.* Solid friction between soft filaments. *Nat. Mater.* **14,** 583–588 (2015).
43. Doodhi, H., Katrukha, E. A., Kapitein, L. C. & Akhmanova, A. Mechanical and geometrical constraints control kinesin-based microtubule guidance. *Curr. Biol.* **24,** 1–7 (2014).
44. Ahmadzadeh, H., Smith, D. H. & Shenoy, V. B. Mechanical effects of dynamic binding between tau proteins on microtubules during axonal injury. *Biophys. J.* **109,** 2328–2337 (2015).
45. Bechstedt, S. & Brouhard, G. J. Doublecortin recognizes the 13-protofilament microtubule cooperatively and tracks microtubule ends. *Dev. Cell* **23,** 181–192 (2012).

DOI: 10.1038/ncb3406

## METHODS

**Imaging.** Microtubules were visualized using an objective-based azimuthal ilas2 TIRF microscope (Nikon Eclipse Ti, modified by Roper Scientific) and an Evolve 512 camera (Photometrics). The cell culture conditions on the microscope stage were controlled with the Chamlide TC incubator (kept at 37 °C and 5% $CO_2$). For *in vitro* experiments, the microscope stage was kept at 37 °C by means of a warm stage controller (LINKAM MC60). Excitation was achieved using lasers with wavelengths of 491 and 561 nm (Optical Insights). Time-lapse recording was performed using Metamorph software (version 7.7.5, Universal Imaging). Videos were processed to improve the signal/noise ratio (subtract background, smooth and PureDenoise functions of ImageJ, version 1.47n5). The kymographs corresponding to the time-lapse sequences were drawn using ImageJ. Images were taken every 300 ms to 5 s (*in vitro*) and 3 s to 7 s (microtubule dynamics *in vivo*) or 10 s to 2 min (cell migration). For *in vitro* experiments showing incorporation of labelled tubulin in photodamaged microtubules, 30 successive individual images were overlaid and background subtracted.

**Live cell imaging.** PtK2 cells stably expressing GFP-tubulin (a gift from F. Perez, Curie Institute, Paris, France) were cultured on glass coverslips for microscopy. The PtK2 cell line (Sigma Aldrich) was transfected with Lipofectamine 2000 (Thermo Fisher Scientific) according to a protocol with the photo-conversion protein fused to tubulin mEOS2-tubulin (a gift from M. Davidson, Florida State University, Florida, USA; Addgene plasmid no. 57431). All cell lines were tested monthly for mycoplasma contamination. No cell lines used in this study were found in the database of commonly misidentified cell lines that is maintained by ICLAC and NCBI Biosample. We did not attempt to authenticate them. For long-time imaging (10 min, time frame 4 s) after photo-conversion the stable PtK2 GFP-tubulin cell line was transfected with the mEOS2-tubulin construct to overcome bleaching of the unconverted green signal. Photo-conversion was achieved with a 100 mW/405 nm laser used at 9% power, performing 15 repetitions within a field size varying between 12 μm × 12 μm to 30 μm × 30 μm.

**Fixation.** Cells expressing mEOS2-tubulin were fixed 2 min after photo-conversion. Cells were detergent-extracted with BRB80 + 4 mM EGTA supplemented with 0.2% Triton X-100 at 37° for 15 s. Glutaraldehyde and Triton X-100 were added to a final concentration of 0.5% each and cells were fixed for 10 min. Cells were rinsed twice using PBS supplemented with 1% Triton X-100 and incubated twice with 1% $NaBH_4$ in PBS for 7 min. Cells were rinsed in PBS and imaged. Ten cells from four independent experiments were analysed.

**Laser-induced microtubule photodamage.** Laser-induced microtubule photodamage was performed using a Laser illuminator iLas2 (Roper Scientific) set up on an inverted microscope (Ti-E, Nikon) with a ×100 Nikon APO TIRF oil-immersion objective plus an optical lens ×1.45. iLas2 is a dual-axis galvanometer-based optical scanner that focuses the laser beam on the sample (diffraction-limited spot size) over the whole field of view of the camera. Laser displacement, exposure time, frequency and repetition rate were controlled using Metamorph software (version 7.7.9.0, Universal Imaging). To damage the microtubules of the GFP-tubulin or mEos2-tubulin cell line, a 200 mW/491 nm laser was used at 40% power, performing 300 repetitions within a field size of approximately 1 μm × 1 μm. To analyse the long-term effect of laser-induced photodamage with respect to rescue, microtubules were repeatedly photodamaged along the lattice (twice or three times). This increased the lifetime of the microtubule and the damage farthest away from the plus tip was taken into account for the analysis.

We then analysed the effect of locally increased microtubule lifetime due to laser damaged in cells. PtK2 GFP-tubulin cells were imaged over 10 min. We photodamaged single microtubules within a region of the cell margin for 5–7 min. Within the same time frame we simultaneously applied the same laser energy next to microtubules at a distant cell margin region (Supplementary Fig. 7). The mean fluorescent intensity of GFP-tubulin was measured in both areas before (0 min) and after (10 min) laser impact. After subtraction of the intensity decrease due to photobleaching, the ratio of fluorescent intensity before and after laser damage was calculated for the site within the cells where microtubules were damaged and the site where the laser was applied next to the microtubules. Sixteen cells were analysed from four different experiments.

For *in vitro* experiments, ATTO-488-labelled microtubules were damaged using a 100 mW/491 nm laser with a ×60 Nikon APO TIRF oil-immersion objective. To test the effects of frequency (corresponding to the number of points per second) and laser power, GMPCPP-capped microtubules were damaged in the absence of free tubulin and the frequency was varied between 1,000 $s^{-1}$ and 10,000 $s^{-1}$ and the laser power between 3% and 100% of the maximum power (Supplementary Fig. 3). The GMPCPP cap was removed using a laser pulse to initiate depolymerization. At low laser power and frequency, microtubules depolymerized without pausing. At high laser power and low frequency, microtubules were cut at the laser-damage site and immediately depolymerized afterwards. At low laser power and high frequency, most microtubules either broke, pausing for a short time before depolymerization, or paused at the laser-damage site. At high laser power and frequency, microtubules mostly paused at the damage site. For all other experiments involving laser damage *in vitro*, low laser power (4–9%) and frequency (2,500 $s^{-1}$) were chosen.

**Tubulin purification and labelling.** Tubulin was purified from fresh bovine brain by three cycles of temperature-dependent assembly and disassembly in Brinkley buffer 80 (BRB80 buffer: 80 mM PIPES pH 6.8, 1 mM EGTA and 1 mM $MgCl_2$ plus 1 mM GTP)[46]. MAP-free neurotubulin was purified by cation-exchange chromatography[47] (EMD SO, 650 M, Merck) in 50 mM PIPES, pH 6.8, supplemented with 1 mM $MgCl_2$ and 1 mM EGTA. Purified tubulin was obtained after a cycle of polymerization and depolymerization. Fluorescent tubulin (ATTO-488- and ATTO-565-labelled tubulin) and biotinylated tubulin were prepared as previously described[48]. Microtubules from neurotubulin were polymerized at 37 °C for 30 min and layered onto cushions of 0.1 M NaHEPES, pH 8.6, 1 mM $MgCl_2$, 1 mM EGTA, 60% v/v glycerol; we resuspended the pellet in 0.1 M NaHEPES, pH 8.6, 1 mM $MgCl_2$, 1 mM EGTA, 40% glycerol and labelled by adding 1/10 volume 100 mM ATTO-488 NHS ester; we stopped the reaction by adding 2 volumes 160 mM PIPES, 2 mM $MgCl_2$, 2 mM EGTA, 100 mM potassium glutamate and 40% v/v glycerol, and then microtubules were sedimented onto cushions of BRB80 supplemented with 60% glycerol. Microtubules were resuspended in BRB80, and a second cycle of polymerization and depolymerization was performed before use.

**Cover glass micropatterning.** The micropatterning technique was adapted from ref. 37. Cover glasses were cleaned by successive chemical treatments: 30 min in acetone, 15 min in ethanol (96%), rinsing in ultrapure water, 2 h in Hellmanex III (2% in water, Hellmanex), and rinsing in ultrapure water. Cover glasses were dried using nitrogen gas flow and incubated for three days in a solution of tri-ethoxy-silane-PEG (30 kDa, Creative PEGWorks) or a 1:10 mix of tri-ethoxy-silane-PEG-biotin and tri-ethoxy-silane-PEG at 1 mg $ml^{-1}$ in ethanol 96% and 0.02% HCl, with gentle agitation at room temperature. Cover glasses were then successively washed in ethanol and ultrapure water, dried with nitrogen gas, and stored at 4 °C. Passivated cover glasses were placed into contact with a photomask (Toppan) with a custom-made vacuum-compatible holder and exposed to deep ultraviolet light (7 mW $cm^{-2}$ at 184 nm, Jelight) for 3 min. Deep ultraviolet exposure through the transparent micropatterns on the photomask created oxidized micropatterned areas on the PEG-coated cover glasses.

**Microfluidic circuit fabrication and flow control.** The microfluidic device was fabricated in PDMS (Sylgard 184, Dow Corning) using standard photolithography and soft lithography. The master mould was fabricated by patterning 50-μm-thick negative photoresist (SU8 3050, Microchem) by photolithography using a custom-made photolithographic mask (La Composite). A positive replica was fabricated by replica moulding PDMS against the master. Before moulding, the master mould was vapour silanized (trichloro(1H,1H,2H,2H-perfluorooctyl)silane, Sigma) for easier lift-off. Two inlet/outlet ports were made in the PDMS device using 0.5 mm soft substrate punches (UniCore 0.5, Ted Pella). Connectors to support the tubing were made out of PDMS cubes (0.5 cm side length) with a 1.2-mm-diameter through-hole. The connectors were bonded to the chip ports using still liquid PDMS as glue, which was used to coat the interface between the chip and the connectors, and was then rapidly cured on a hotplate at 120 °C. Teflon tubing (Tefzel, inner diameter: 0.03′, outer diameter: 1/16′, Upchurch Scientific) was inserted into the port serving as an outlet. Tubing with 0.01′ inner and 1/16′ outer diameter was used to connect the inlet, via a three-way valve (Omnifit Labware) that could be opened and closed manually, to a computer-controlled microfluidic pump (MFCS-4C, Fluigent). Flow inside the chip was controlled using the MFCS-Flex control software (Fluigent).

**Microtubule growth on micropatterns.** Microtubule seeds were prepared at 10 μM tubulin concentration (20% ATTO-565- or ATTO-488-labelled tubulin and 80% biotinylated tubulin) in BRB80 supplemented with 0.5 mM GMPCPP at 37 °C for 1 h. The seeds were incubated with 1 μM Taxotere (Sigma) at room temperature for 30 min and were then sedimented by centrifugation at 30 °C and resuspended in BRB80 supplemented with 0.5 mM GMPCPP and 1 μM Taxotere. Seeds were stored in liquid nitrogen and quickly warmed to 37 °C before use.

For experiments involving exchange of the solution after microtubule growth, the PDMS chip was placed on a micropatterned cover glass and fixed on the microscope stage. The chip was perfused with neutravidin (25 μg $ml^{-1}$ in BRB80; Pierce) and washed with BRB80. Microtubule seeds were flowed into the chamber at high flow rates perpendicularly to the micropatterned lines to ensure proper orientation of the seeds. Non-attached seeds were washed out immediately using BRB80 supplemented with 1% BSA. Seeds were elongated with a mix containing 12–20 μM of tubulin (20% labelled) in BRB80 supplemented with 50 mM NaCl, 25 mM NaPi, 1 mM GTP, an oxygen scavenger cocktail (20 mM dithiothreitol,

1.2 mg ml$^{-1}$ glucose, 8 μg ml$^{-1}$ catalase and 40 μg ml$^{-1}$ glucose oxidase), 0.1% BSA and 0.025% methyl cellulose (1500 cp, Sigma). For experiments showing tubulin incorporation after photodamage, a solution of 100% labelled tubulin was perfused before applying the laser damage. GMPCPP caps were grown by supplementing the before mentioned buffer with 0.5 mM GMPCPP (Jena Bioscience) and using 10 μM tubulin (100% labelled). Only microtubules growing in the direction of flow were analysed. For depolymerization experiments, the same mix as for microtubule elongation was used, without adding free tubulin to it.

For rescue experiments after photodamage, a flow cell chamber with an approximate volume of 40 μl was constructed with double-sided tape (70 μm height) between a micropatterned cover glass and a passivated glass slide. The chamber was perfused with 25 μg ml$^{-1}$ neutravidin (Pierce) and washed with 300 μl of BRB80. Microtubule seeds were perfused and non-attached seeds were removed by washing with 300 μl BRB80 supplemented with 1% BSA. Seeds were elongated with a mix containing 12 μM of tubulin (20% labelled and 80% unlabelled tubulin) as described above. Only microtubule plus ends were considered for analysis.

For repair and rescue experiments after photodamage, microtubules were grown with red-fluorescent tubulin (20% labelled with ATTO-565 and 80% unlabelled, 20 μM) from micropatterns. Microtubules were then protected from depolymerization by growing a cap at microtubule ends with 0.5 mM GMPCPP and 10 μM tubulin. The solution was then replaced by 20 μM ATTO-488-labelled tubulin (100% labelled) and microtubules were photodamaged. After waiting approximately 2 min, the solution was replaced by red-fluorescent tubulin (18 μM, 20% labelled) and microtubule dynamics were initiated by removing the GMPCPP cap with a laser pulse at high intensity.

For repair and pause experiments in the presence of GMPCPP- and GTP-tubulin, microtubules were grown with red-fluorescent tubulin at 20 μM (20% labelled). Microtubules were then capped as described above with GMPCPP-tubulin. Laser damage was initiated either in the presence of 10 μM green-fluorescent GMPCPP-tubulin or 15 μM green-fluorescent GTP-tubulin (100% labelled). After waiting approximately 2 min, the solution was replaced by 10 μM red-fluorescent GTP-tubulin (20% labelled) and depolymerization was initiated by cutting the GMPCPP cap with a laser pulse at high intensity after a delay of 200–400 s.

**Microtubule crossing experiment.** For microtubule crossing and rescue experiments, microtubules were grown from seeds randomly attached via neutravidin to cover glasses passivated with a mix of tri-ethoxy-silane-PEG-biotin and tri-ethoxy-silane-PEG. Microtubule dynamics were imaged for 30 min. A flow cell chamber with an approximate volume of 40 μl, and two entry and two exits sites was constructed with double-sided tape (70 μm height) between a glass coverslip functionalized with SiPEG-Biotin[49] and a passivated glass slide (SiPEG 30 kDa). The chamber was perfused with 25 μg ml$^{-1}$ neutravidin (Pierce) for 1 min and washed with 300 μl of BRB80. Microtubules were polymerized for 30 min from microtubule seeds (0.5 μM) in a tube with an elongation mix containing BRB80, 1 mM GTP and 20 μM of tubulin (10% ATTO-565-labelled and 90% biotinylated tubulin). The long microtubules were perfused into the chamber from two sites with a 90° orientation towards each other. A stabilization mix containing BRB80, 0.5 mM GMPCPP and 10 μM ATTO-565-labelled tubulin was perfused into the chamber from both entry sites. After incubation for 5 min the stabilization mix was washed with 300 μl BRB80. The incorporation mix containing BRB80, 1 mM GTP and 20 μM ATTO-488-labelled tubulin was perfused from both sites and incubated for 7 min before washing with 300 μl BRB80 and imaging. The incorporation of green tubulin within a distance of 1 μm from the crossing site was taken into account as repair sites. Three hundred crossing sites from three independent experiments were analysed.

**EB3 binding to photodamage sites *in vitro*.** Red-fluorescent microtubule seeds were randomly attached via neutravidin to cover glasses passivated with a mix of tri-ethoxy-silane-PEG-biotin and tri-ethoxy-silane-PEG. Seeds were elongated with red-fluorescent free tubulin (20% labelled, 16 μM) in the presence of 100 nM EB3-GFP and standard buffer (see above) with 60 mM NaCl.

For experiments in the absence of free tubulin, microtubules were grown in a microfluidic chamber from red-fluorescent seeds attached to micropatterns. Microtubules were grown with red-fluorescent free tubulin (20% labelled, 20 μM) and protected from depolymerization with a cap of GMPCPP-tubulin (0.5 mM GMPCPP, 10 μM tubulin). Before photodamage, the solution was replaced by 100 nM EB3-GFP[50] in standard buffer with 60 mM NaCl without free tubulin.

**Statistics and reproducibility.** All statistical analyses were performed using GraphPad Prism 6.0 or Microsoft Excel software. All results presented in graphs are the mean ± s.d. Each exact *n* value is indicated in the corresponding figure or figure legend. No statistical method was used to predetermine sample size. No samples were excluded from the analyses. The investigators were not blinded to allocation during experiments and outcome assessment. A paired *t*-test was used in Fig. 7b. A Chi-square test was used in Fig. 5c. All experiments without quantification were independently performed at least three times and the representative data are shown.

**Data availability.** All data that support the conclusions are available from the authors on request.

46. Shelanski, M. L. Chemistry of the filaments and tubules of brain. *J. Histochem. Cytochem.* **21,** 529–539 (1973).
47. Malekzadeh-Hemmat, K., Gendry, P. & Launay, J. F. Rat pancreas kinesin: identification and potential binding to microtubules. *Cell. Mol. Biol. (Noisy-le-grand).* **39,** 279–285 (1993).
48. Hyman, A. *et al.* Preparation of modified tubulins. *Methods Enzymol.* **196,** 478–485 (1991).
49. Portran, D. *et al.* MAP65/Ase1 promote microtubule flexibility. *Mol. Biol. Cell* **24,** 1964–1973 (2013).
50. Komarova, Y. A. Mammalian end binding proteins control persistent microtubule growth. *J. Cell Biol.* **184,** 691–706 (2009).

DOI: 10.1038/ncb3406

nature cell biology

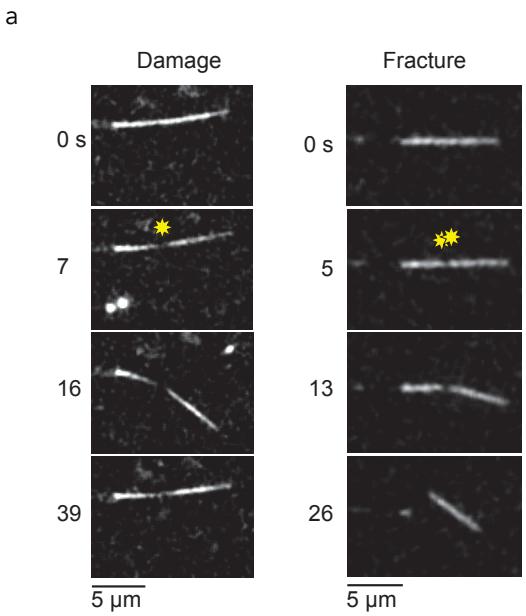


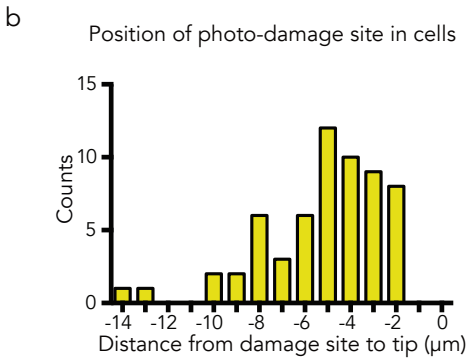


**Supplementary Figure 1** Effect of laser intensity on photo damage induced on microtubules. (a) Examples of microtubules damaged with different laser intensities. Left panel: Microtubule damaged at intermediate laser intensity. The microtubule was structurally damaged, as shown by the kinked shape it displayed when submitted to flow. No severing occurred. Right panel: At high laser intensity, microtubules were cut. (b) Histogram of the distance of the photo-damage site with respect to the tip (set to zero).

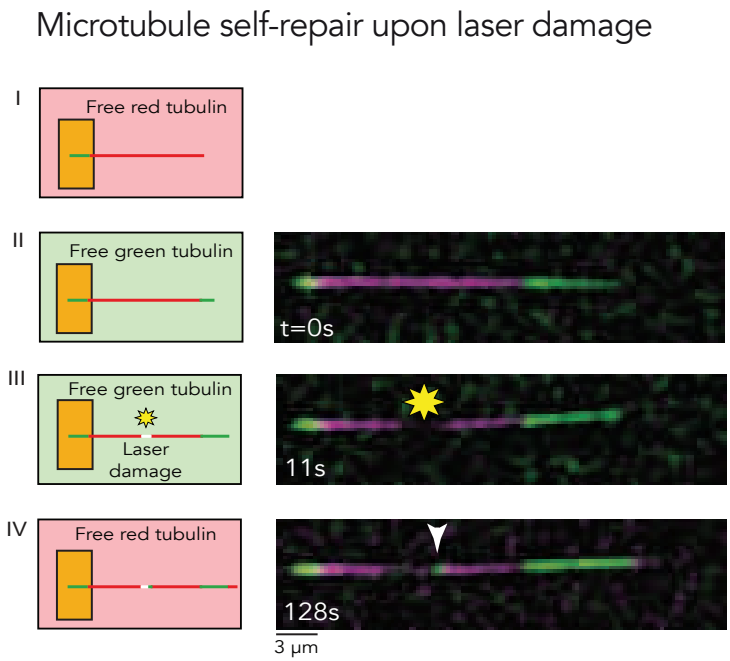


**Supplementary Figure 2** Microtubules self-repair at photo damage sites. Microtubules were grown in the device shown in figure 4a. Green microtubule seeds were elongated with red free tubulin (step I). Photo damage (yellow star) was induced in the presence of green tubulin (step II). After a two-minute delay, the medium was changed again for red tubulin (step IV). Free fluorescent tubulin dimers were removed and replaced with non-fluorescent dimers to visualize microtubules. The white arrow point at the incorporation of green tubulin along the pre-existing red microtubule following laser-induced damage.

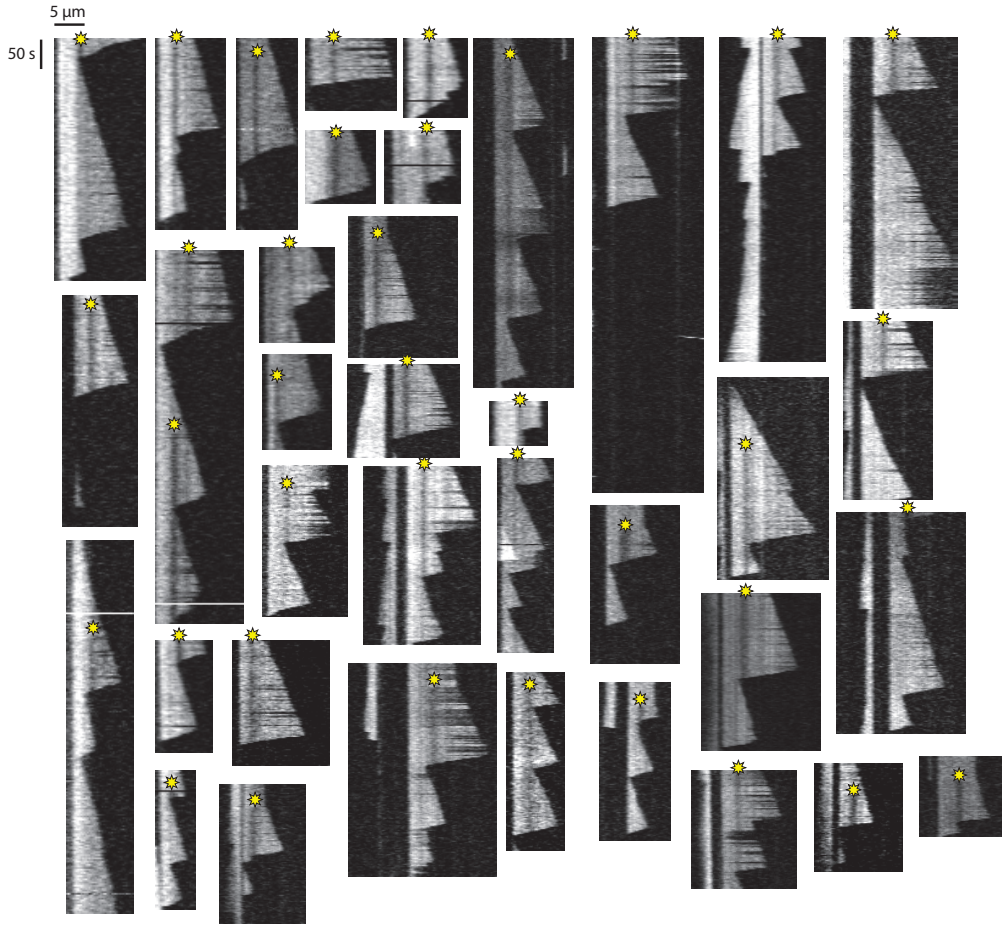


**Supplementary Figure 3** Microtubules rescue at photo damage sites. Kymographs of microtubules showing rescue or depolymerization at photo damage sites (yellow star), analogous to Figure 4e.

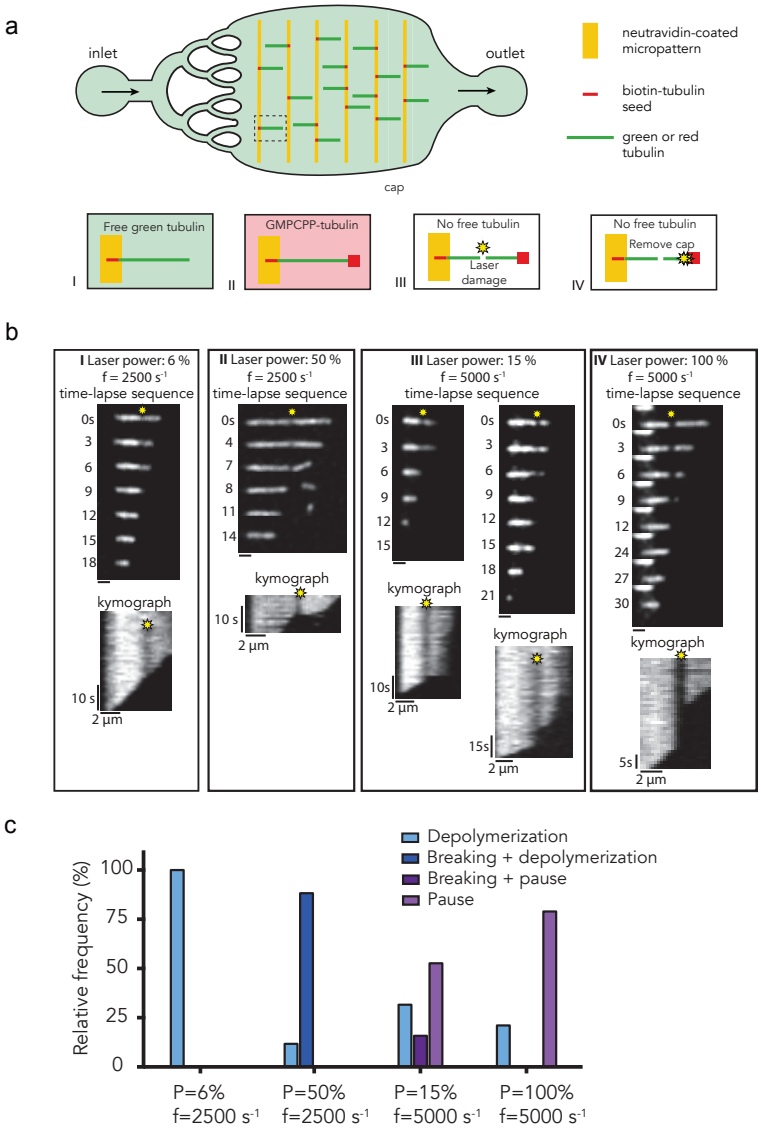


**Supplementary Figure 4** Effect of laser power and frequency on microtubule photo-damaging. (a) Red microtubule seeds were elongated with green free tubulin (step I). A GMPCPP cap was grown at the microtubule tip to avoid spontaneous depolymerization (step II). Photo damage was induced in the absence of free tubulin to avoid microtubule self-repair (step III). Depolymerization was initiated by removing the GMPCPP cap with a laser pulse at high intensity (step IV). In the absence of free tubulin, microtubule could not grow but only depolymerize. The laser-induced damage could only temporally interrupt microtubule depolymerisation (pause). High laser power could break the microtubule. (b) At low laser power and frequency (I), such as the one used throughout the study, photo damaged microtubules depolymerized without pausing. At high laser power and low frequency (II), microtubules broke at the laser damage site and immediately started to depolymerize after fracture. At low laser power and high frequency (III), most microtubules either broke, pausing for a short time before depolymerization (left panel), or paused at the laser damage site (right panel). At high laser power and frequency (IV), microtubules usually paused at the damage site before resuming depolymerization, suggesting that the laser power had a cauterizing effect on the microtubule lattice. (c) Quantification of the events shown in b. Between 17 and 24 events were monitored per condition in 4 independent experiments.

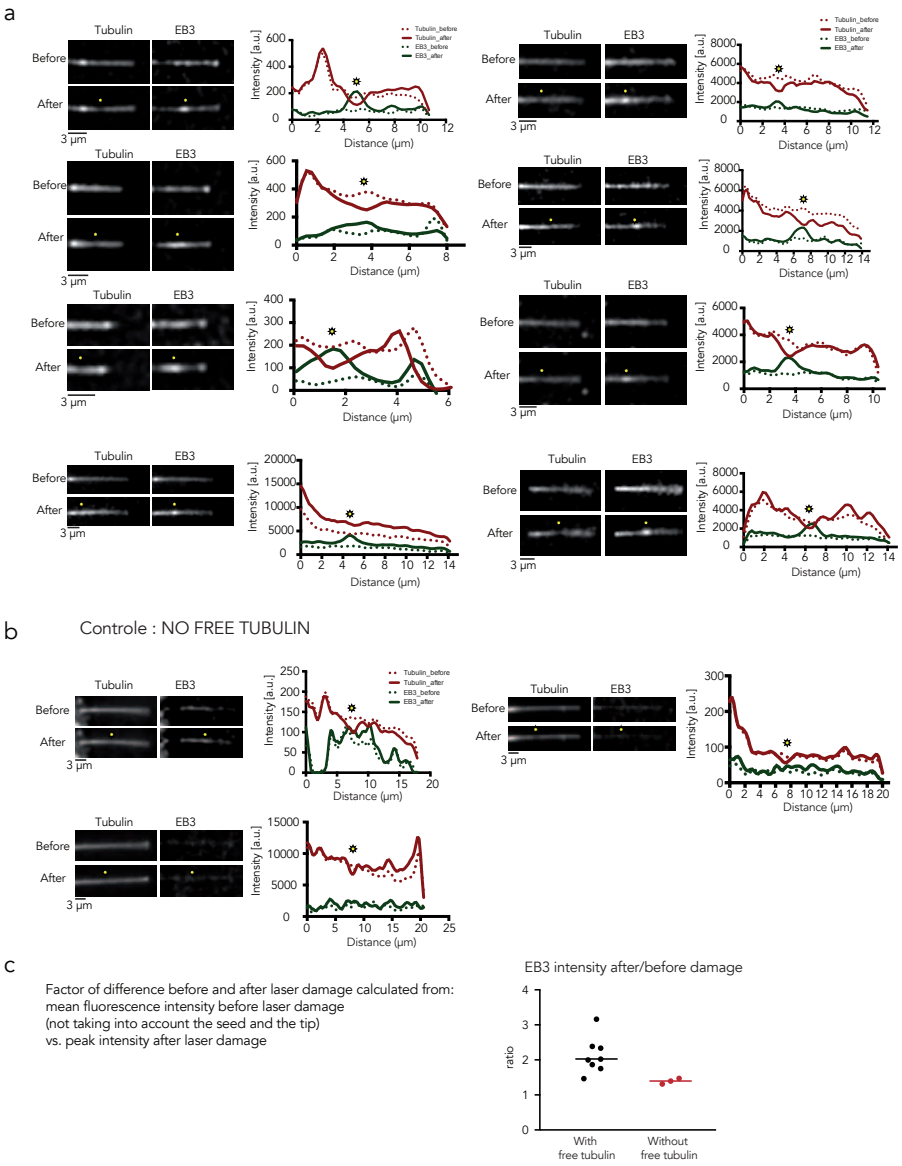


**Supplementary Figure 5** EB1 recruitment at microtubule repair sites. (a) EB3 recruitment at repair sites in the presence of free tubulin. Red microtubules were photodamaged in the presence of red-fluorescent free tubulin dimers and EB3-GFP. Images show microtubule fluorescence in the red (left) and green (right) channels, before (top) and after (bottom) the laser-induced damage. The graph shows fluorescent linescans along this microtubule before and after the damage. The yellow star represents the damaged site. (b) Absence of EB3 recruitment at repair sites in the absence of free tubulin. Same experiment in the absence of free tubulin. (c) Quantification of the effect of laser damage on the ratio of EB3 intensity after/before.

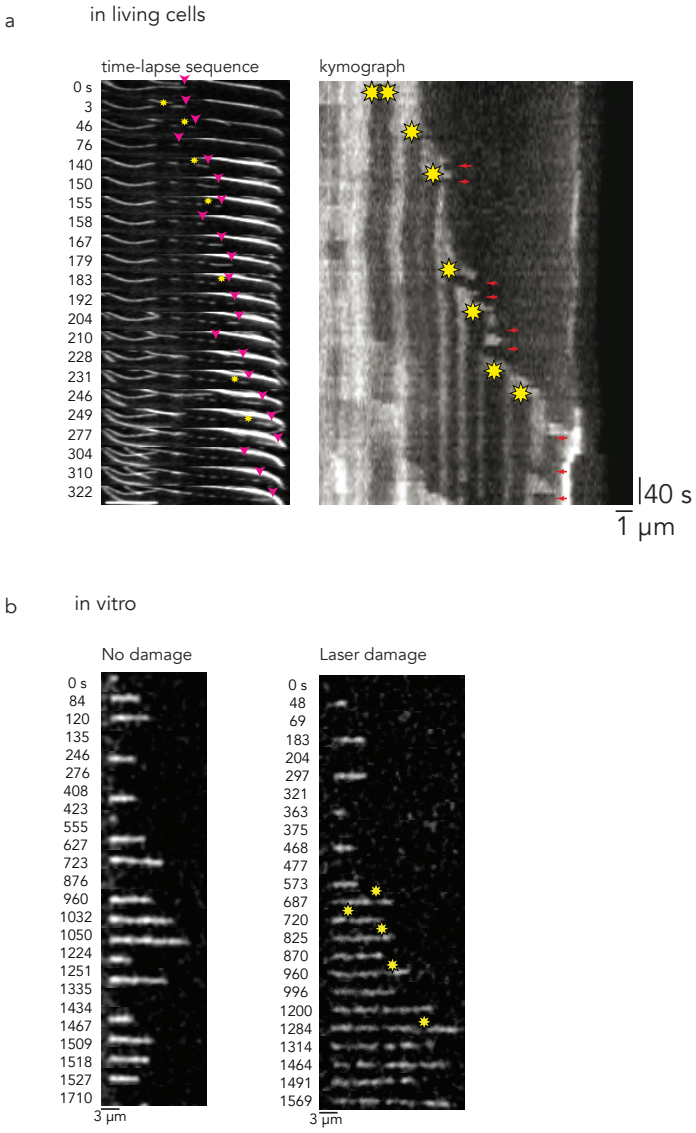


**Supplementary Figure 6** Laser photo damage promotes microtubule growth. (a) Time lapse and kymograph of a microtubule in vivo with multiple photo-damage sites. Microtubule was photo-damaged (yellow stars) close to the tip, promoting multiple rescue events (red arrowhead). Though catastrophe events were frequent, this microtubule was protected from complete depolymerization by the photo damage. Scale bar is 5 µm. (b) Time lapse of a growing microtubule in vitro without or with laser damage. Left, a growing microtubules in absence of laser damage. Right, a growing microtubule in presence of repeated laser damages. Image sequences corresponding to the kymographs shown in Fig. 6a.

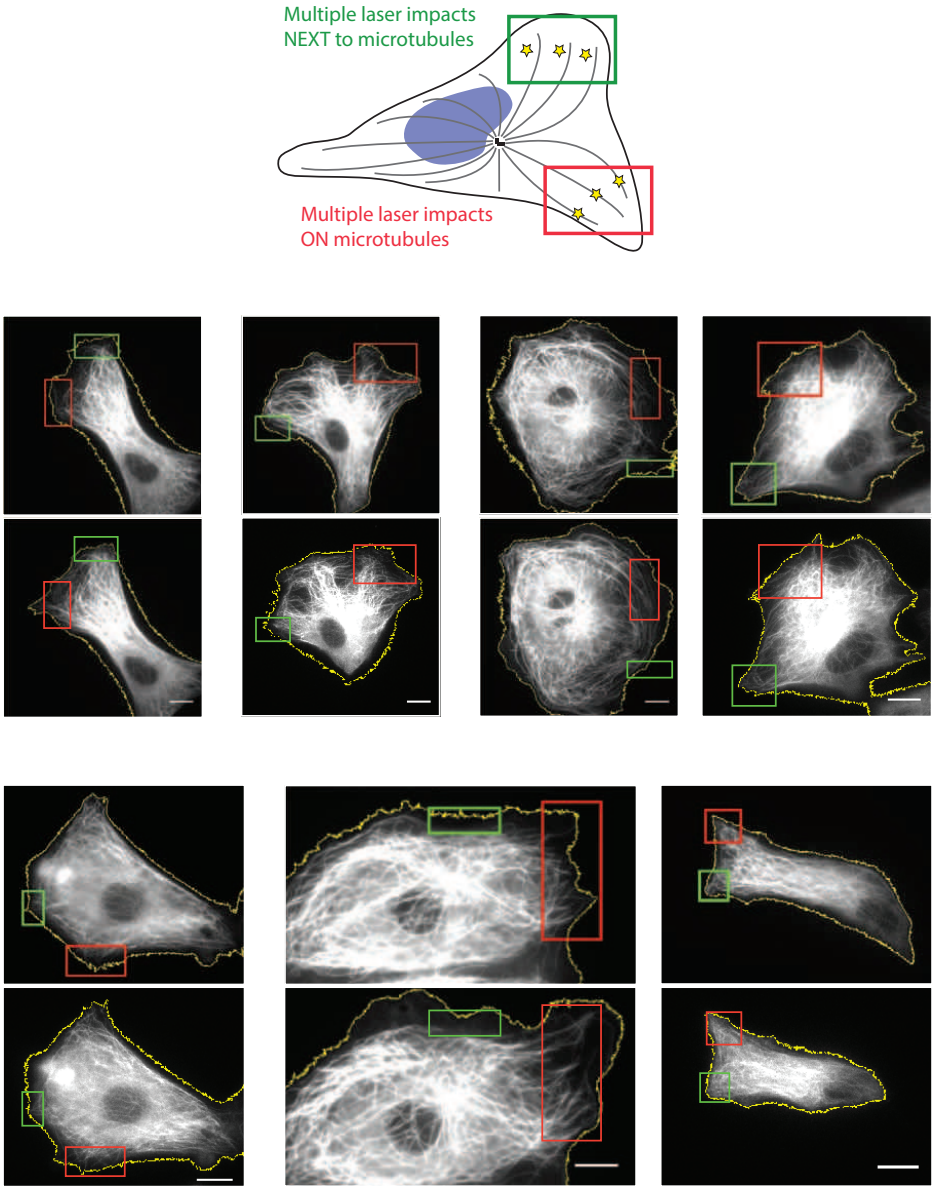


**Supplementary Figure 7** Self-repair biases microtubule dynamic instability in vivo. The sheme illustrates laser induced photo-damages either on the microtubules, in the red region, or next to the microtubules, in the green region. The images show the cell before (top) and after (bottom) the shooting. Comparison of the left and right cell margin pre- and post-photo-damage. Scale bar is 5 µm.

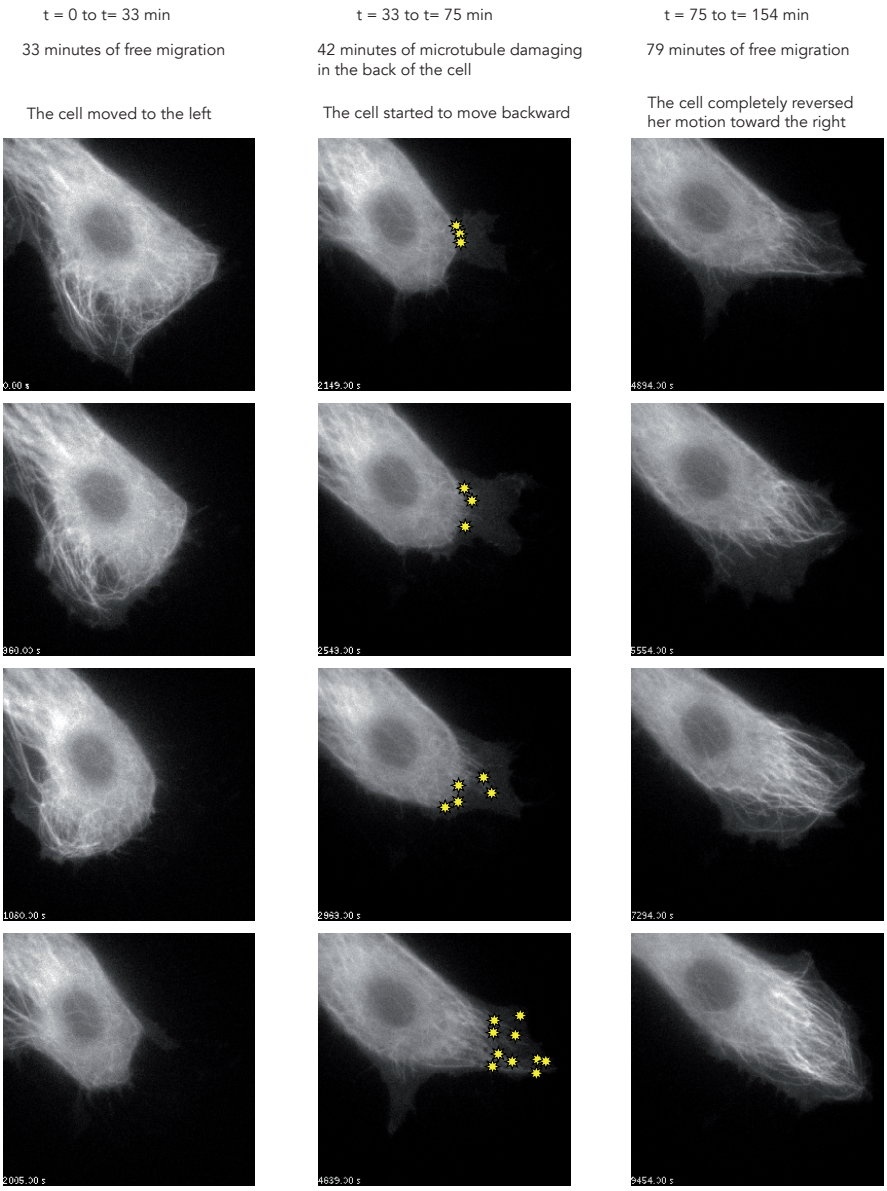


**Supplementary Figure 8** Laser-induced photo damage on microtubules influences cell migration. Time series montage of a migrating PTK2 GFP-tubulin cell. Cell migrated 33 min prior photo-damage to the left upper corner of the field of view. Photo-damage at the retracting cell edge (yellow stars) from t=33 min to t=75 min changed migration direction towards the photo-damage site. Even after the laser-induced photo-damage was stopped the cell continued the motion towards the bottom right corner of the field of view.

# SUPPLEMENTARY INFORMATION

**Supplementary Video Legends**

**Supplementary video 1** PTK2 cell expressing mEos2 post photo-conversion. The microtubule tips grow by incorporating converted tubulin dimers (magenta).

**Supplementary video 2** PTK2 cell expressing mEos2 post photo-conversion. Converted free tubulin dimers (magenta) diffused through the cytoplasm. Signal of converted dimers (magenta) was observed at the growing tips as well as in spot-like structures along the length of pre-existing microtubules (green). Video related to Fig. 1a.

**Supplementary video 3** Self-repair sites are rescue sites. Overview and detail of PTK2 cell expressing mEos2 post photo-conversion. Incorporation (arrow) of converted tubulin dimers (magenta) in pre-existing microtubule (green). Rescue event occurs exactly at the site of incorporation (arrow). Video related to Fig. 2a.

**Supplementary video** 4 The localization of rescue events in cells are frequently at microtubule crossing site. White arrow indicates the microtubule tip. Red circle highlights the rescue at microtubule crossing site. PTK2 cells stable expressing GFP-tubulin.

**Supplementary video 5** Representative sites of laser induced photo-damage (red circle) within the cell margin and near the nucleus of PTK2 GFP-tubulin cells. Microtubules undergo rescue at photo-damage sites. Arrow highlights the dynamic microtubule tip pre- and post-rescue. Video related to Fig. 3c.

**Supplementary video 6** Detail of microtubule rescue at photo-damage site in vivo. Multiple rescues at photo-damage site are occurring occasionally, bottom video. Red circle highlights the rescue at photo-damage site. Arrow highlights the dynamic microtubule tip pre- and post-rescue. Video related to Fig. 3d,e.

**Supplementary video 7** Microtubule rescuing at a photo damage site in vitro. The upper panel shows a microtubule without laser damage; in these conditions, microtubules rarely undergo spontaneous rescue. The lower panel shows a microtubule rescuing several times at a laser damage site (red circle) before complete depolymerization. Video related to Fig. 4e.

**Supplementary video 8** Microtubule rescue at cross-over. The video shows the growth of non-micropatterned and non-photo-damaged microtubules. Microtubule depolymerisation was stopped at the site where microtubules cross each other.

**Supplementary video 9** Laser damage increases microtubule length and life-time. The upper panel shows a microtubule without laser damage and infrequent rescue events. In the lower panel, the microtubule was damaged repeatedly close to the tip (red circles), inducing rescue and making the microtubule grow longer and longer. Video related to Figure 6a.

**Supplementary video 10** Microtubules rescue and over growth upon repeated photo-damages. PTK2 GFP-tubulin cell. Photo-damage on single microtubule (red dots) or next to microtubules (green dots). Microtubule number and length increased at the site of microtubule photo-damage (red dots) and decreased on the opposite site (green dots). The cell spread toward the site where microtubules were photo-damaged. Video related to Figure 7.

**Supplementary video 11** Reoriented migration by photo-damaged microtubules. PTK2 GFP-tubulin cell migrated 34 min prior photo-damage to the left upper corner of the field of view. Photo-damage of single microtubule (red dots) at the retracting cell edge from t=33 min to t=75 min changed migration direction towards the photo-damage site. Even after the offset of photo-damage cell continued the motion towards the right. Video related to Supplementary Figure 8.

### 2.2.2 Conclusions and perspectives

The two major conclusions of the study are that, firstly, microtubules in cells incorporate tubulin into their lattice, confirming the *in vitro* findings of the first study and pointing to their relevance *in vivo*. Secondly, it shows that microtubule damage can lead to rescue at the damage site after tubulin incorporation. The combination of *in vitro* and *in vivo* experiments shows that, on the one hand, no other cellular factors like MAPs are needed for rescue after damage. On the other hand, microtubule damage is an efficient way to increase rescue in cells, and by biasing microtubule rescue in certain areas of the cell, cell migration can be influenced. Furthermore, the damage induced rescue sites appear plus end like, as they present areas of preferential EB binding, indicating the presence of GTP tubulin (see Fig. 5d and S5 of the second study). Relating the results of the present study to the findings of Dimitrov *et al.* (Dimitrov *et al., 2008*), it seems likely that the presence of GTP stretches they observed are due to tubulin incorporation, rather than remnants from microtubule polymerization.

One of the aspects that remain to be explored is the molecular basis of the laser induced damage. Though it is apparent that dimers are removed from the lattice, as demonstrated by kinked shapes and severed microtubules at high intensities, this does not hint to the distribution of the damage on a molecular scale: Are single dimers removed within a big area? Or are big chunks of neighboring dimers removed at the same time? What is more, GTP hydrolysis at the microtubule tip was shown to be rather fast, occurring on the order of seconds (Melki *et al.*, 1996). It therefore needs to be further explored how GTP tubulin incorporation after laser damage can induce rescue after as much as 800 s.

Several scenarios could explain this discrepancy: GTP hydrolysis might be slowed down compared to the microtubule tip due to different incorporation mechanisms

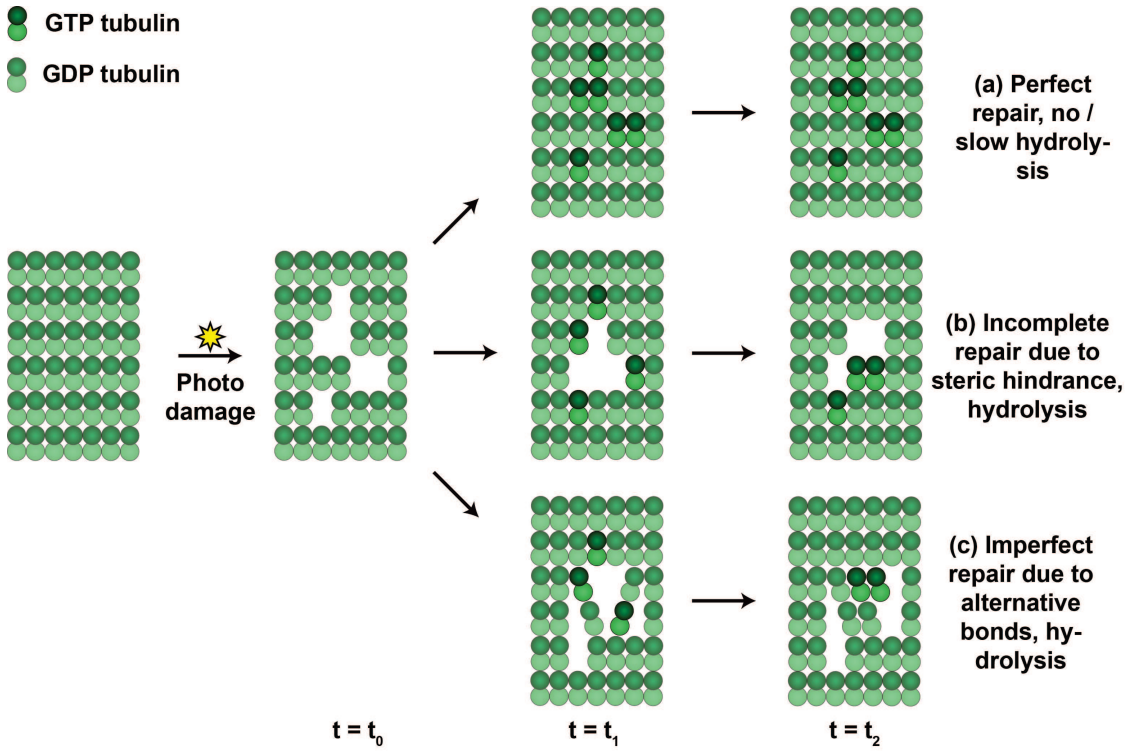


Figure 21: *Possible mechanisms of photo damage induced rescue. Photo damage leads to dimer dissociation, and probably creates irregular holes in the lattice. There are different possibilities how subsequent repair could lead to a prolonged rescue probability: (a) GTP tubulin dimers from the solution, which fill up the gaps in the lattice, may not / slowly hydrolyze due to a different incorporation pathway compared to the microtubule tip. Non-hydrolyzed GTP tubulin stabilizes the lattice locally and could therefore lead to rescue. (b) Repair may be incomplete due to steric hindrance by neighboring dimers, hampering the incorporation of new dimers. On the one hand, this could lead to dissociation of GDP dimers with less than four direct neighbors, and subsequent replacement by GTP dimers. On the other hand, dimers with a missing upper, longitudinal neighbor may hydrolyze more slowly. (c) Repair may be imperfect, creating longitudinal bonds between neighboring protofilaments. Dimers with missing neighbors could dissociate from the lattice and lead to tubulin turnover, until the lattice is fully healed.*

(see Fig. 21, scenario (a)). Intermediate conformational states such as they have been proposed to occur at the plus end when sheet-like structures close into a tube could be suppressed, hindering hydrolysis. Another possibility is that the incorporation of new tubulin dimers may be limited by steric hindrance due to the surrounding dimers (see Fig. 21, scenario (b)). Alushin *et al.* showed that longitudinal interdimer contacts undergo compaction upon hydrolysis (Alushin *et al.*, 2014), so that a GTP dimer might not easily fit in a place where there are already two longitudinal neighbors. The more neighbors there are, the more stably bound the dimer, but the more difficult it may be for the dimer to reach that site in the first place. This explanation would fit with the fact that the recovery of microtubule stiffness observed in the first study takes rather long. At the same time, GDP dimers with missing neighbors could have an increased off-rate, and would eventually be replaced by GTP dimers, leading to a rescue effect that could last much longer than hydrolysis rates of individual dimers suggest. On the other hand, hydrolysis may be slowed down or absent in dimers with a missing longitudinal neighbor at the beta subunit, as the alpha subunit of the incoming dimer is known to trigger hydrolysis at the microtubule plus end (Choi *et al.*, 1998; Nogales *et al.*, 1998; Nogales *et al.*, 1999; Anders and Botstein, 2001). Thirdly, the laser damage may be rather extensive and subsequent repair imperfect, e.g. by interconnecting different protofilaments longitudinally (see Fig. 21, scenario (c)). This would cause some dimers to have less than four direct neighbors, and it would lead to strain in the interdimer bonds, which could subsequently favor dimer dissociation and GTP tubulin incorporation, until the lattice is fully 'healed'.

To clearly distinguish between these possibilities, it would be necessary to image the photo damage site. This, however, is very challenging, as it requires first to damage the microtubule, to stabilize it and then to image it with atomic force microscopy or another high-resolution imaging technique that allows visualization on the scale of single dimers. Another way to shed light on the matter would be to estimate the

GTP hydrolysis time, e.g. by measuring EB binding to the damage site over time after removal of free tubulin dimers.

The relevance of damage induced rescue could be further tested by using other, more physiological means of inducing damage: As shown in the present study, crossing microtubules have a higher probability to rescue at the crossing site, while tubulin incorporation is also observed at crossings (see Fig. 4a, b and c of the second study). This is probably due to friction induced damage. The effect of friction would be interesting to further investigate, as based on the observations of tubulin incorporation and rescue in cells it seems to be even more important for rescue than microtubule bending (see Fig. 2e of the second study). Though crosslinking of microtubules at crossing sites *in vivo* could play a role by physically stabilizing the depolymerizing microtubule at the crossing site, the *in vitro* experiments show that even without crosslinkers, microtubule crossing can lead to rescue. This is interesting as microtubule interfilament friction is rather low (Sanchez *et al.*, 2011). Like the first study, it shows that even small forces can have a considerable effect on microtubule mechanics and behavior.
Further characterizing friction induced rescue could e.g. provide more information about how long the effect of damage on rescue lasts in a cellular context. Another interesting aspect is tubulin incorporation observed in bundled microtubules: In cells, it is challenging to quantify the influence of bundling as the number of microtubules in a bundle is usually difficult to estimate, and crosslinking proteins may be involved. *In vitro* sliding of bundled microtubules could therefore be used to induce friction along the entire microtubules, and subsequent tubulin incorporation and rescue behavior could be quantified. This would be of particular interest for neuronal microtubules, which are often bundled.

Finally, although damage induced rescue does not require the presence of proteins other than GTP tubulin, it would be interesting to investigate if other molecular players assist rescue *in vivo*. It might therefore be tested if proteins which are known to recognize the GTP tubulin conformation (like EB) or have been described as rescue factors are involved. For example, CLIP-170 has been shown to act as a rescue factor in cells; it has been hypothesized that it does so by binding tubulin dimers and recruiting them to shortening microtubules, favoring switching back to growth (Komarova *et al.*, 2002; Arnal *et al*, 2004). CLASP also seems to contribute to rescue by locally binding along the microtubule lattice and binding tubulin dimers to restart growth (Al-Bassam *et al.*, 2010). The influence of EB on rescue efficiency at damage sites *in vitro* could not be evaluated in the current study due to the inherent changes in microtubule dynamics upon addition of EB.

### 2.2.3 Limitations of the study

Though it provides a reliable way of inducing damage at a known location, the use of photo damage is non-physiological and therefore may be seen as a limitation. Furthermore, Niedermayer *et al.* showed that light exposure can lead to permanent crosslinking of fluorescently labelled actin monomers, causing abrupt pauses during depolymerization (Niedermayer *et al.*, 2012). Indeed the present study shows that microtubules which were exposed to high frequency laser pulses, corresponding to a short exposure of individual spots within a given area, paused at the damage site during disassembly in the absence of free tubulin (see Fig. S4 of the second study). This indicates that crosslinking of dimers can be induced by light exposure, similarly to actin dimerization described by Niedermayer *et al.* At lower frequencies, no pauses in depolymerization were observed, suggesting that rescue events observed in the presence of free tubulin at these parameters were effectively due to the incorporation of new tubulin, rather than to the crosslinking of dimers in the lattice.

In addition, the *in vitro* experiments showing increased rescue at crossing sites and the correlation found *in vivo* between microtubule bending / crossing, tubulin incorporation and rescue demonstrate that damage induced rescue indeed takes place, and confirm the physiological relevance of the findings.

Furthermore, minus end dynamics have not been included in the study. Their dynamic behavior is different from plus ends, and it would therefore be interesting to include them in subsequent studies.

# 3 Conclusions and Perspectives

In this thesis, the effect of mechanical stress on microtubule mechanics was studied. It was found that microtubules soften when exposed to repeated, moderate bending forces, showing that they are subject to material fatigue. Interestingly, microtubules can self-heal, while incorporating tubulin dimers from the solution into their lattice. The inherent capacity to self-repair is a remarkable feature that makes microtubules stand apart from most engineered materials. An important aspect of these findings is that microtubule dynamics is not exclusive to plus and minus ends: A microtubule is not simply a homogeneous, inert lattice with active ends.
The incorporation of tubulin dimers from the solution into a damage site along the microtubule lattice has some interesting consequences: Newly incorporated tubulin is GTP-bound. GTP tubulin stretches have been proposed to rescue depolymerizing microtubules (Dimitrov *et al.*, 2008; Tropini *et al.*, 2012), and indeed, as shown in the second study, photo damaged areas can lead to rescue. EB proteins recognize the damage sites, making them appear as plus end-like structures.

The microtubule GDP lattice is inherently in a metastable state, where even small events like the loss of a few GTP tubulin dimers at the tip or a slight stabilization of the shrinking microtubule may be enough to tip the balance between phases of growth and shrinkage (Gardner *et al.*, 2011; Hunyadi *et al.*, 2007, Rice *et al.*, 2008). Similarly, GDP tubulin dissociation from the lattice outside the tip region could be induced by minor changes in (internal or external) conditions. In their study of microtubule bending in living cells, Odde *et al.* raised the possibility of curvature enhanced tubulin dissociation as a mechanism of microtubule breaking (Odde *et al.*, 1999). Dissociation is likely to happen preferentially in areas of increased pre-stress or missing neighbors (e.g. at lattice defects), and can probably be enhanced by external forces like bending, which help dimers to overcome the energy barrier and

leave the lattice.

The 1D model of a growing microtubule, which assumes the dissociation rate ($k_{off}$) to be independent of the free tubulin concentration, does not do justice to the complexity of the microtubule tip structure (van Buren *et al.*, 2005; Gardner *et al.*, 2011): Growing microtubule tips become more tapered at higher tubulin concentrations, so that tubulin subunits at the tip are more likely to have less neighbors than in the case of blunt ends. They therefore fall off more rapidly, leading to a dissociation rate that increases with the free tubulin concentration. Similarly, it may be necessary to consider lattice on- and off-rates that depend on the presence of neighbors in the lattice.

Though the presence of defects in cellular microtubules has not yet been proven, *in vivo* data from the second study shows that microtubules incorporate tubulin into their lattice, and Dimitrov *et al.* provided evidence for GTP tubulin patches along the microtubule lattice in cells (Dimitrov *et al.*, 2008).

An important question is whether microtubule damage plays a specific role in cells, or if damage caused by mechanical forces is the price that the cell pays to maintain a prestressed lattice that can do work during disassembly. An area where microtubule damage occurs is an area of high (mechanical) activity in the cell, caused e.g. by internal contractile actomyosin structures or external forces, and it might be useful for the cell to remodel its microtubule network in those areas. Remodeling could occur in two different ways: Through increased rescue, or by breaking. Overall, cells could use microtubule damages to either (passively or actively) selectively stabilize or destabilize microtubule networks in areas of high mechanical stress. By (passive) incorporation of GTP tubulin at damage sites that are caused by increased mechanical stress, microtubules undergo frequent rescues and could e.g. deliver cellular components for an appropriate response to external forces, and make the cell eventually move towards the source of stress. On the other hand, microtubules seem to

be preferentially cut by katanin at lattice defects (Davis *et al.*, 2002; Díaz-Valencia *et al.*, 2011) and katanin has been proposed to act specifically at regions of high curvature (Davis *et al.*, 2002). Katanin also severs microtubules at crossover sites in *Arabidopsis* (Zhang *et al.*, 2013). Damage could therefore mark a mechanically stressed microtubule as to be replaced since katanin would preferentially cut microtubules that are curved or in other ways exposed to mechanical forces. The severed microtubule could then depolymerize, initiating retraction of the cell from the site of stress. Alternatively, the newly generated plus end, if it does not depolymerize, would explore the intracellular space and locally remodel the microtubule network. In general, local microtubule damage could be a way for cells to tag those damaged areas for specific actions. Apart from rescue and severing, upon GTP tubulin incorporation, damaged areas could attract proteins that e.g. initiate microtubule branching, or crosslinking with other cytoskeletal components.
The second study showed that microtubules have an increased rescue frequency at crossover sites, and also incorporate tubulin at those sites. In microtubule bundles that are bent, microtubules are forced to slide past each other, as e.g. an early study of microtubules in cilia showed (Satir, 1968). Like crossing microtubules, sliding microtubules might incorporate tubulin due to friction induced damage. Cellular microtubules that are organized in bundles, like in axons, may therefore either benefit from specific stabilizing factors that inhibit sliding induced damage, or have an increased damage induced tubulin turnover at the lattice.

In summary, this thesis explored how mechanical stress affects microtubules. It opened new perspectives to investigate two important aspects of microtubule behavior: Firstly, microtubule repair in response to mechanical stress induced damage could help to better understand the structural role of microtubules in cells and explain how microtubules are able to sustain repeated bending stress without breaking. Secondly, incorporation of GTP tubulin after microtubule damage could help to ex-

plain microtubule rescue in cells, and lead to a better understanding of microtubule dynamic behavior *in vivo*. In general, this work provides evidence that more attention needs to be brought to the dynamic properties of the GDP microtubule lattice far from the tip, which so far has received little consideration compared to plus and minus ends.

# A References


Akhmanova, A., & Steinmetz, M. O. (2010). **Microtubule +TIPs at a glance.** *Journal of Cell Science*, 123(20), 3415–3419.

Al-Bassam, J., Kim, H., Brouhard, G., van Oijen, A., Harrison, S. C., & Chang, F. (2010). **CLASP promotes microtubule rescue by recruiting tubulin dimers to the microtubule.** *Developmental Cell*, 19(2), 245–258.

Alushin, G. M., Lander, G. C., Kellogg, E. H., Zhang, R., Baker, D., & Nogales, E. (2014). **High-resolution microtubule structures reveal the structural transitions in alpha-beta-tubulin upon GTP hydrolysis.** Cell, 157(5), 1117–1129.

Amos, L., & Klug, A. (1974). **Arrangement of subunits in flagellar microtubules.** *Journal of Cell Science*, 14(3), 523–549.

Ananthakrishnan, R., & Ehrlicher, A. (2007). **The forces behind cell movement.** *International Journal of Biological Sciences*, 3(5), 303–317.

Anders, K. R., & Botstein, D. (2001). **Dominant-lethal alpha-tubulin mutants defective in microtubule depolymerization in yeast.** *Molecular Biology of the Cell*, 12(12), 3973–3986.

Ayaz, P., Ye, X., Huddleston, P., Brautigam, C. A., & Rice, L. M. (2012). **A TOG:alpha-beta-tubulin complex structure reveals conformation-based mechanisms for a microtubule polymerase.** *Science*, 337(6096), 857-860.

Baba, S. A. (1972). **Flexural rigidity and elastic constant of cilia.** *The Journal of Experimental Biology*, 56(2), 459–467.

Bartolini, F., & Gundersen, G. G. (2006). **Generation of noncentrosomal microtubule arrays.** *Journal of Cell Science*, 119(20), 4155–4163.

Battle, C., Ott, C. M., Burnette, D. T., Lippincott-Schwartz, J., & Schmidt, C. F. (2015). **Intracellular and extracellular forces drive primary cilia movement.** *PNAS*, 112(5), 1410–1415.

Bayley, P. M., Schilstra, M. J., & Martin, S. R. (1990). **Microtubule dynamic instability: numerical simulation of microtubule transition properties using a lateral cap model.** *Journal of Cell Science*, 95(1), 33–48.

Bechstedt, S., & Brouhard, G. J. (2012). **Doublecortin recognizes the 13-protofilament microtubule cooperatively and tracks microtubule ends.** *Developmental Cell*, 23(1), 181–192.

Bechstedt, S., & Brouhard, G. J. (2013). **Fluorescence-based assays for microtubule architecture.** *Methods in Cell Biology*, 115, 343-354.

Bicek, A. D., Tüzel, E., Demtchouk, A., Uppalapati, M., Hancock, W. O., Kroll, D. M., & Odde, D. J. (2009). **Anterograde microtubule transport drives microtubule bending in LLC-PK1 epithelial cells.** *Molecular Biology of the Cell*, 20(12), 2943–2953.

Bieling, P., Laan, L., Schek, H., Munteanu, E. L., Sandblad, L., Dogterom, M., ... Surrey, T. (2007). **Reconstitution of a microtubule plus-end tracking system in vitro.** *Nature*, 450(7172), 1100–1105.

Boal, D. (2002). **Mechanics of the cell.** *Cambridge University Press.*

Bormuth, V., Varga, V., Howard, J., & Schäffer, E. (2009). **Protein friction limits diffusive and directed movements of kinesin motors on microtubules.** *Science*, 325(5942), 870–873.

Bowne-Anderson, H., Zanic, M., Kauer, M., & Howard, J. (2013). **Microtubule dynamic instability: A new model with coupled GTP hydrolysis and multistep catastrophe.** *BioEssays*, 35(5), 452–461.

Brangwynne, C. P., MacKintosh, F. C., Kumar, S., Geisse, N. A., Talbot, J., Mahadevan, L., ... Weitz, D. A. (2006). **Microtubules can bear enhanced compressive loads in living cells because of lateral reinforcement.** *Journal of Cell Biology*, 173(5), 733–741.

Brangwynne, C. P., MacKintosh, F. C., & Weitz, D. A. (2007). **Force fluctuations and polymerization dynamics of intracellular microtubules.** *PNAS*, 104(41), 16128–16133.

Brangwynne, C. P., Koenderink, G. H., MacKintosh, F. C., & Weitz, D. A. (2008). **Nonequilibrium microtubule fluctuations in a model cytoskeleton.** *Physical Review Letters*, 100(11), 1–4.

Bré, M. H., & Karsenti, E. (1990). **Effects of brain microtubule-associated proteins on microtubule dynamics and the nucleating activity of centrosomes.** *Cell Motility and the Cytoskeleton*, 15(2), 88–98.

Bré, M. H., Pepperkok, R., Hill, A. M., Levilliers, N., Ansorge, W., Stelzer, E. H. K., & Karsenti, E. (1990). **Regulation of microtubule dynamics and nucleation during polarization in MDCK II cells.** *Journal of Cell Biology*, 111(6), 3013–3021.

Brouhard, G. J. (2015). **Dynamic instability 30 years later: Complexities in microtubule growth and catastrophe.** *Molecular Biology of the Cell*, 26(7), 1207–1210.

Buey, R. M., Daz, J. F., & Andreu, J. M. (2006). **The nucleotide switch of tubulin and microtubule assembly: A polymerization-driven structural change.** *Biochemistry*, 45(19), 5933-5938.

Buxbaum, R. E., & Heidemann, S. R. (1988). **A thermodynamic model for force integration and microtubule assembly during axonal elongation.** *Journal of Theoretical Biology*, 134(3), 379–390.

Carlier, M. F., & Pantaloni, D. (1981). **Kinetic analysis of guanosine 5'-triphosphate hydrolysis associated with tubulin polymerization.** *Biochemistry*, 20(7), 1918–1924.

Carlier, M. F., Didry, D., & Pantaloni, D. (1987). **Microtubule elongation and guanosine 5'-triphosphate hydrolysis. Role of guanine nucleotides in microtubule dynamics.** *Biochemistry*, 26(14), 4428–37.

Cassimeris, L., Pryer, N. K., & Salmon, E. D. (1988). **Dynamic instability in living cells.** *The Journal of Cell Biology*, 107(6), 2223–2231.

Cassimeris, L. (1993). **Regulation of microtubule dynamic instability.** *Cell Motility and the Cytoskeleton*, 26(4), 275–281.

Charras, G. T., & Horton, M. A. (2002). **Single cell mechanotransduction and its modulation analyzed by atomic force microscope indentation.** *Biophysical Journal*, 82(6), 2970–2981.

Choi, H.-J., Kang, S. W., Yang, C.-H., Rhee, S. G., & Ryu, S.-E. (1998). **Tubulin and FtsZ form a distinct family of GTPases.** *Nature Structural Biology*, 5(6), 451–458.

Chrétien, D., & Wade, R. H. (1991). **New data on the microtubule surface lattice.** *Biology of the Cell*, 71(1), 161–174.

Chrétien, D., Metoz, F., Verde, F., Karsenti, E., & Wade, R. H. (1992). **Lattice defects in microtubules: Protofilament numbers vary within individual microtubules.** *Journal of Cell Biology*, 117(5), 1031–1040.

Chrétien, D., Fuller, S. D., & Karsenti, E. (1995). **Structure of growing microtubule ends: Two-dimensional sheets close into tubes at variable rates.** *Journal of Cell Biology*, 129(5), 1311–1328.

Coombes, C. E., Yamamoto, A., Kenzie, M. R., Odde, D. J., & Gardner, M. K. (2013). **Evolving tip structures can explain age-dependent microtubule catastrophe.** *Current Biology*, 23(14), 1342–1348.

Cordier, P., Tournilhac, F., Soulié-Ziakovic, C., & Leibler, L. (2008). **Self-healing and thermoreversible rubber from supramolecular assembly.** *Nature*, 451(7181), 977–980.

Cueva, J. G., Hsin, J., Huang, K. C., & Goodman, M. B. (2012). **Posttranslational acetylation of alpha-tubulin constrains protofilament number in native microtubules.** *Current Biology*, 22(12), 1066–1074.

Desai, A., & Mitchison, T. J. (1997). **Microtubule polymerization dynamics.** *Annual Review of Cell and Developmental Biology*, 13(1), 83–117.

Díaz, J. F., Valpuesta, J. M., Chacón, P., Diakun, G., & Andreu, J. M. (1998). **Changes in microtubule protofilament number induced by taxol binding to an easily accessible site: Internal microtubule dynamics.** *Journal of Biological Chemistry*, 273(50), 33803–33810.

Díaz-Valencia, J. D., Morelli, M. M., Bailey, M., Zhang, D., Sharp, D. J., & Ross, J. L. (2011). **Drosophila katanin-60 depolymerizes and severs at microtubule defects.** *Biophysical Journal*, 100(10), 2440–2449.

Dimitrov, A., Quesnoit, M., Moutel, S., Cantaloube, I., Poüs, C., & Perez, F. (2008). **Detection of GTP-tubulin conformation in vivo reveals a role for GTP remnants in microtubule rescues.** *Science*, 322(5906), 1353–1356.

Dogterom, M., & Yurke, B. (1997). **Measurement of the force-velocity relation for growing microtubules.** *Science*, 278(5339), 856–860.

Dos Remedios, C. G., Chhabra, D., Kekic, M., Dedova, I. V., Tsubakihara, M., Berry, D. A., & Nosworthy, N. J. (2003). **Actin binding proteins: regulation of cytoskeletal microfilaments.** *Physiol Rev*, 83(2), 433–473.

Dumont, E. L. P., Do, C., & Hess, H. (2015). **Molecular wear of microtubules propelled by surface-adhered kinesins.** *Nature Nanotechnology*, 10(2), 166-169.

Dye, R. B., Fink, S. P., & Williams, R. C. (1993). **Taxol-induced flexibility of microtubules and its reversal by MAP-2 and Tau.** *Journal of Biological Chemistry*, 268(10), 6847–6850.

Efremov, A., Grishchuk, E. L., Mcintosh, J. R., & Ataullakhanov, F. I. (2007). **In search of an optimal ring to couple microtubule depolymerization to processive chromosome motions.** *PNAS*, 104(48), 19017-19022.

Ellis, R. J. (2001). **Macromolecular crowding: Obvious but underappreciated**. *Trends in*

*Biochemical Sciences*, 26(10), 597–604.

Eriksson, J. E., Dechat, T., Grin, B., Helfand, B., Mendez, M., Pallari, H. M., & Goldman, R. D. (2009). **Introducing intermediate filaments: From discovery to disease.** *Journal of Clinical Investigation*, 119(7), 1763–1771.

Evans, L., Mitchison, T. I. M., & Kirschner, M. (1985). **Influence of the centrosome of nucleated microtubules on the structure of isolated centrosomes.** *J. Cell Biol.*, 100(4), 1185–1191.

Fletcher, D. A., & Mullins, R. D. (2010). **Cell mechanics and the cytoskeleton.** *Nature*, 463(7280), 485–492.

Fulton, A. B. (1982). **How crowded is the cytoplasm?** *Cell*, 30(2), 345–347.

Gardner, M. K., Charlebois, B. D., Janosi, I. M., Howard, J., Hunt, A. J., & Odde, D. J. (2011). **Rapid microtubule self-assembly kinetics.** *Cell*, 146(4), 582–592.

Gardner, M. K., Zanic, M., Gell, C., Bormuth, V., & Howard, J. (2011). **Depolymerizing kinesins Kip3 and MCAK shape cellular microtubule architecture by differential control of catastrophe.** *Cell*, 147(5), 1092–1103.

Gardner, M. K., Zanic, M., & Howard, J. (2013). **Microtubule catastrophe and rescue.** *Current Opinion in Cell Biology*, 25(1), 14-22.

Gittes, F., Mickey, B., Nettleton, J., & Howard, J. (1993). **Flexural rigidity of microtubules and actin filaments measured from thermal fluctuations in shape.** *Journal of Cell Biology*, 120(4), 923–934.

Gundersen, G. G., & Bulinski, J. C. (1988). **Selective stabilization of microtubules oriented toward the direction of cell migration.** *PNAS*, 85(16), 5946–5950.

Guo, H., Xu, C., Liu, C., Qu, E., Yuan, M., Li, Z., ... Zhang, D. (2006). **Mechanism and dynamics of breakage of fluorescent microtubules.** *Biophysical Journal*, 90(6), 2093–2098.

Gupta, M., Sarangi, B. R., Deschamps, J., Nematbakhsh, Y., Callan-Jones, A., Margadant, F., ... Ladoux, B. (2015). **Adaptive rheology and ordering of cell cytoskeleton govern matrix rigidity sensing.** *Nature Communications*, 6, 1-9.

Gupton, S. L., Salmon, W. C., & Waterman-Storer, C. M. (2002). **Converging populations of f-actin promote breakage of associated microtubules to spatially regulate microtubule turnover in migrating cells.** *Current Biology*, 12(22), 1891–1899.

Haase, K., Pelling, A. E., & Haase, K. (2015). **Investigating cell mechanics with atomic force microscopy.** *Interface*, 12(104), .

Hammond, J. W., Huang, C.-F., Kaech, S., Jacobsen, C., Banker, G., & Kristen, J. V. (2010). **Posttranslational modifications of tubulin and the polarized transport of kinesin-1 in neurons.** *Molecular Biology of the Cell*, 21(22), 572–583.

Hawkins, T., Mirigian, M., Selcuk Yasar, M., & Ross, J. L. (2010). **Mechanics of microtubules.** *Journal of Biomechanics*, 43(1), 23–30.

Hawkins, T. L., Mirigian, M., Li, J., Yasar, M. S., Sackett, D. L., Sept, D., & Ross, J. L. (2012). **Perturbations in microtubule mechanics from tubulin preparation.** *Cellular and Molecular Bioengineering*, 5(2), 227–238.

Heidemann, S. R., Kaech, S., Buxbaum, R. E., & Matus, A. (1999). **Direct observation of the mechanical behaviors of the cytoskeleton in living fibroblasts.** *Cell*, 145(1), 109–122.

Henderson, E., Haydon, P. G., & Sakaguchi, D. S. (1992). **Actin filament dynamics in living glial cells imaged by atomic force microscopy.** *Science*, 257(5078), 1944–1946.

Hendricks, A. G., Holzbaur, E. L. F., & Goldman, Y. E. (2012). **Force measurements on cargoes in living cells reveal collective dynamics of microtubule motors.** *PNAS*, 109(45), 18447–18452.

Herrmann, H., & Aebi, U. (2000). **Intermediate filaments and their associates: Multi-**

**talented structural elements specifying cytoarchitecture and cytodynamics.** *Current Opinion in Cell Biology*, 12(1), 79–90.

Hosek, M., & Tang, J. X. (2004). **Polymer-induced bundling of F actin and the depletion force.** *Physical Review E*, 69(5), 051907.

Huber, F., Schnauß, J., Rönicke, S., Rauch, P., Müller, K., Fütterer, C., & Käs, J. (2013). **Emergent complexity of the cytoskeleton: From single filaments to tissue.** *Advances in Physics*, 62(1), 1–112.

Huber, F., Boire, A., López, M. P., & Koenderink, G. H. (2015). **Cytoskeletal crosstalk: When three different personalities team up.** *Current Opinion in Cell Biology*, 32, 39–47.

Hunyadi, V., & Jánosi, I. M. (2007). **Metastability of Microtubules Induced by Competing Internal Forces.** *Biophysical Journal*, 92(9), 3092–3097.

Janson, M. E., & Dogterom, M. (2004). **A bending mode analysis for growing microtubules: evidence for a velocity-dependent rigidity.** *Biophysical Journal*, 87(4), 2723–2736.

Janson, M. E., & Dogterom, M. (2004). **Scaling of microtubule force-velocity curves obtained at different tubulin concentrations.** *Physical Review Letters*, 92(24), 248101–248104.

Jean, D. C., Baas, P. W., & Black, M. M. (2012). **A novel role for doublecortin and doublecortin-like kinase in regulating growth cone microtubules.** *Human Molecular Genetics*, 21(26), 5511–5527.

Katsuki, M., Drummond, D. R., & Cross, R. A. (2014). **Ectopic A-lattice seams destabilize microtubules.** *Nature Communications*, 5, 3094.

Kent, I. A., Rane, P. S., Dickinson, R. B., Ladd, A. J. C., & Lele, T. P. (2016). **Transient pinning and pulling: A mechanism for bending microtubules.** *Plos One*, 11(3), e0151322.

Kinoshita, K., Arnal, I., Desai, A., Drechsel, D. N., & Hyman, A. A. (2001). **Reconstitution of physiological microtubule dynamics using purified components.** *Science*, 294(5545),

1340–1343.

Kirmizis, D., & Logothetidis, S. (2010). **Atomic force microscopy probing in the measurement of cell mechanics.** *International Journal of Nanomedicine*, 5(1), 137–145.

Kirschner, M. W., Williams, R. C., Weingarten, M., & Gerhart, J. C. (1974). **Microtubules from mammalian brain: Some properties of their depolymerization products and a proposed mechanism of assembly and disassembly.** *PNAS*, 71(4), 1159–1163.

Kollman, J. M., Merdes, A., Mourey, L., & Agard, D. A. (2011). **Microtubule nucleation by gamma-tubulin complexes.** *Nature Reviews Molecular Cell Biology*, 12(11), 709–21.

Komarova, Y. A., Vorobjev, I. A., & Borisy, G. G. (2002). **Life cycle of MTs: Persistent growth in the cell interior, asymmetric transition frequencies and effects of the cell boundary.** *Journal of Cell Science*, 115(17), 3527–3539.

Komarova, Y. A., Akhmanova, A. S., Kojima, S. I., Galjart, N., & Borisy, G. G. (2002). **Cytoplasmic linker proteins promote microtubule rescue in vivo.** *The Journal of Cell Biology*, 159(4), 589–599.

Komarova, Y., De Groot, C. O., Grigoriev, I., Gouveia, S. M., Munteanu, E. L., Schober, J. M., ... Akhmanova, A. (2009). **Mammalian end binding proteins control persistent microtubule growth.** *Journal of Cell Biology*, 184(5), 691–706.

Kuchnir Fygenson, D., Braun, E., & Libchaber, A. (1994). **Phase diagram of microtubules.** *Physical Review E*, 50(2), 1579–1588.

Kueh, H. Y., & Mitchison, T. J. (2010). **Structural Plasticity in Actin and Tubulin Polymer Dynamics.** *Science*, 325(5943), 960–963.

Kurachi, M., Hoshi, M., & Tashiro, H. (1995). **Buckling of a single microtubule by optical trapping forces: Direct measurement of microtubule rigidity.** *Cell Motility and the Cytoskeleton*, 30(3), 221–228.

Laan, L., Roth, S., & Dogterom, M. (2012). **End-on microtubule-dynein interactions and pulling-based positioning of microtubule organizing centers.** *Cell Cycle*, 11(20), 3750–3757.

Laan, L., Pavin, N., Husson, J., & Romet-lemonne, G. (2012). **Cortical dynein controls microtubule dynamics to generate pulling forces that reliably position microtubule asters.** *Cell*, 148(3), 502–514.

Lang, I., Sassmann, S., Schmidt, B., & Komis, G. (2014). **Plasmolysis: Loss of turgor and beyond.** *Plants*, 3(4), 583–593.

Ledbetter, M. C., & Porter, K. R. (1964). **Morphology of microtubules of plant cell.** *Science*, 144(3620), 872–874.

Leung, C. L., Sun, D., Zheng, M., Knowles, D. R., & Liem, R. K. H. (1999). **Microtubule actin cross-linking factor (MACF): A hybrid of dystonin and dystrophin that can interact with the actin and microtubule cytoskeletons.** *Journal of Cell Biology*, 147(6), 1275–1285.

Levy, S. F., LeBoeuf, A. C., Massie, M. R., Jordan, M. A., Wilson, L., & Feinstein, S. C. (2005). **Three- and four-repeat tau regulate the dynamic instability of two distinct microtubule subpopulations in qualitatively different manners: Implications for neurodegeneration.** *Journal of Biological Chemistry*, 280(14), 13520–13528.

Li, C., Li, J., Goodson, H. V., & Alber, M. S. (2014). **Microtubule dynamic instability: the role of cracks between protofilaments.** *Soft Matter*, 10(12), 2069–2080.

Lin, Y.-C., Koenderink, G. H., MacKintosh, F. C., & Weitz, D. A. (2011). **Control of non-linear elasticity in F-actin networks with microtubules.** *Soft Matter*, 7(3), 902.

Mandato, C. A., & Bement, W. M. (2003). **Actomyosin transports microtubules and microtubules control actomyosin recruitment during Xenopus oocyte wound healing.** *Current Biology*, 13(13), 1096–1105.

Mandelkow, E., Mandelkow, E., & Milligan, R. A. (1991). **Microtubule dynamics and microtubule caps: a time-resolved cryo-electron microscopy study.** *The Journal of Cell Biology*,

114(5), 977–991.

Margolin, G., Gregoretti, I. V., Cickovski, T. M., Li, C., Shi, W., Alber, M. S., & Goodson, H. V. (2011). **The mechanisms of microtubule catastrophe and rescue: implications from analysis of a dimer-scale computational model.** *Molecular Biology of the Cell*, 23(4), 642–656.

Martin, D. S. (2013). **Measuring microtubule persistence length using a microtubule gliding assay.** *Methods in Cell Biology*, 115, 13-25.

Maurer, S. P., Cade, N. I., Bohner, G., Gustafsson, N., Boutant, E., & Surrey, T. (2014). **EB1 accelerates two conformational transitions important for microtubule maturation and dynamics.** *Current Biology*, 24(4), 372–384.

McIntosh, J. R., Morphew, M. K., Grissom, P. M., Gilbert, S. P., & Hoenger, A. (2009). **Lattice structure of cytoplasmic microtubules in a cultured mammalian cell.** *Journal of Molecular Biology*, 394(2), 177–182.

Melki, R., Fievez, S., & Carlier, M.-F. (1996). **Continuous monitoring of P(i) release following nucleotide hydrolysis in actin or tubulin assembly using 2-amino-6-mercapto-7-methylpurine ribonucleoside and purine-nucleoside phosphorylase as an enzyme-linked assay.** *Biochemistry*, 35(37), 12038–12045.

Menéndez, M., Rivas, G., Díaz, J. F., & Andreu, J. M. (1998). **Control of the structural stability of the tubulin dimer by one high affinity bound magnesium ion at nucleotide N-site.** *Journal of Biological Chemistry*, 273(1), 167–176.

Mickey, B., & Howard, J. (1995). **Rigidity of microtubules is increased by stabilizing agents.** *Journal of Cell Biology*, 130(4), 909–917.

Mimori-Kiyosue, Y. (2011). **Shaping microtubules into diverse patterns: Molecular connections for setting up both ends.** *Cytoskeleton*, 68(11), 603–618.

Mogilner, A., & Oster, G. (2003). **Force generation by actin polymerization II: The elastic**

**ratchet and tethered filaments.** *Biophysical Journal*, 84(3), 1591–1605.

Molodtsov, M. I., Ermakova, E. A., Shnol, E. E., Grishchuk, E. L., McIntosh, J. R., & Ataullakhanov, F. I. (2005). **A molecular-mechanical model of the microtubule.** *Biophysical Journal*, 88(5), 3167–3179.

Molodtsov, M. I., Grishchuk, E. L., Efremov, A. K., McIntosh, J. R., & Ataullakhanov, F. I. (2005). **Force production by depolymerizing microtubules: a theoretical study.** *PNAS*, 102(12), 4353–4358.

Murphy, E. B., & Wudl, F. (2010). **The world of smart healable materials.** *Progress in Polymer Science*, 35(1-2), 223–251.

Nawaz, S., Sánchez, P., Bodensiek, K., Li, S., Simons, M., & Schaap, I. A. T. (2012). **Cell viscoelasticity measured with AFM and optical trapping at sub-micrometer deformations.** *PLoS ONE*, 7(9), e45297.

Nawrotek, A., Knossow, M., & Gigant, B. (2011). **The determinants that Govern microtubule assembly from the atomic structure of GTP-tubulin.** *Journal of Molecular Biology*, 412(1), 35–42.

Needleman, D. J., Ojeda-Lopez, M. A., Raviv, U., Ewert, K., Miller, H. P., Wilson, L., & Safinya, C. R. (2005). **Radial compression of microtubules and the mechanism of action of taxol and associated proteins.** *Biophysical Journal*, 89(5), 3410–3423.

Niedermayer, T., Jegou, A., Chieze, L., Guichard, B., Helfer, E., Romet-Lemonne, G., ... Lipowsky, R. (2012). **Intermittent depolymerization of actin filaments is caused by photo-induced dimerization of actin protomers.** *PNAS*, 109(27), 10769–10774.

Nogales, E., Wolf, S. G., & Downing, K. H. (1998). **Structure of the alpha beta tubulin dimer by electron crystallography.** *Nature*, 391(6663), 199–203.

Nogales, E., Whittaker, M., Milligan, R. A., & Downing, K. H. (1999). **High-resolution model of the microtubule.** *Cell*, 96(1), 79–88.

Odde, D. J., Cassimeris, L., & Buettner, H. M. (1995). **Kinetics of microtubule catastrophe assessed by probabilistic analysis.** *Biophysical Journal*, 69(3), 796–802.

Odde, D. J., Ma, L., Briggs, A. H., DeMarco, A., & Kirschner, M. W. (1999). **Microtubule bending and breaking in living fibroblast cells.** *Journal of Cell Science*, 112(19), 3283–3288.

Olmstedt, J. B., & Borisy, G. G. (1975). **Ionic and nucleotide requirements for microtubule polymerization in vitro.** *Biochemistry*, 14(13), 2996-3005.

Omary, M. B., Ku, N. O., Tao, G. Z., Toivola, D. M., & Liao, J. (2006). **"Heads and tails" of intermediate filament phosphorylation: Multiple sites and functional insights.** *Trends in Biochemical Sciences*, 31(7), 383–394.

Pallavicini, C., Levi, V., Wetzler, D. E., Angiolini, J. F., Benseñor, L., Despósito, M. A., & Bruno, L. (2014). **Lateral motion and bending of microtubules studied with a new single-filament tracking routine in living cells.** *Biophysical Journal*, 106(12), 2625–2635.

Pampaloni, F., Lattanzi, G., Jonás, A., Surrey, T., Frey, E., & Florin, E.-L. (2006). **Thermal fluctuations of grafted microtubules provide evidence of a length-dependent persistence length.** *PNAS*, 103(27), 10248–10253.

Pecqueur, L., Duellberg, C., Dreier, B., Jiang, Q., Wang, C., Pluckthun, A., ... Knossow, M. (2012). **A designed ankyrin repeat protein selected to bind to tubulin caps the microtubule plus end.** *PNAS*, 109(30), 12011–12016.

Pertz, O. (2010). **Spatio-temporal Rho GTPase signaling - where are we now?** *Journal of Cell Science*, 123(11), 1841–1850.

Piehl, M., & Cassimeris, L. (2003). **Organization and dynamics of growing microtubule plus ends during early mitosis.** *Molecular Biology of the Cell*, 14(3), 916-925.

Portran, D., Zoccoler, M., Gaillard, J., Stoppin-Mellet, V., Neumann, E., Arnal, I., ... Vantard, M. (2013). **MAP65/Ase1 promote microtubule flexibility.** *Molecular Biology of the Cell*,

24(12), 1964–1973.

Portran, D., Gaillard, J., Vantard, M., & Thery, M. (2013). **Quantification of MAP and molecular motor activities on geometrically controlled microtubule networks.** *Cytoskeleton*, 70(1), 12–23.

Prahlad, V., Yoon, M., Moir, R. D., Vale, R. D., & Goldman, R. D. (1998). **Rapid movements of vimentin on microtubule tracks: Kinesin-dependent assembly of intermediate filament networks.** *Journal of Cell Biology*, 143(1), 159–170.

Prota, A. E., Bargsten, K., Zurwerra, D., Field, J. J., Díaz, J. F., Altmann, K.-H., & Steinmetz, M. O. (2013). **Molecular mechanism of action of microtubule-stabilizing anticancer agents.** *Science*, 339(6119), 587–591.

Rice, L. M., Montabana, E. A., & Agard, D. A. (2008). **The lattice as allosteric effector: Structural studies of alphabeta- and gamma-tubulin clarify the role of GTP in microtubule assembly.** *PNAS*, 105(14), 5378–5383.

Roll-Mecak, A., & Mcnally, F. J. (2010). **Microtubule severing enzymes.** *Current Opinion in Cell Biology*, 22(1), 96-103.

Rotsch, C., Braet, F., Wisse, E., & Radmacher, M. (1997). **AFM imaging and elasticity measurements on living rat liver macrophages.** *Cell Biology International*, 21(11), 685–696.

Salmon, W. C., Adams, M. C., & Waterman-Storer, C. M. (2002). **Dual-wavelength fluorescent speckle microscopy reveals coupling of microtubule and actin movements in migrating cells.** *Journal of Cell Biology*, 158(1), 31–37.

Sanchez, T., Welch, D., Nicastro, D., & Dogic, Z. (2011). **Cilia-like beating of active microtubule bundles.** *Science*, 333(6041), 456–459.

Satir, P. (1968). **Further studies on the cilium Tip and a 'sliding filament' model of ciliary motility.** *The Journal of Cell Biology*, 39(1), 77–94.

Schaap, I. A. T., de Pablo, J. J., & Schmidt C F. (2004). **Resolving the molecular structure of microtubules under physiological conditions with scanning force microscopy.** *European Biophysics Journal*, 33(5), 462–467.

Schaap, I. A. T. (2006). **Nano-scale mechanics of protein and DNA assemblies.** *PhD thesis, Vrije University 2006.*

Schaefer, A. W., Kabir, N., & Forscher, P. (2002). **Filopodia and actin arcs guide the assembly and transport of two populations of microtubules with unique dynamic parameters in neuronal growth cones.** *Journal of Cell Biology*, 158(1), 139–152.

Schaller, V., Weber, C., Semmrich, C., Frey, E., & Bausch, A. R. (2010). **Polar patterns of driven filaments.** *Nature*, 467(7311), 73–77.

Scheele, R. B., Bergen, L. G., & Borisy, G. G. (1982). **Control of the structural fidelity of microtubules by initiation sites.** *Journal of Molecular Biology*, 154(3), 485–500.

Schek, H. T., Gardner, M. K., Cheng, J., Odde, D. J., & Hunt, A. J. (2007). **Microtubule assembly dynamics at the nanoscale.** *Current Biology*, 17(17), 1445–1455.

Sept, D., Baker, N. A., & McCammon, J. A. (2003). **The physical basis of microtubule structure and stability.** *Protein Science*, 12(10), 2257–2261.

Song, Y., & Brady, S. T. (2015). **Post-translational modifications of tubulin: Pathways to functional diversity of microtubules.** *Trends in Cell Biology*, 25(3), 125–136.

Spedden, E., White, J. D., Naumova, E. N., Kaplan, D. L., & Staii, C. (2012). **Elasticity maps of living neurons measured by combined fluorescence and atomic force microscopy.** *Biophysical Journal*, 103(5), 868–877.

Spitzer, J., & Poolman, B. (2009). **The role of biomacromolecular crowding, ionic strength, and physicochemical gradients in the complexities of life's emergence.** *Microbiology and Molecular Biology Reviews*, 73(2), 371–88.

Srayko, M., Kaya, A., Stamford, J., & Hyman, A. A. (2005). **Identification and characterization of factors required for microtubule growth and nucleation in the early C. elegans embryo.** *Developmental Cell*, 9(2), 223–236.

Stiess, M., Maghelli, N., Kapitein, L. C., Gomis-Ruth, S., Wilsch-Brauninger, M., Hoogenraad, C. C., ... Bradke, F. (2010). **Axon extension occurs independently of centrosomal microtubule nucleation.** *Science*, 327(5966), 704–707.

Su, X., Ohi, R., & Pellman, D. (2012). **Move in for the kill: Motile microtubule regulators.** *Trends in Cell Biology*, 22(11), 567–575.

Sui, H., & Downing, K. H. (2010). **Structural basis of interprotofilament interaction and lateral deformation of microtubules.** *Structure*, 18(8), 1022–1031.

Sun, D., Leung, C. L., & Liem, R. K. (2001). **Characterization of the microtubule binding domain of microtubule actin crosslinking factor (MACF): Identification of a novel group of microtubule associated proteins.** *Journal of Cell Science*, 114(1), 161–172.

Taute, K. M., Pampaloni, F., Frey, E., & Florin, E. L. (2008). **Microtubule dynamics depart from the wormlike chain model.** *Physical Review Letters*, 100(2), 028102.

Tolomeo, J. a, & Holley, M. C. (1997). **Mechanics of microtubule bundles in pillar cells from the inner ear.** *Biophysical Journal*, 73(4), 2241–2247.

Tropini, C., Roth, E. A., Zanic, M., Gardner, M. K., & Howard, J. (2012). **Islands containing slowly hydrolyzable GTP analogs promote microtubule rescues.** *PLoS ONE*, 7(1), e30103.

Valiron, O., Arnal, I., Caudron, N., & Job, D. (2010). **GDP-tubulin incorporation into growing microtubules modulates polymer stability.** *Journal of Biological Chemistry*, 285(13), 17507–17513.

VanBuren, V., Odde, D. J., & Cassimeris, L. (2002). **Estimates of lateral and longitudinal bond energies within the microtubule lattice.** *PNAS*, 99(9), 6035– 6040.

VanBuren, V., Cassimeris, L., & Odde, D. J. (2005). **Mechanochemical model of microtubule structure and self-assembly kinetics.** *Biophysical Journal*, 89(5), 2911–2926.

Vandecandelaere, A., Pedrotti, B., Utton, M. A., Calvert, R. A., & Bayley, P. M. (1996). **Differences in the regulation of microtubule dynamics by microtubule-associated proteins MAP1B and MAP2.** *Cell Motility and the Cytoskeleton*, 35(2), 134–146.

van der Vaart, B., Akhmanova, A., & Straube, A. (2009). **Regulation of microtubule dynamic instability.** *Cell Motility and the Cytoskeleton*, 37(5), 1007–1013.

Wade, R. H., Chrétien, D., & Job, D. (1990). **Characterization of microtubule protofilament numbers. How does the surface lattice accommodate?** *Journal of Molecular Biology*, 212(4), 775–786.

Wadsworth, P. (1999). **Regional regulation of microtubule dynamics in polarized, motile cells.** *Cell Motility and the Cytoskeleton*, 42(1), 48–59.

Wagner, O. I., Rammensee, S., Korde, N., Wen, Q., & Janmey, P. A. (2009). **Softness, strength and self-repair in Intermediate filament networks.** *Experimental Cell Research*, 313(10), 2228–2235.

Walker, R. A., Brien, O., Pryer, K., Soboeiro, M. E., Voter, W. A., Erickson, H. P., & Salmon, E. D. (1988). **Dynamic instability of individual microtubules analyzed by light microscopy: Rate constants and transition frequencies.** *The Journal of Cell Biology*, 107(4), 1437–1448.

Wang, N., Butler, J. P., & Ingber, D. E. (1993). **Mechanotransduction across the cell surface and through the cytoskeleton.** *Science*, 260(5111), 1124–1127.

Wang, N., Naruse, K., Stamenovic, D., Fredberg, J. J., Mijailovich, S. M., Tolic-Nørrelykke, I. M., ... Ingber, D. E. (2001). **Mechanical behavior in living cells consistent with the tensegrity model.** *PNAS*, 98(14), 7765–7770.

Waterman-Storer, C. M., & Salmon, E. D. (1997). **Actomyosin-based retrograde flow of microtubules in the lamella of migrating epithelial cells influences microtubule dynamic**

**instability and turnover and is associated with microtubule breakage and treadmilling.** *Journal of Cell Biology*, 139(2), 417–434.

Waterman-Storer, C. M., Worthylake, R. A., Liu, B. P., Burridge, K., & Salmon, E. D. (1999). **Microtubule growth activates Rac1 to promote lamellipodial protrusion in fibroblasts.** *Nature Cell Biology*, 1(1), 45–50.

Wieczorek, M., Bechstedt, S., Chaaban, S., & Brouhard, G. J. (2015). **Microtubule-associated proteins control the kinetics of microtubule nucleation.** *Nature Cell Biology*, 17(7), 907–918.

Winans, A. M., Collins, S. R., & Meyer, T. (2016). **Waves of actin and microtubule polymerization drive microtubule-based transport and neurite growth before single axon formation.** *eLife*, 5, e12387.

Wu, H. W., Kuhn, T., & Moy, V. T. (1998). **Mechanical properties of L929 cells measured by atomic force microscopy: effects of anticytoskeletal drugs and membrane crosslinking.** *Scanning*, 20(5), 389–397.

Wu, Z., Wang, H. W., Mu, W., Ouyang, Z., Nogales, E., & Xing, J. (2009). **Simulations of tubulin sheet polymers as possible structural intermediates in microtubule assembly.** *PLoS ONE*, 4(10), e7291.

Wu, Z., Nogales, E., & Xing, J. (2012). **Comparative studies of microtubule mechanics with two competing models suggest functional roles of alternative tubulin lateral interactions.** *Biophysical Journal*, 102(12), 2687–2696.

Zaoui, K., Honoré, S., Isnardon, D., Braguer, D., & Badache, A. (2008). **Memo - RhoA - mDia1 signaling controls microtubules, the actin network, and adhesion site formation in migrating cells.** *Journal of Cell Biology*, 183(3), 401–408.

Zanic, M., Stear, J. H., Hyman, A. A., & Howard, J. (2009). **EB1 recognizes the nucleotide state of tubulin in the microtubule lattice.** *PLoS ONE*, 4(10), e7585.

Zanic, M., Widlund, P. O., Hyman, A. A., & Howard, J. (2013). **Synergy between XMAP215 and EB1 increases microtubule growth rates to physiological levels.** *Nature Cell Biology*, 15(6), 688-693.

# B Summary

Microtubules play an important role in many cellular functions. They can be highly bent by intracellular forces, yet how mechanical stress affects microtubules and how they tolerate the vast forces exerted on them remains unknown.

In this thesis, the effect of mechanical stress on microtubule mechanical properties is studied. It is found that the stiffness of microtubules decreases when they are exposed to repeated bending forces, revealing that they are subject to material fatigue. Pre-existing defects in the lattice seem to be present weak points in the microtubules, where mechanical stresses concentrate and generate more extensive damage.

Interestingly, microtubules are able to recover their initial stiffness while incorporating new tubulin dimers from the solution into their lattice, demonstrating their self-healing properties. It also shows that microtubule dynamics is not exclusive to the plus and minus ends of microtubules, challenging established paradigms.

Tubulin dimers that are incorporated into the microtubule lattice are GTP bound. GTP tubulin is known to be more stably bound in the lattice, and is thought to promote microtubule rescue. Indeed, this thesis shows that tubulin incorporation into the lattice far from the tip in response to microtubule damage can lead to rescue events. This finding opens up a new perspective on an aspect of microtubule dynamic instability that so far is poorly understood.

**Résumé**

Les microtubules - qui définissent la forme des axones, des cils et des flagelles, et qui servent de rails pour le transport intracellulaire-subissent de fortes contraintes exercées par les forces intracellulaires. La structure des microtubules et leur rigidité peuvent en théorie être affectées par des contraintes physiques. Cependant, il reste à établir comment les microtubules tolèrent de telles forces et quelles sont les conséquences de ces forces sur la structure des microtubules. En utilisant un dispositif de microfluidique, j'ai pu montrer que la rigidité des microtubules diminue progressivement à chaque cycle de courbure induit par des contraintes hydrodynamiques. Comme dans d'autres exemples de fatigue des matériaux, l'application de contraintes mécaniques sur des défauts pré-existants le long des microtubules est responsable de la génération de dommages plus étendus. Ce processus rend les microtubules moins rigides. J'ai pu aussi montrer que les microtubules endommagés peuvent se réparer en intégrant de nouveaux dimères de tubuline à leur surface et de récupérer ainsi leur rigidité initiale. Nos résultats démontrent que les microtubules sont des matériaux biologiques ayant des propriétés d'auto-réparation, et que la dynamique des microtubules ne se produit pas exclusivement à leurs extrémités. La mise en évidence de ces nouvelles propriétés permet de montrer comment les microtubules peuvent s'adapter à des contraintes mécaniques.